U.S. ARMY COMBAT CAPABILITIES DEVELOPMENT COMMAND CHEMICAL BIOLOGICAL CENTER

ABERDEEN PROVING GROUND, MD 21010-5424

Effects of Complex Features, Surfaces, and Interfaces on Post-Decontamination Vapor Emission from Contaminated Materials

Neil A. Hawbaker
Brent A. Mantooth
Thomas P. Pearl
RESEARCH AND TECHNOLOGY DIRECTORATE

January 2022

REPORT DOCUMENTATION PAGE		*Form Approved* *OMB No. 0704-0188*

1. REPORT DATE *(DD-MM-YYYY)* XX-01-2022	2. REPORT TYPE Final	3. DATES COVERED *(From - To)* May 2019 – Jan 2021

4. TITLE AND SUBTITLE
Effects of Complex Features, Surfaces, and Interfaces on Post-Decontamination Vapor Emission from Contaminated Materials

5a. CONTRACT NUMBER

5b. GRANT NUMBER

5c. PROGRAM ELEMENT NUMBER

6. AUTHOR(S)
Hawbaker, Neil A.; Mantooth, Brent A.; Pearl, Thomas P.

5d. PROJECT NUMBER
CB10409

5e. TASK NUMBER

5f. WORK UNIT NUMBER

7. PERFORMING ORGANIZATION NAME(S) AND ADDRESS(ES)
Director, DEVCOM CBC, ATTN: FCDD-CBR-PD, APG, MD 21010-5424

8. PERFORMING ORGANIZATION REPORT NUMBER
DEVCOM CBC-TR-1734

9. SPONSORING / MONITORING AGENCY NAME(S) AND ADDRESS(ES)
Defense Threat Reduction Agency, Joint Science and Technology Office, 8725 John J. Kingman Road, MSC 6201, Fort Belvoir, VA 22060-6201

10. SPONSOR/MONITOR'S ACRONYM(S)
DTRA JSTO

11. SPONSOR/MONITOR'S REPORT NUMBER(S)

12. DISTRIBUTION / AVAILABILITY STATEMENT
Approved for public release: distribution unlimited.

13. SUPPLEMENTARY NOTES

14. ABSTRACT: (Limit 200 words)
Complex features such as capillaries, screw threads, and material interfaces may act to entrain chemical warfare agents (CWAs) and resist decontamination. Representative features of various sizes and geometries for both bare and painted metals were contaminated with the CWA simulant 2,5-lutidine, and the vapor emission rate was determined using atmospheric pressure mass spectrometry. It was found that complex features composed of either bare metals (i.e., steel) or painted materials (i.e., polyurethane-based paint applied to steel) gave significantly different vapor emission profiles when compared with the same materials in a flat configuration. Contaminants entrained in capillary features were not completely removed using a water-rinse procedure, which would result in significant vapor emission risk. Scale-up calculations showed that small levels of capillary entrainment may account for a significant portion of the post-decontamination vapor hazard. These studies demonstrate that decontamination of complex features must be considered in decontaminant development and hazard assessments.

15. SUBJECT TERMS

Complex features	Chemical warfare agent (CWA)	Vapor emission	Entrainment
Off-gassing simulant	Decontamination	Capillary action	Mass transfer

16. SECURITY CLASSIFICATION OF			17. LIMITATION OF ABSTRACT	18. NUMBER OF PAGES	19a. NAME OF RESPONSIBLE PERSON Renu B. Rastogi
a. REPORT U	b. ABSTRACT U	c. THIS PAGE U	UU	104	19b. TELEPHONE NUMBER *(include area code)* (410) 436-7545

Standard Form 298 (Rev. 8-98)
Prescribed by ANSI Std. Z39.18

Blank

PREFACE

The use of either trade or manufacturers' names in this report does not constitute an official endorsement of any commercial products. This report may not be cited for purposes of advertisement.

This report has been approved for public release.

<u>Acknowledgments</u>

Blank

CONTENTS

FIGURES

TABLES

Blank

EFFECTS OF COMPLEX FEATURES, SURFACES, AND INTERFACES ON POST-DECONTAMINATION VAPOR EMISSION FROM CONTAMINATED MATERIALS

1. INTRODUCTION

1.1 Overview and Context

Decontamination is of paramount importance for reducing and eliminating hazards posed to civilians and soldiers in the event of a chemical warfare agent (CWA) attack or accidental release. CWAs are toxic, small molecules with diverse chemical structures and mechanisms of action on the human body, but all are capable of causing death or injury.[1,2] Personnel in a contaminated area can be exposed through inhalation of toxic vapors (vapor hazard) or through direct contact (contact hazard) when interacting with a contaminated surface or material.[3] A decontamination technology is any means of hazard mitigation aimed at reducing the exposure risk. These technologies may focus on physical removal, reactive destruction, or encapsulation of the chemical agent.[1,2]

In the case of vapor hazards, the evaluation of vapor emission from assets has traditionally started with laboratory measurements of vapor flux from asset-relevant materials in a flat horizontal configuration (i.e., panels). The time-dependent vapor emission profiles (i.e., source terms), are unique to each contaminant–material–decontaminant combination and are used in scaling calculations to represent vapor emission for full-sized assets. Briefly, the whole is equal to the sum of the parts; the total asset source term is calculated as the sum of emission rates from all materials and features on the asset.[3] However, real assets have textures and interfaces that can significantly influence agent retention and the ability of a decontaminant to access and remove agent from these features. Previous testing has not systematically characterized how contaminants in these types of features contribute to vapor source terms.

Determining the impact of complex features such as grooves and material interfaces on vapor emission has so far been a major challenge for estimating real-world decontaminant performance. These types of features on assets can promote chemical agent entrainment and thereby limit decontaminant access and effectiveness. Although agent is retained, it is not entirely clear to what extent the entrained agent contributes to vapor emission. These features vary widely in size and geometry, so accurately estimating their influence on decontamination is difficult. Early exposure assessment calculation approaches have attempted to account for the contribution of complex features to vapor hazards by invoking estimated higher-magnitude source terms for nonflat horizontal surfaces, but they lack laboratory data to fully support these assumptions. The focus of this work is to clarify that picture and to assess how complex features contribute to vapor emission both before and after decontamination (Figure 1). The work documented in this report demonstrates that entrained contaminants in complex features can be the dominant vapor sources from assets; therefore, it is critically important to include them in the analysis of hazard mitigation technologies. The exclusive use of flat, horizontal material test data could cause potential exposure risks to personnel to be significantly underestimated.
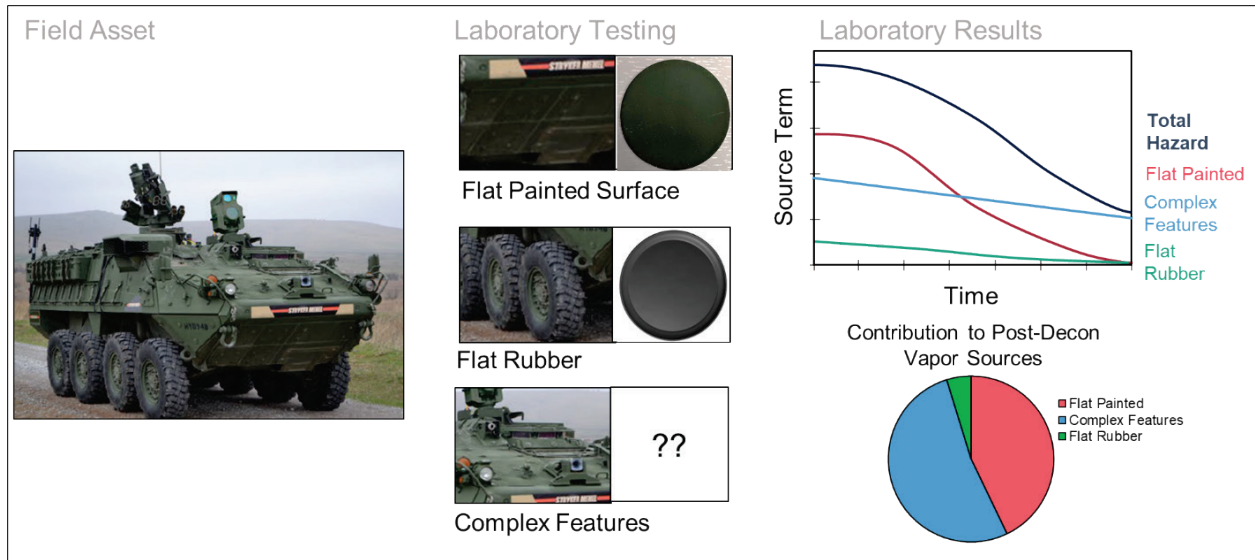
Figure 1. Example of how laboratory testing is used to evaluate decontaminant performance on a real-world asset.

Complex features restrict decontaminant access to entrained bulk liquid contaminant, thereby reducing the efficacy of a decontamination process. A liquid contaminant entrained within a complex feature may only interact with a liquid decontaminant across a small area, leaving much of the bulk liquid inaccessible to the decontaminant solution (Figure 2). Traditional liquid decontaminants were developed with a focus on liquid-phase reactivity, and researchers have not addressed how entrained contaminant can be displaced and mitigated. Until this point, studies on vapor emission of complex features after decontamination have been extremely limited. This study focuses on understanding how feature size, geometry, and material composition change vapor emission of a volatile contaminant after application of an aqueous solution.
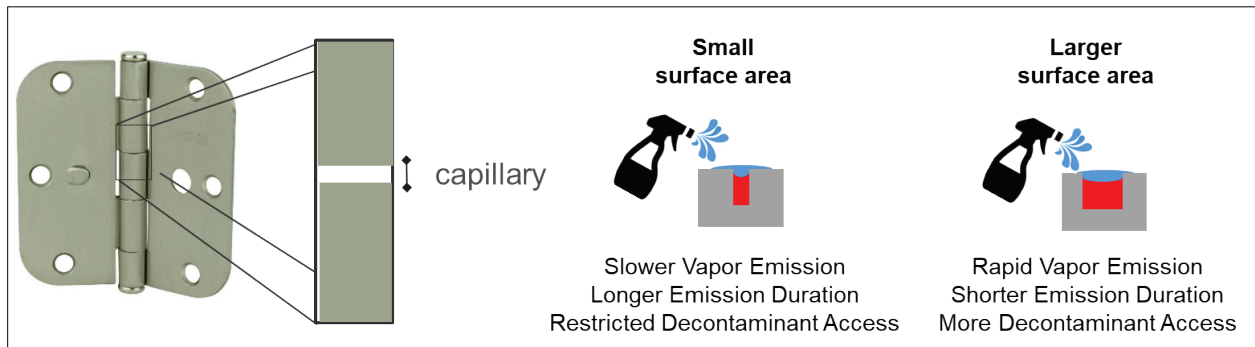
Figure 2. Capillary action explains how complex features influence contaminant retention and the resulting contaminant distribution in and on the material, decontaminant performance, and vapor emission.

To characterize the vapor emission profiles from these features, measurements of vapor emitted mass (VEM) from materials as a function of time are required. Traditionally, solid sorbent tubes (SSTs) were used to collect vapor samples over time. The SSTs were then analyzed for accumulated mass as a function of chemical species using tools such as gas or liquid chromatography.[3] Although SSTs offer excellent sensitivity and chemical species selectivity to quantify collected agent mass vapor, there are several disadvantages to this sampling technique, including limited dynamic range (approximately two decades for a specific sampling schedule), poor time resolution (typically, two samples per hour), and significant labor associated with collection of each sample. The ability to characterize and use vapor source terms, especially from complex features, requires higher time resolution (on the order of minutes) and a larger dynamic range (approximately five decades). As a result, a new vapor sampling strategy and method was developed that was based on an atmospheric pressure real-time gas analyzer.

The primary objective of this work was to determine whether liquid contaminant entrained in complex features is likely to be a significant contributor to pre- and post-decontamination vapor hazards. Additionally, this work aimed to develop a set of complex features that can be tested at laboratory scale to represent features on actual assets. It was *not* envisioned that these laboratory complex test fixtures would exactly replicate the features found on a real-world asset (e.g., depth, width, length, and internal volume), but instead that they would allow for an evaluation of the effects of capillary entrainment. This type of analysis will inform the methodology, including the types of features to be evaluated, for development and evaluation of decontaminants in the future (Figure 3). This work included several subgoals, and each is covered in a specific section of this report:

- Section 2: development of real-time techniques for vapor monitoring and development of laboratory-scale complex features;

- Section 3: influence of complex features on vapor emission from untreated surfaces;

- Section 4: influence of complex features on vapor emission from water-rinsed surfaces;

- Section 5: estimated contribution of complex features in a scale-up calculation; and

- Section 6: discussion of the scope and impacts of results.
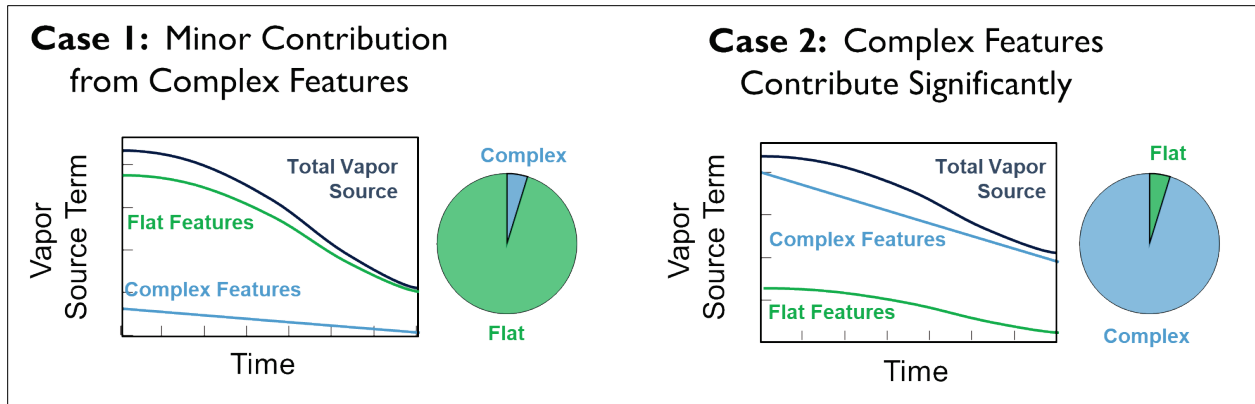
Figure 3. Sensitivity analysis: How do complex features contribute
to the post-decontamination hazard?

The results provided in this report demonstrate that contaminant associated with even a few complex features on an asset can significantly contribute to the overall vapor hazard, both before and after decontamination. For example, it is shown that for steel, after a water-rinse treatment process, the VEM from a capillary feature can be 100,000 times greater than that observed from the flat material. In a similar test on a polyurethane (PU) coating, the material with capillary features exhibited 450 times greater VEM than the flat material. The contributions and effects of capillary features are significant in evaluating decontamination efficacy and post-decontamination vapor exposure hazard. The data provided here provide guidance on which feature sizes and geometries are the largest contributors to the overall emission hazard. This helps focus the evaluation of hazards from post-decontaminated materials on the most relevant and important features. Lastly, this work also highlights a need for updated protocols for decontaminant development and evaluation.

1.2   Scientific Background

Small-scale laboratory studies provide the foundation for developing and evaluating decontaminant technologies to be used under field conditions. In laboratory studies, decontaminant performance can be measured quickly, accurately, and safely. An effective decontaminant must be able to mitigate the hazard posed by the contaminated asset or surface as a result of:

- accessing the contaminated area,

- interacting with absorbed and bulk contamination, and

- directly neutralizing or extracting contaminant for subsequent neutralization.

Each of these primary roles of a decontaminant is governed by different underlying physics and chemistry. All three must be considered during development and evaluation. Robust laboratory techniques are continually being developed and refined by science and technology organizations for the test and evaluation (T&E) community.[3] Typical laboratory studies focus on application of a liquid decontaminant (via pipette) to flat horizontal materials. However, the end use of a decontaminant in the field includes application of the technology to three-dimensional (3D) materials with unique textures and geometries.

4

The ability to decontaminate a material depends on the contaminant distribution on the material and the resulting accessibility of the contaminant to the decontaminant. Contaminant distribution is influenced by several contaminant–material interactions, including sorption into the material, capillary action, and surface wetting, as shown in Figure 4. Due to these factors, certain material–contaminant combinations are more difficult to decontaminate than others. An understanding of the key physical and chemical processes needs to inform decontaminant development to ensure that decontaminant formulations are capable of solving the correct problem.

The factors driving sorption and surface wetting have been covered in previous publications,[4,5] so these topics are only briefly discussed here. The focus of this work is on nonporous materials that are used on assets (such as metals and coatings) and flexible sealants, which can broadly be categorized as polymeric or polymer composite materials.

Absorption describes the permeation of chemicals into a material. The mechanism of ingress greatly depends on the material, with some materials (e.g., stainless steel) being completely impermeable to liquid contaminants, while others (e.g., silicone elastomer) are more susceptible to rapid contaminant absorption. The rate of permeation depends on the diffusivity of the contaminant in the material, which can be measured experimentally by infrared spectrometry or microbalance gravimetry. The diffusivity can depend on the chemical environment presented by the material and the chemical properties of the contaminant, such as molecular size and polarity. Typically, contaminant sorption results in a larger decontamination challenge; for example, liquid decontaminants applied to a surface have less direct access to the absorbed contaminant mass in the bulk of the material.[6,7] Contaminant absorbed into a paint or a coating can present a long-lasting contact and vapor hazard, as the chemical will slowly migrate to the surface even after the bulk surface contamination is removed. Decontaminants must be formulated to either extract or displace the contaminant that has been absorbed into the material without altering or damaging the material in question; in other words, the decontaminated material or asset must still be functional after treatment. Decontaminants that can access absorbed materials may use surfactants or co-solvents to help extract the contaminant, swell the material to accelerate extraction, or use solvent to displace material-bound contaminant.[6,7] Decontamination of absorbed contaminant remains a significant challenge for flat surfaces and will likely be even more difficult for complex features.

Absorption	Wetting	Capillary Action

CWA Absorbing into the Material

CWA Spreading Across the Surface

CWA Becomes Entrained in Small Capillaries

Decontamination Challenge:
Removing CWA absorbed into the material.

Decontamination Challenge:
CWA is spread across the material.

Decontamination Challenge:
Accessing contaminant entrained in capillaries.

Driving Forces:
Diffusion
Bulk Liquid Flow

Driving Forces:
Surface Roughness

Driving Forces:
Capillary Size
Interfacial Tension

Contributing Factors :
Polarity (agent)
Molecular Size (agent)
Polymer Composition (material)

Contributing Factors :
Surface Tension (agent)
Surface Roughness (material)
Surface Energy (material)

Contributing Factors :
Surface Tension (agent)
Surface Energy (material)
Capillary Size (material)

Figure 4. Contaminant–material interactions that govern distribution of contamination at surfaces and interfaces.

Surface wetting describes how a liquid contaminant interacts with a material surface (Figure 5). Over time, partly wetting droplets can spread across the material and lead to increased surface area of interaction and a different boundary condition for contaminant absorption relative to a non-spreading case. When contaminant is spread out on a surface, the rate of evaporation increases, which can result in a greater short-term vapor hazard that may have a shorter vapor emission duration. Wetting and spreading lead to larger surface areas to be decontaminated, and may lead to the possibility of contaminant spreading beyond the initial contamination location (e.g., into harder-to-decontaminate complex features). However, wetting may also provide a mechanism for an entrained bulk liquid to spread out of capillary entrainment. Wetting has been shown to be influenced by surface roughness, as contaminant spreads through microcapillaries on the material surface. For smoother surfaces, interfacial tension also plays a role. If the surface energy of the material is greater than the surface tension of the contaminant, wetting will occur. The rate of spreading is increased as the disparity between surface tension and surface energy grows. Surface wetting is dependent on both the contaminant and the material, and different contaminant–material combinations result in different behaviors. Examples of wetting behaviors of CWAs on common materials are shown in Figure 6.
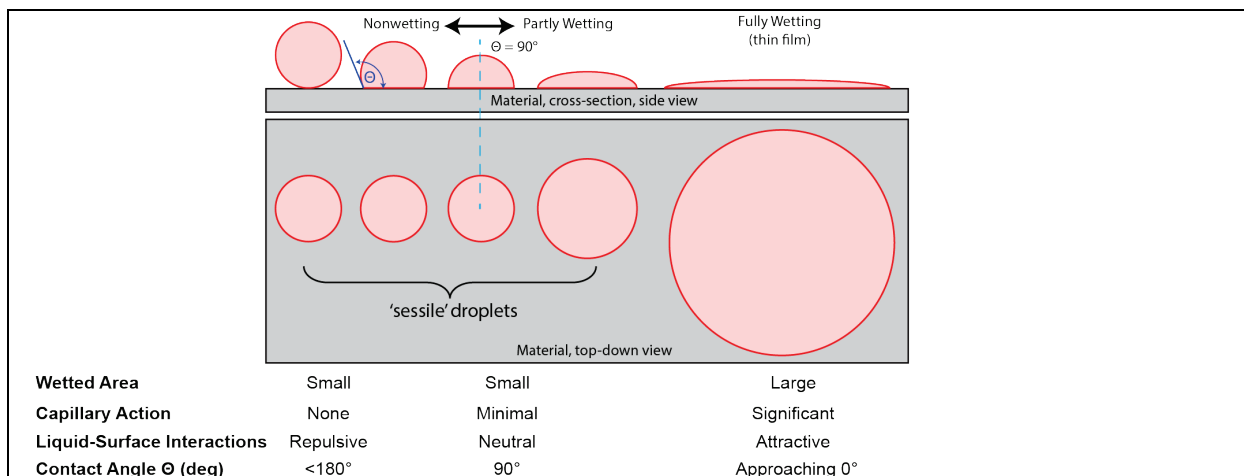
Figure 5. The range of wetting and contact angles that can be observed and the resulting magnitudes of capillary action.
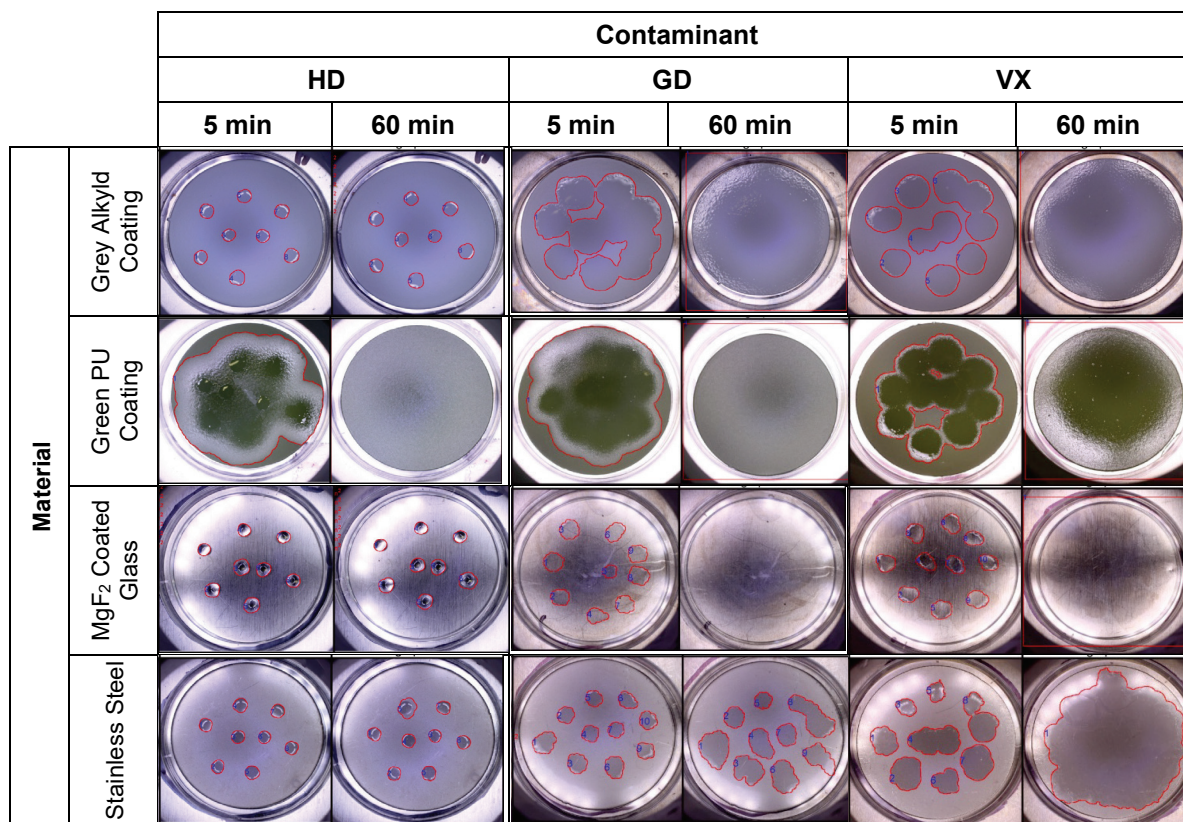
Figure 6. Top-down photography of wetting on four different materials with three CWAs. Comparison between liquid distribution at 5 and 60 min after deposition of droplets illustrates differences in wetting behavior. HD (mustard agent), bis-(2-chloroethyl)sulfide; GD, pinacolyl methylphosphonofluoridate; VX, [2-(diisopropylamino)ethyl]-O-ethyl methylphosphonothioate.

Accounting for material wetting and contaminant sorption are important when considering how complex features influence vapor emission and decontamination. As shown in Figure 7, different contaminant–material combinations give rise to different wetting and sorption behaviors. Although there are varying degrees of contaminant wetting and absorption, contaminant–material combinations can be loosely described as wetting or sessile (non-wetting) for liquid spreading and sorptive or impermeable (non-sorptive) for contaminant uptake into the material. Defining the wetting and absorption behaviors of materials and contaminants relevant to an asset under study will help researchers determine which decontaminant attributes are required to reduce the hazard.
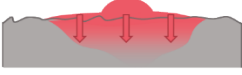
Figure 7. Wetting and sorption matrix for various contaminant–material combinations.

For contaminant entrained within capillary features, capillary action is the primary driving force for liquid movement. Capillary action is the flow of liquid based on forces associated with wetting. This mechanism allows for contaminant to travel within the threads on a screw or at a narrow interface between two materials. Contaminant entrained in these areas is more difficult to access with a liquid decontamination solution. Moreover, the smaller exposed surface area also slows the rate of contaminant evaporation and thereby leads to an increased vapor emission time duration. This results in a reduction in the vapor source term magnitude but a significant increase in the time over which vapor emission would occur.

Movement of fluid in capillary features is largely governed by fluid dynamics. The Young–Laplace equation shows that capillary pressure (P_c) depends on interfacial tension (γ), the wetting angle (θ), and the size of a capillary feature (r_c):

$$P_c = \frac{2\gamma\cos\theta}{r_c} \tag{1}$$

Increased P_c corresponds to greater effects on flow into the capillary features. Each of the variables that determine P_c are influenced differently by the physical properties of the contaminant and material, as shown in Figure 8. Capillary size (r_c) is a material-only property and is not influenced by the properties of the CWA. P_c is inversely proportional to r_c, meaning the effect is more pronounced as the capillary becomes smaller (<10 mm when $\gamma = 40$ mN/m). Contact angle (θ) describes the wettability of the surface with CWA. Highly wetting conditions (θ near 0°) result in high capillary pressures, whereas non-wetting conditions (θ near 90°) resist entrainment in capillary features. The P_c is directly proportional to cos θ; therefore, it decreases nonlinearly as θ approaches 90°. Interfacial tension is a correlated property. Like contact angle, interfacial tension depends on the surface tension of the contaminant and the surface energy of the material. For a solid–liquid interface, the interfacial tension is related to the adhesive force between the liquid droplet and the solid substrate. Capillary pressure increases linearly as the interfacial tension increases. Interfacial tension and contact angle are related: low contact angle (high wettability) correlates with high interfacial tension.
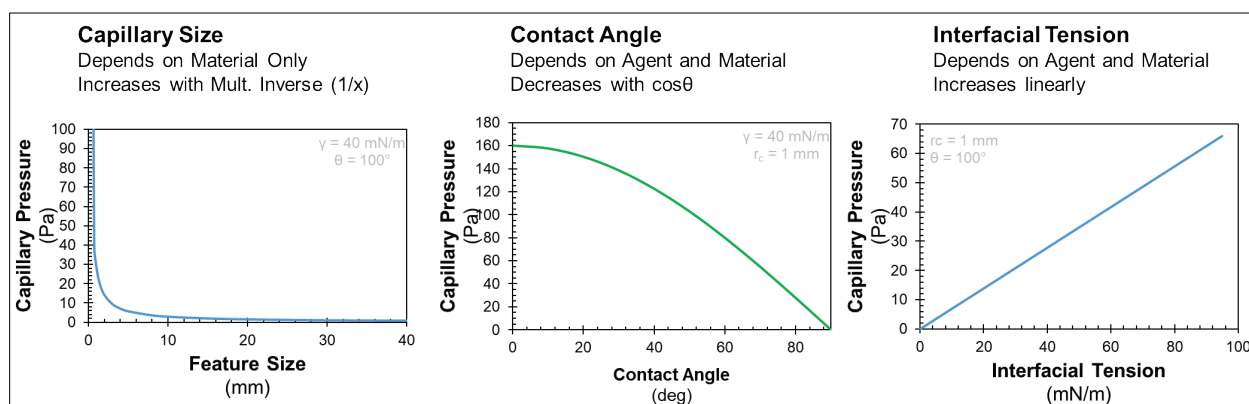
Figure 8. Influence of feature size (r_c) contact angle (θ), and interfacial tension (γ) on capillary pressure (P_c). In each case, two of the three parameters (r_c, θ, and, γ) are held constant as indicated in the insets. The values used for θ and γ represent the contact angle (100°)[8] and interfacial tension (40 mN/m)[9] for polydimethylsiloxane and water, respectively.

Understanding the physics behind capillary pressure[10] helps to highlight key areas of decontaminant and material development. Highly wetting contaminants are more likely to become entrained in capillary features, and this effect is amplified at smaller feature sizes. From a material-development perspective, the best way to avoid entrainment in capillary features is to use materials with low surface energies that resist wetting by the contaminant, or to design assets with a minimal number of capillary structures. This increases the contact angle and interfacial tension, thereby reducing the capillary pressure. This can also inform decontaminant development, where removing contaminant from capillary features is a significant problem. As shown in Figure 8, the driving factors behind capillary entrainment are feature size, surface wetting, and interfacial tension. These factors likely play a role in contaminant retention, decontamination burden, and vapor emission behavior.

Decontamination of capillary features has been underexplored. However, understanding the fundamental physics can help inform what decontaminant attributes are likely to be important and what features may be the hardest to decontaminate. Many CWAs have a

lower surface tension (25–40 mN/m at 25 °C) than typical aqueous decontaminant solutions (~75 mN/m at 25 °C).[11] Therefore, CWAs are more likely to spread over a surface and experience capillary entrainment when compared to aqueous decontaminants. Moreover, many CWAs exhibit poor water solubility, so removal via extraction is also limited for aqueous decontaminants. This shows that contaminant solubility and surface tension may be potential areas for optimization of an aqueous decontaminant for better performance on capillary features.

Constrained geometries that give rise to capillary-driven liquid transport influence contaminant distribution on the material and decontaminant access to the entrained contaminant. On a flat horizontal surface, agent may be sorbed into the material or reside on the surface as a liquid. When applied to the surface of contaminated material, a liquid decontaminant can easily access the surface-bound contaminant liquid but will have more limited access to the sorbed contaminant. The introduction of capillary features can significantly alter the agent distribution on the material and create entrained agent within the capillary features. Furthermore, the presence of these capillary features can alter the flow of decontaminant and impact contaminant removal. Lastly, capillary features can alter how the entrained agent may be emitted from the feature as a vapor, which is the principal focus of this report.

Based on the anticipated trends with capillary pressure and the flow restrictions, it was hypothesized that the effect would be dependent on the size of the feature (Table 1). Systems involving small features are likely to result in capillary entrainment and to be influenced by fluid flow restrictions. As the feature size increases, the capillary pressure and flow restrictions decrease, which potentially decreases the entrained contaminant and enables better accessibility. At some threshold size, features are large enough that they behave similarly to flat panels.

Table 1. Qualitative Effects of Complex Feature Size on Capillary Action, Fluid Flow Restrictions, and the Ability to Decontaminate the Feature

Capillary Feature Size	Capillary Action	Decontaminant Fluid Flow Restrictions	Ability to Decontaminate
Small (e.g., <0.04 mm)	Likely to draw liquid into feature, if wetting	Highly restrictive to fluid flow	May be highly challenging compared to flat panel
Moderate (e.g., <0.5 mm)	May draw liquid into feature, if wetting	Restrictive to fluid flow	Challenging compared to flat panel
Large (e.g., >0.5 mm)	Minimal effects	Minimally restrictive to fluid flow	Similar to flat panel

This study provides an initial data set that highlights some potentially important factors for understanding the decontamination of complex features. Although a full scope of contaminant–material combinations was not investigated, these results provide insight into the influence of wetting on vapor emission and decontamination of complex features.

2. EXPERIMENTAL APPROACH

2.1 Development of a Real-Time Vapor Monitoring Method

The aim of this study was to determine whether contamination associated with complex features contributes significantly to the overall vapor hazard posed by a contaminated asset. This requires the ability to measure the vapor emission profiles from a variety of feature sizes and geometries. The large number of geometries, feature sizes, and materials requires a screening technique that is flexible and accurate. Several requirements were identified for the experimental design:

- a means of measuring vapor emission with a wide dynamic range for analyte flux and high time resolution capable of easily resolving extremely varied vapor profiles from contaminated and decontaminated materials;

- an analytical instrument connected to the chamber, with a regulated flow of a carrier gas as the sampling medium;

- the ability to measure vapor emission under ambient conditions (e.g., non-vacuum and room temperature);

- a methodology with a short duty cycle for data collection to allow for rapid throughput; and

- test fixtures that accurately represent real-world complex features while being small enough to be tested.

With these requirements in mind, a method was developed using atmospheric pressure mass spectrometry (AP-MS) for analysis. The AP-MS system was connected to a vapor microchamber of the same construction and design as that used for vapor test measurements, in which SSTs were used for analyte collection. Test fixtures were developed to mimic common complex geometries found on assets composed of either stainless steel and/or PU paint-coated steel, and the high-vapor-pressure simulant 2,5-lutidine was used as a test contaminant. The subsequent sections detail each aspect of the measurement approach.

2.2 Vapor Microchamber

A vapor chamber of the same construction and style as that used in vapor sampling manifolds plumbed to SSTs facilitated the measurement of vapor emission rates using AP-MS.[12] This standardized test microchamber and sampling approach meets the criteria discussed in *Chemical Contaminant and Decontaminant Test Methodology Source Document* (SD2ED)[3] and is based upon concepts presented in ASTM-D5116.[13] Schematics of the chamber are provided in Figure 9. Briefly, dry nitrogen flows over the surface of a material that is located in the sealed vapor chamber in a laminar flow limit. This carrier gas serves as the sampling medium for the emitted vapor from a contaminated material. The internal volume of the chamber (V) is 3.2×10^{-5} m^3, and the typical flow rate (Q) is 150 mL/min (2.5×10^{-6} m^3/s). The microchamber has a cross-sectional area (A) of 5×10^{-4} m^2 (6.3×79 mm, height × width) at the midpoint, resulting in an average airspeed (Q/A) of 0.005 m/s. Prior to the measurement, the material is contaminated with a specific number of liquid contaminant droplets (N).
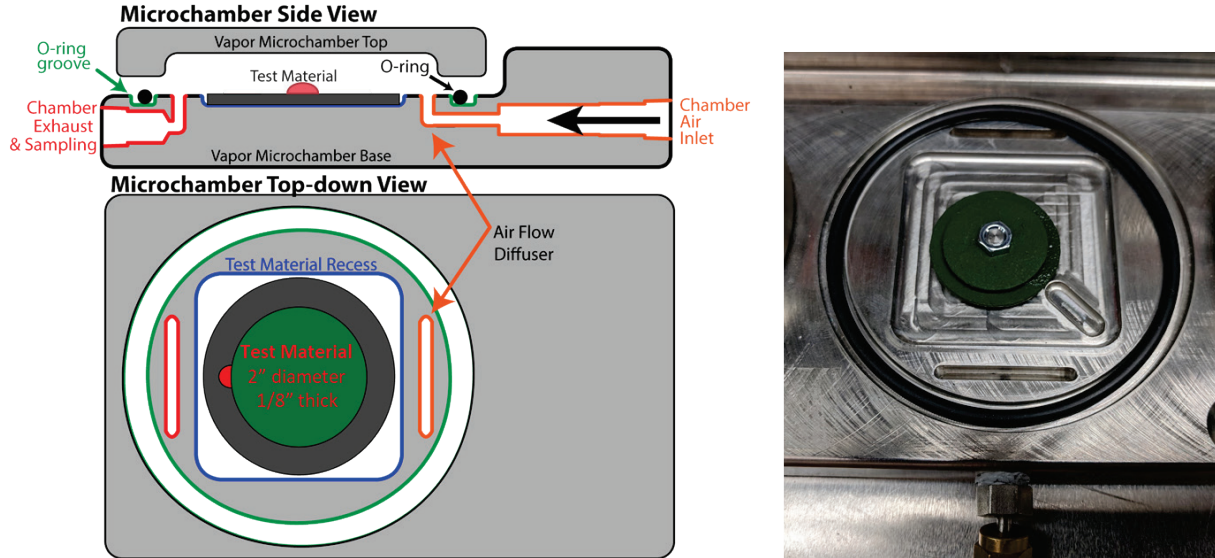
Figure 9. Schematic and photograph of a vapor microchamber used to contain the test materials.

The mass balance equation describes the relationship of vapor emission, *E(t)*, and the resulting vapor concentration in the vapor microchamber as a function of time, *C(t)*:

$$\frac{\mathrm{d}C}{\mathrm{d}t} = E(t)\frac{N}{V} - C(t)\frac{Q}{V} \qquad (2)$$

where

    E(t) is the emission rate (mg/min/drop),
    N   is the number of contaminant droplets applied to the test material (drops),
    V   is the microchamber volume (m^3),
    C(t) is the vapor concentration (mg/m^3), and
    Q   is the airflow rate through the chamber (m^3/min).

Appendix B provides the derivation showing that the emission rate for the microchamber geometry and test conditions at the U.S. Army Combat Capabilities Development Command Chemical Biological Center (DEVCOM CBC; Aberdeen Proving Ground, MD) can be determined using a simplified equation:

$$E(t) = \frac{C(t)Q}{N} \qquad (3)$$

Thus, the emission rate can be directly determined from the microchamber exhaust concentration, which is quantified using the AP-MS. Details on quantification of the exhaust gas concentration are provided in Appendix B.

Previous vapor test methods, including methods in the SD2ED,[3] used the liquid wetted area of the material to indicate the emission rate as mass emitted per unit area. The inclusion of complex features does not facilitate the use of a wetted area-based emission rate

because of the variable geometries of the features. Instead, the emission rate here is normalized per droplet. This should enable the characterization and scaling of different-geometry features based on how much contaminant is applied to a feature. This requires droplet volume to be fixed and uniform for testing and implies that the droplet volume used in testing corresponds to the volume that would be used in in any scale-up calculations.

2.3   AP-MS

Contaminants trapped within constrained geometries such as screw threads, grooves, and material interfaces may exhibit vapor emission profiles that vary greatly from the well-studied flat horizontal surfaces. Monitoring these diverse emission profiles presents a large challenge for traditional vapor sampling using SSTs. The collection time for solid sorbent vapor sampling is determined based on reasonable estimates of the predicted vapor emission. When the vapor emission profile is unknown, over- or under-sampling of the vapor can lead to measurements falling outside the calibration limits. Therefore, use of traditional vapor sampling techniques may prove tedious when attempting to study the possibility of highly variable vapor emission from complex features.

Real-time AP-MS provides an alternative method for monitoring vapor emission. In this technique, vapor emission is monitored continuously by a residual gas analyzer that samples the effluent vapor flow from a contaminated panel (or other feature). In these studies, the Cirrus 3-XD commercial system (MKS Instruments; Andover, MA) was used for trace gas analyses in research laboratories and industrial applications. The instrument has high sensitivity, particularly for low mass-to-charge ratio (*m/z*) ions, with a minimum detectable concentration of <15 ppb for argon and nitrogen gases. This technique overcomes some of the shortcomings of obtaining vapor measurements with SSTs by using mass spectrometry to measure the real-time analyte concentration in a vapor stream. The high scan rate allows for a data point to be collected every few seconds, which results in a drastic improvement in time resolution as compared to SSTs. The instrument exhibits a large dynamic range, with approximately 5 orders of magnitude between the highest and lowest quantifiable concentrations for the analytes of interest. This large dynamic range allows for the analysis of the full vapor emission profile for the conditions evaluated in this study. Finally, this method eliminates the need for complex sampling schedules and sidesteps the labor- and analysis-intensive process of collecting and analyzing sorbent tubes. A comparison of the two techniques is provided in Figure 10.
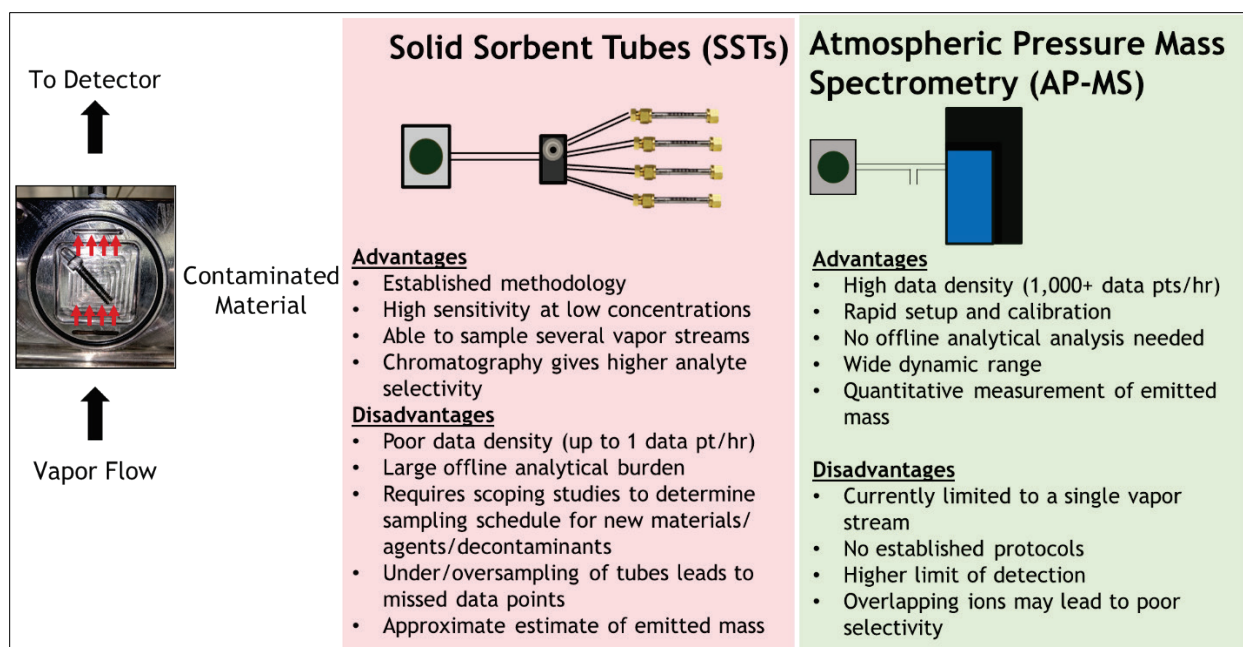
Figure 10. Comparison of SST and AP-MS vapor monitoring methods.

This work includes real-time vapor monitoring via AP-MS using CWA simulants in a fume hood. Use of simulants allows for benchmarking of the instrument in a safe environment, so that the system can be properly adapted for use in surety operations. In the current configuration, a contaminated panel (or other material) is placed in a vapor chamber. A flow of argon, nitrogen, or air is introduced to the contaminated item, and the effluent vapor is sampled using a narrow diameter capillary. The mass spectrometer is a vacuum instrument that requires a low pressure (10^{-6} Torr) for optimum operation. To analyze the ambient-pressure (760 Torr) vapor effluent, a pressure reduction is needed. A backing (rough) pump and a turbomolecular pump are used to pull the vapor effluent through the capillary and aperture restriction, respectively (20 mL/min flow rate at the inlet). The pressure reduction due to the drop in conductance over the capillary and the aperture combined with the differential pumping of the gas manifold and measurement chamber result in a low enough pressure to allow for direct electron impact gas ionization and extraction. Ions pass through a quadrupole mass filter based on *m/z*, en route to detection with a Faraday cup or an electron multiplier. A schematic of this system is provided in Figure 11.

Instrument response was calibrated using a vapor stream of known analyte concentration that was generated through dilution of a saturated stream. Regular control samples were included in the testing conditions to verify that calibration was maintained. The AP-MS could accurately analyze simulant concentrations ranging from 1 to 500 mg/m^3 (0.3–100 ppm). Concentrations below this value fell within the noise of the instrument and could not be accurately quantified (the signal-to-noise ratio was less than 3:1). At the flow rates used in this study, the detection limits correlate with emission rates of 0.15–75 µg/min. Details on detector calibration, ionization conditions, and data analysis are given in Appendix C.
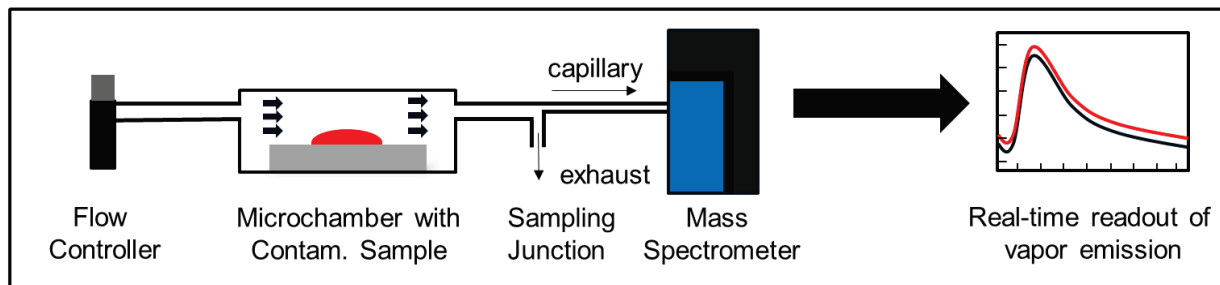
Figure 11. Experimental setup for monitoring the vapor effluent using AP-MS.

2.4   Contaminant and Materials Type Selection

        The principal goal of these studies was to highlight the feature geometries and sizes that lead to the most contaminant retention and prolonged vapor emission. Different contaminants will spread, absorb, and evaporate differently, based on physical properties and chemical structure. CWA simulants closely match one or more of the chemical and physical properties of a chemical agent but have a lower toxicity.[12] For this study, a single chemical simulant was used that was selected based on testing throughput and ease of analysis by mass spectrometry. 2,5-Lutidine was chosen as a simulant for GB (sarin; (*RS*)-propan-2-yl methylphosphonofluoridate) based on these criteria as well as the Decontamination Sciences Branch's familiarity in working with this compound on the influence of hydrogen bonding interactions on mass transport in polymeric materials.[6] Preliminary measurements with 2,5-lutidine showed rapid vapor emission (1–8 h) as compared with the traditional HD simulant, methyl salicylate (1–4 days) (Figure 12). Faster vapor emission gives greater throughput and allows for more complex feature sizes, materials, and geometries to be probed.

		2,5-Lutidine	GB (Sarin)	Methyl Salicylate	HD (Mustard)
	Chemical Structure				
Vapor Emission	**Boiling Point**	144°C	147°C	220°C	216°C
	Vapor Pressure	2.4 Torr	2.5 Torr	0.08 Torr	0.10 Torr
Liquid Spreading	**Surface Tension**	30 dyn/cm	26 dyn/cm	39 dyn/cm	43 dyn/cm
	Throughput	1-8 hours/test		16-100 hours/test	

Figure 12. Physical properties and chemical structures of GB, HD,
and associated simulants at 20 °C.

Selection of an appropriate simulant requires an understanding of the key properties that are relevant to the phenomena being studied.[12,14] In this case, the important factors were the the chemical contaminant retention in the capillary features and the vapor emission rate. Retention is controlled by surface wetting and feature size. Although feature size is a material-dependent property, surface wetting is influenced by the surface tension of the contaminant, as well as the surface energy and surface roughness of the material used. It can be anticipated that 2,5-lutidine and GB will have similar wetting behavior on smooth surfaces due to similarities in surface tension.

The vapor emission rate is controlled by the exposed surface area and the vapor pressure (a contaminant property). 2,5-Lutidine and GB have extremely similar vapor pressures at room temperature (2.4 and 2.5 Torr, respectively) and will have similar vapor emission rates given the exposed surface areas are the same. Therefore, it can be anticipated that 2,5-lutidine will loosely mimic capillary entrainment and vapor emission of GB. Similarly, both GB and 2,5-lutidine are highly water soluble at room temperature and can be dissolved by an aqueous water rinse. Although the data generated may not reflect the influences for every contaminant–material combination, they do provide an initial estimate of the feature sizes, geometries, and materials that provide the largest contribution to the vapor source.

As with any simulant study, it is essential to understand how the simulant data will inform or predict the behavior of chemical agents with different properties. The factors influencing capillary entrainment and vapor can be divided into three categories:

1. factors only influenced by the material;

2. factors influenced by both the material and contaminant; and

3. factors only influenced by the contaminant.

As shown in Figure 13, capillary size is only determined by the material, whereas surface wetting and absorption rate are impacted by both the material and the contaminant. Vapor pressure is a physical property of a contaminant. The relative importance of each of these factors is unknown and may change with the operational context of the study. The simulant data generated using 2,5-lutidine can help highlight the contribution of material-dictated properties such as capillary size. If capillary size is the dominant factor in controlling vapor emission, the simulant data should reflect the trends for other contaminants.
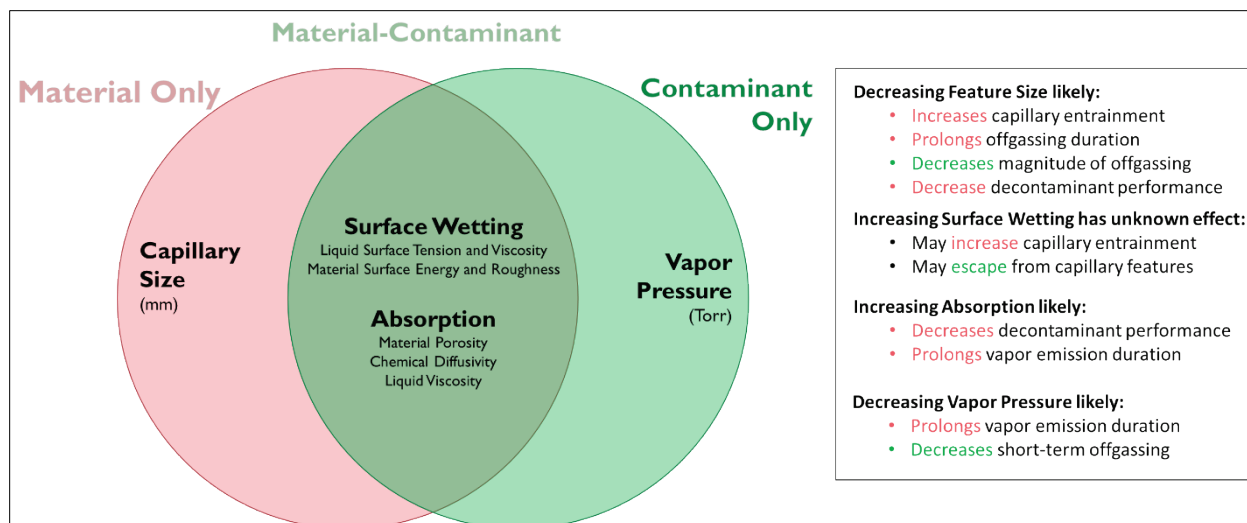
Figure 13. Factors influencing vapor emission and capillary entrainment.

Absorption and surface wetting are controlled by both material and contaminant properties. These properties are hard to mimic with simulant data, and the important properties change depending on the context. Absorption and transport of liquid-phase contaminants in nonporous materials like polymers can occur via multiple diffusion mechanisms (e.g., Fickian diffusion) as a function of chemical interactions between the solid and the absorbing chemical or capillary uptake routes promoted by the material surface and bulk layer morphology. Surface wetting is governed by different dynamics on rough surfaces than it is on smooth surfaces. The ability to translate simulant data to different cases will depend on the operational context, the materials being used, and the agents being studied.

In general, this study has focused on two different chemical–material combinations: (1) stainless steel, a smooth material for which 2,5-lutidine does not wet the surface and does not absorb into the material and (2) PU-based paint, a rough material for which 2,5-lutidine wets the surface and absorbs into the bulk. The data generated using simulants may roughly translate to agents in those use cases.

The influence of capillary features will change based on the materials, agents, age time, and decontaminant procedures, which are all dictated by the operational context. This study helps provide a broad understanding of whether entrainment in capillary features is important to consider in decontaminant development and if so, what factors influence capillary retention the most.

2.5   Laboratory-Scale Complex Features

Evaluation of decontamination efficacy uses representative configurations of materials that can be easily tested in the laboratory. Although flat and vertical surfaces have been extensively studied on the laboratory scale, complex features have only been investigated in select cases. The approach is to consider a selection of common feature types to identify prevailing trends associated with contaminant retention and decontamination burden for complex geometries and materials. For this study, it was necessary to create mimics to represent sizes,

materials, and geometries of complex features found on real-world items, specifically for the case of a military vehicle. A secondary goal was to develop features that should be easy to produce and test at laboratory scale.

Cleanup of a contaminated vehicle, which is essential for military response after a CWA release, may present a significant decontamination challenge. Vehicles contain many small complex features such as door hinges, weather stripping, tire and rim interfaces, screw threads on lug nuts, and utility mounts. An initial survey of several military vehicles was performed to determine which complex features were most common, specifically for exterior exposed surfaces. The aim was to catalog observations that describe complex features on representative vehicles in three areas:

- types of complex feature geometries,

- range of complex feature sizes, and

- classes of common materials.

As shown in Figure 14, four key feature geometries were found on the surfaces of the examined vehicles. Rather than sampling materials from decommissioned vehicles, these features were reproduced in the laboratory. This ensured that materials were compatible with the experimental apparatus and could be reproducibly tested. The variability associated with materials on fielded vehicles as a function of age and usage is not considered in this study. Capillaries, small grooves, or slits were found at door hinges, on weather stripping, in tire grooves, at the vehicle hood and gas covers, and many other places. These capillaries can be created in the laboratory using three stacked washers, where one is a small-diameter shim of variable thickness placed between the other two. Capillary features can entrain contaminant through capillary action, which limits the surface area for evaporation and restricts decontaminant access. Another common capillary type is screw threads, where the threads act as a capillary channel that leads to a larger reservoir. These were seen throughout the vehicle including on lug nuts, tow hooks, and other bolted areas. These features were recreated in the laboratory using bolts or standoffs threaded into flat-head or set screws. Another common feature size were holes and recessions on the vehicle surface. These features were found on mounting brackets and hardware. Contaminant located in a recessed area is protected from certain directional sprays of liquid decontaminant as well as from wind, which may limit decontaminant efficacy and emission rate, respectively. These recessed areas were represented in the laboratory using one-sided standoffs. Lastly, interfaces between two materials were common on vehicle exteriors. Material interfaces were found at door junctions, weather stripping, tire mounts, and throughout the vehicle exterior. At the laboratory scale, these interfaces could be represented by washers of dissimilar materials bolted together.
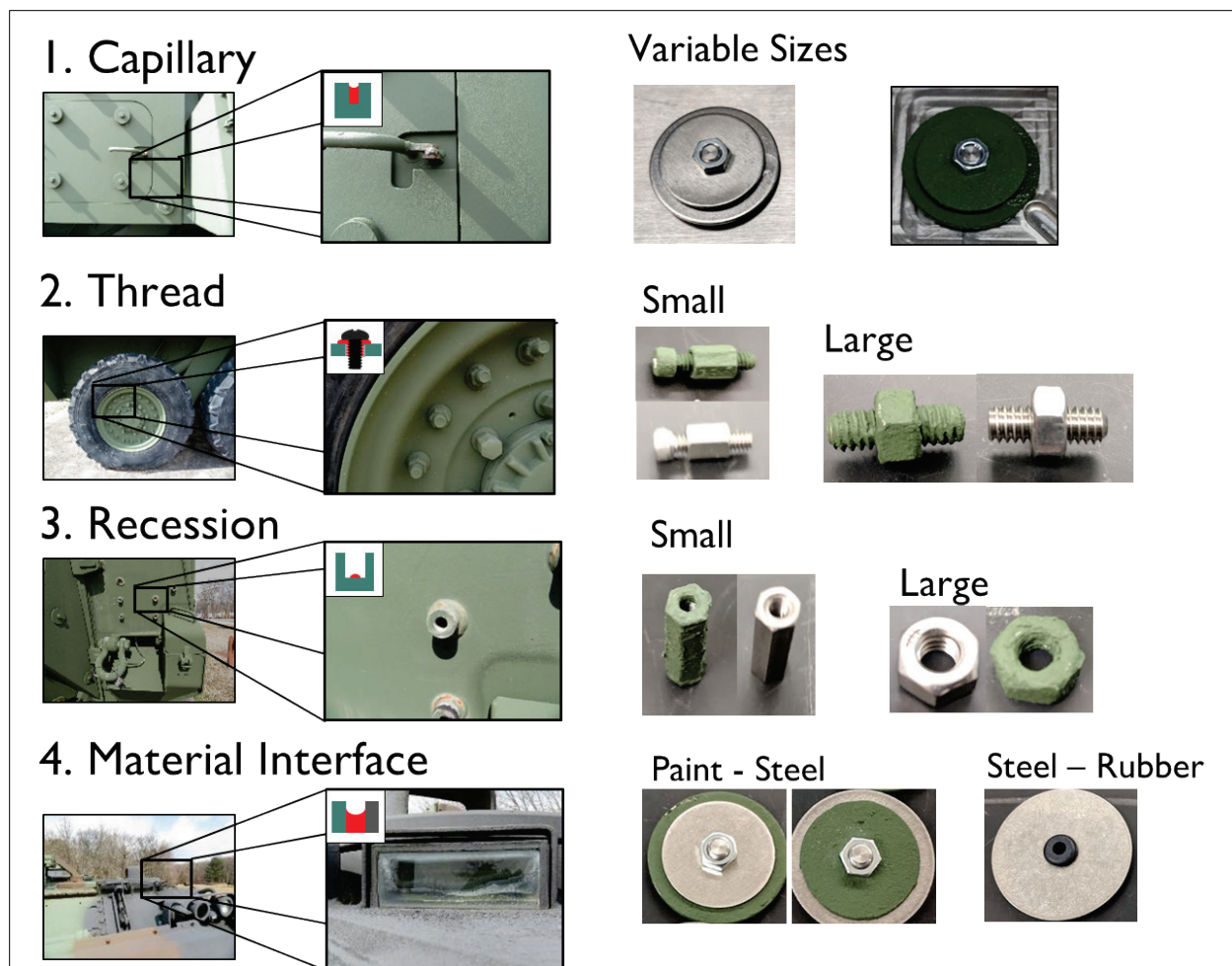
Figure 14. Common complex feature geometries found on vehicles.

In addition to shape, feature size and material composition both play important roles in contaminant retention in capillary features. As discussed in Section 1.2, the size of a capillary plays a dominant role in determining the extent of capillary retention. One of the primary objectives of this work was to determine which feature sizes lead to significant retention of CWAs. To do this, capillary features of a specific type needed to be created of variable sizes or widths. This was done using washers separated by a steel shim, as shown in Figure 15. Using the shimming method, capillary features were generated between 0.025 mm (0.001 in.) and 1.5 mm (0.060 in.).
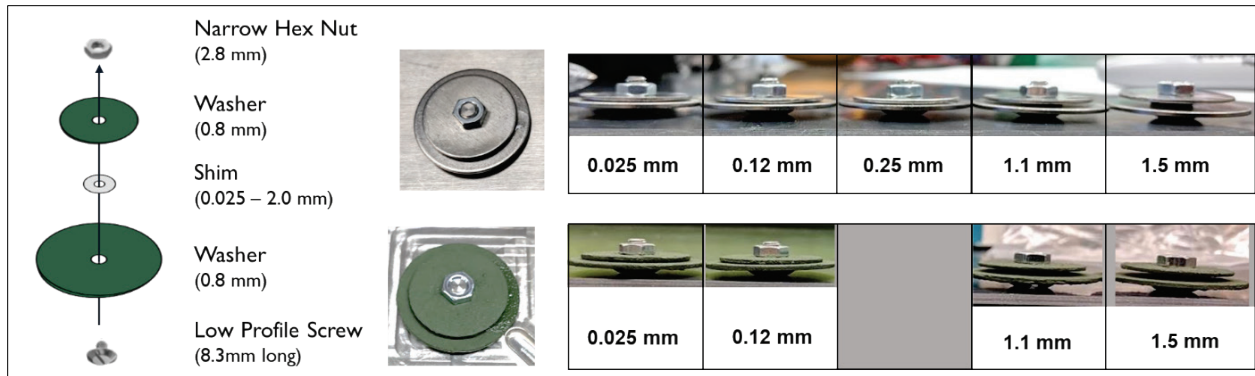
Figure 15. Varied capillary feature sizes created using shimmed washers.

Painted surfaces were created by coating steel features with a low-gloss, PU-based coating applied using a high-volume, low-pressure sprayer. This laboratory preparation for the paint may differ from industrial application using a certified specification and may have unknown impacts on contaminant spreading and absorption. However, this method allowed for rapid turnaround in material preparation and should be sufficient for this sensitivity analysis testing.

3.   INFLUENCE OF COMPLEX FEATURES ON VAPOR EMISSION: NO LIQUID DECONTAMINATION

3.1   Background and Approach

In the absence of any decontamination procedure, vapor emission will occur from contaminated surfaces. The emission of toxic vapors provides a significant inhalation risk to personnel near a contaminated surface. Understanding the extent of that risk is a complex process dictated by environmental conditions (e.g., wind speed and temperature), distance from the asset, contaminant toxicity, and the source terms that describe emission rate. Source terms quantify how vapor emission changes over time for each contaminated material and can be used to compare how the intensity and duration of vapor emission changes as a function of material and contaminant. Characterizing the vapor source terms leads to an understanding of the duration and magnitude of hazards posed to personnel. If the vapor source term is reduced, then the resulting exposure to personnel will be reduced.

It is important to note that the purpose of the vapor test is to measure vapor source terms. The measured chamber concentration does not correspond to the vapor concentration that personnel would be exposed to in operational conditions. As a result, the AP-MS does not need to detect at concentrations as specified in metrics like general population limits (GPLs) or worker population limits (WPLs). The source term can be subsequently used to calculate environmental concentrations; it is the environmental conditions (e.g., enclosed volume, outdoor wind speed, amount of emitting materials, etc.) that determine the lowest concentrations that could occur in the environment that would be compared to the GPL, WPL, or other concentration-based specification. This study focuses exclusively on characterizing the vapor source terms as the environment concentrations resulting in vapor exposure are influenced by factors not associated with the material features or the decontaminant efficacy (i.e., detailed operational context).

This study measures vapor source terms for a variety of complex features and determines how they differ from flat surfaces. One hypothesis is that contaminant entrained within a complex feature may have a severely limited exposed area, which would limit the vapor emission rate. The emission rate may also be hindered by contaminant in recessed areas that are protected from wind, which in turn decreases advection at the boundary and slows evaporation. However, this effect may depend heavily on feature size, geometry, contaminant, and material.

The first goal of this study focused on understanding vapor emission from complex features when no treatment process was applied. A variety of complex features were contaminated, and the vapor emission process was monitored using mass spectrometry. Conditions were selected to address several key questions:

1. How does vapor emission from complex features differ from emission from flat surfaces?
2. Does vapor emission of entrained contaminant vary from wetting to non-wetting materials?
3. Does feature size have a significant impact on entrainment and vapor emission?
4. Does feature geometry have a significant impact on vapor emission?

The results and analysis given in this section provide a basic understanding of how complex feature size, geometry, and material each influences capillary entrainment and vapor source terms. This provides an initial estimate of the key contributing factors driving entrainment and vapor emission. Although the critical dimensions may vary across materials and contaminants, the trends observed in this study provide approximate scales to consider for complex panel efforts.

3.2   Methods and Procedures

For this study, 5 µL drops of 2,5-lutidine were placed on each of the model complex features described in Section 2. The location of the droplet placement (i.e., dosing) depended on the feature geometry (Figure 16). In general, contaminant was applied such that the liquid would be in contact with the capillary feature. For capillaries generated using three washers, contaminant was dosed near the opening to the capillary feature. For screw threads, contaminant was dosed at the interface of the screw thread and the nut or standoff. For recessed areas, contaminant was placed ~10 mm from the entrance of the standoff or nut. Following dosing, the mass of the contaminated object was measured (approximately 4.6 mg of 2,5-lutidine added for a 5 µL drop), and the object was immediately (within 60 s) placed within the vapor microchamber. The lid of the microchamber was closed, and a flowing stream of nitrogen (150 mL/min) was passed over the feature. The concentration of simulant was monitored by AP-MS. A flat horizontal surface was also used as a reference for each of the complex features, whether it was made of stainless steel or PU paint. When no treatment was applied, the mass of the contaminated feature was measured after the vapor emission to determine the overall VEM. This data was used to verify the calibration of the instrument, as described in Appendix C. Identical treatments were used on unpainted stainless steel and features painted with a PU-based coating.
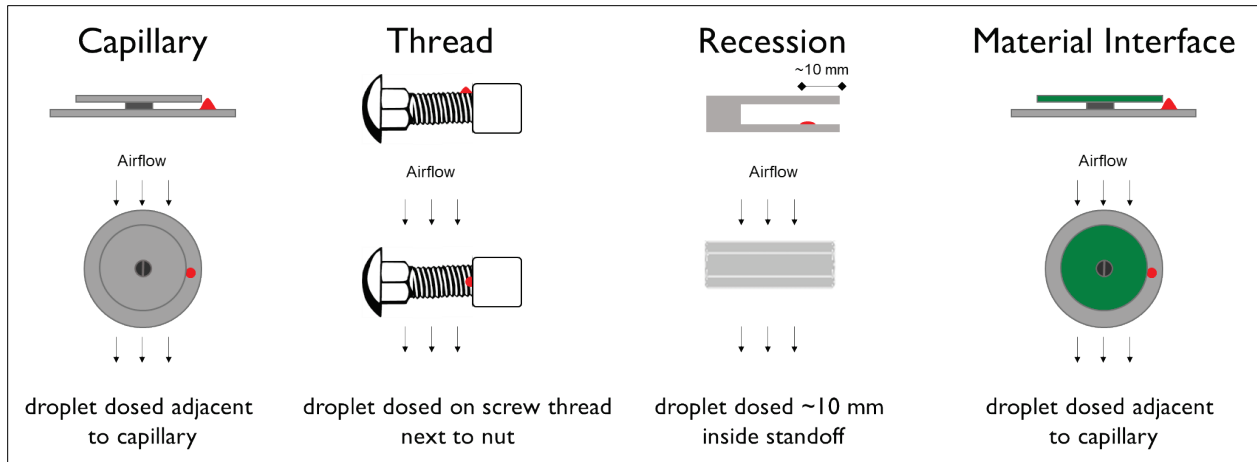
Figure 16. Contaminant dosing locations for complex features.

3.3   Example Data Analysis: Flat Panel Results

To establish a reference data set, vapor emission profiles were measured for droplets placed on a flat panel. When vapor emission from untreated surfaces was analyzed, two metrics were used to describe the source terms:

1. *Peak emission rate* describes the maximum emission rate at any point during the measurement.

2. *Emission duration* describes how long it takes for the available mass that can be emitted to reduce by a certain percentage of the total emitted mass.

The two metrics are used to compare and contrast vapor source terms from the various sample types (i.e., material and feature geometry). For the purpose of screening to identify influential factors, emission duration is based on the percentage of mass emitted. For exposure assessment, it may be more appropriate to define emission duration in terms of a time until a threshold emission rate.

Peak emission rate and overall emission profiles can be determined by analysis of emission rate changes over time, as shown in Figure 17. These emission rate profiles show that source terms vary strongly based on the material. On a bare stainless steel surface, the droplet remains sessile. As the surface area of the droplet remains constant, the emission rate remains constant at 0.1 mg/min for the first 35 min before decreasing rapidly. This contrasts with droplets placed on the coated surface, which exhibited a rapid spike in the first 10 min followed by a rapid decline. This correlates with a droplet that initially spreads across the surface, increasing surface area and thus increasing emission rate. The emission rate declines as the contaminant evaporates, shrinking the exposed surface area. This demonstrates that liquid spreading has a pronounced impact on vapor emission rate. The peak vapor emission rate is much larger on the coated surface (0.7 mg/min) compared with bare metal (0.1 mg/min) because of the differences in liquid spreading.

22
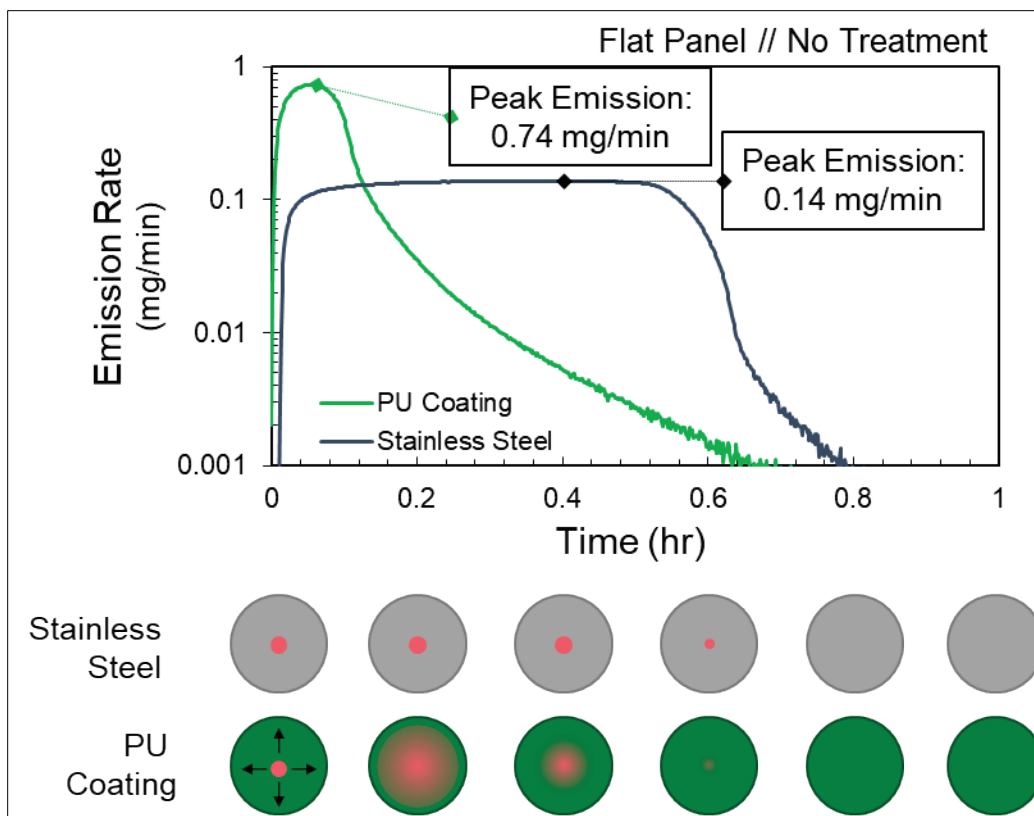
Figure 17. Emission rate vs time for untreated bare stainless steel (gray) and coated surfaces (green). Note that emission rate is on a log scale and spans three decades of magnitude.

These data correspond with cases where the majority of the contaminant was emitted as a vapor. Integrating the emission rate over time provides the VEM, which was 4.5 mg for both steel and the PU coating. Even though the emission profiles are different in magnitude and time, the total VEM was similar. The data may also be analyzed to determine what fraction of vapor was emitted at a given time (Figure 18). This method of data presentation provides the vapor emission duration and determines the length of time required for a given percentage of emitted mass to evaporate. After just over 8 min, 90% of the total emitted mass had evaporated from a coated panel. However, for a stainless steel panel, it took nearly four times longer to reach 90% (32 min). This demonstrates that source terms describing vapor emission from these two materials varied in time and magnitude.
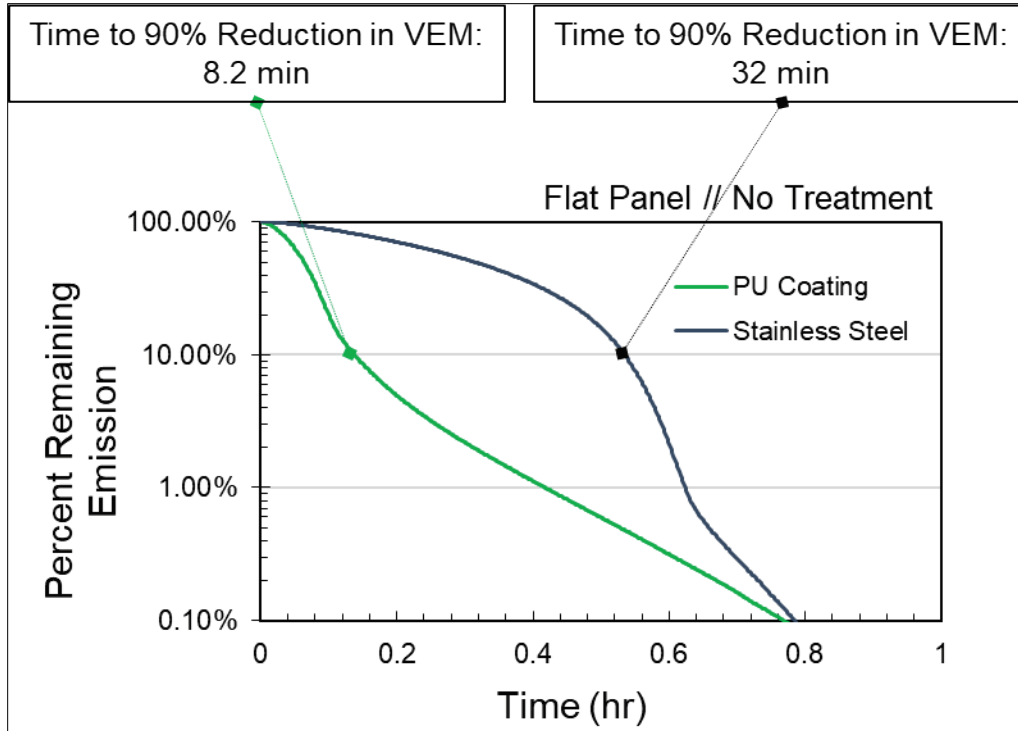
Figure 18. Percent remaining emission vs time for untreated bare stainless steel (gray) and coated surfaces (green).

In general, it was found that source terms measured on stainless steel gave a lower-magnitude peak but longer duration. In contrast, droplets evaporating from the PU-based coating gave a larger peak emission rate, but the emission duration was significantly shorter. This stark difference in vapor source terms can be attributed to the liquid spreading behavior. On non-wetting materials, contaminant surface area remained largely constant, leading to a constant emission rate. On wetting materials, the emission rate changed as the surface area changed, first increasing as the liquid spread on the surface and then decaying as the liquid evaporated.

3.4   Influence of Capillary Feature Size

After a reference was established by measuring the vapor source terms from flat coated and uncoated steel panels, the influence of capillary features was explored. In this study, vapor source terms were measured using capillary features of variable sizes. This data set addressed two key questions:

1. Does capillary entrainment lead to significant changes in vapor source terms?

2. Does capillary feature size significantly influence entrainment?

Capillary features ranging from 0.025 to 1.5 mm were constructed using stainless steel shims placed between two washers (see Section 1.2 for definitions of capillary critical dimensions). Contaminant was placed next to the capillary, and vapor emission was monitored by AP-MS. The vapor emission rates from stainless steel capillary features are provided in

Figure 19. Two distinct source term profiles were observed. Large capillary features (greater than 1.0 mm) gave a vapor emission profile similar to that for flat panels. On these features, vapor emission was constant for approximately 30 min before it significantly subsided. Contaminant entrained within smaller capillaries (0.25 mm or smaller) led to a significantly altered emission profile, which suggests that capillary entrainment may have occurred. In these cases, vapor emission had a significantly lower peak emission rate with a significantly extended emission duration. Across the sample geometries, the VEM was found to be 4.34 ± 0.25 mg, indicating that similar quantities of contaminant were emitting as compared to the flat panel.
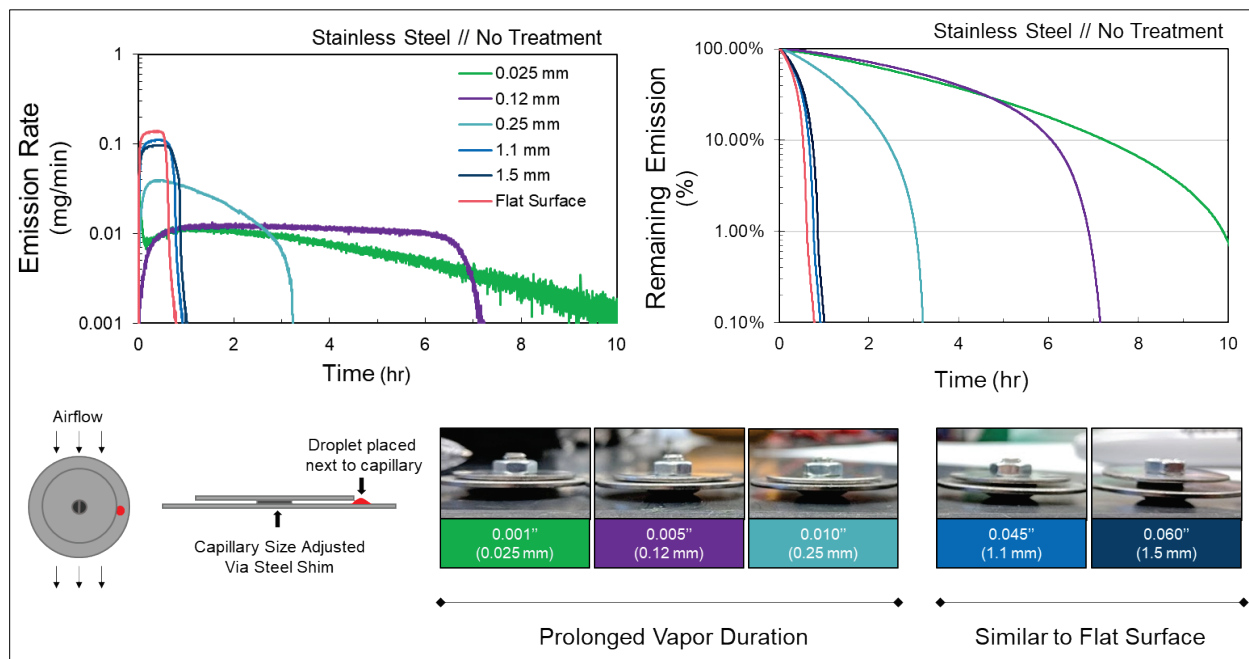
Figure 19. Influence of capillary feature size on vapor source terms on stainless steel.

Peak vapor emission and vapor duration (defined as time until 90% reduction of total VEM) for each stainless steel capillary size are given in Figure 20. For the smallest capillary feature (0.025 mm), the peak vapor emission decreased by 10-fold compared to flat panel. However, the vapor duration was extended from a 0.5 h to over 7 h, a 13-fold increase. This suggests that capillary entrainment led to a significantly longer vapor emission at a lower emission rate as compared with droplets on a flat surface. The change in emission rate may be correlated with a change in exposed surface area. As a droplet enters a capillary feature, the surface area of the boundary may shrink, which decreases the overall emission rate. The size of the capillary feature influences the exposed surface area as well as the capillary pressure drawing the liquid into the capillary feature. For stainless steel, the data suggest that 5 μL liquid droplets of 2,5-lutidine were drawn into capillary features smaller than 0.25 mm. However, the critical feature size may vary for different contaminants, materials, and droplet sizes due to the liquid surface tension of the contaminant as well as the surface energy and roughness of the material.
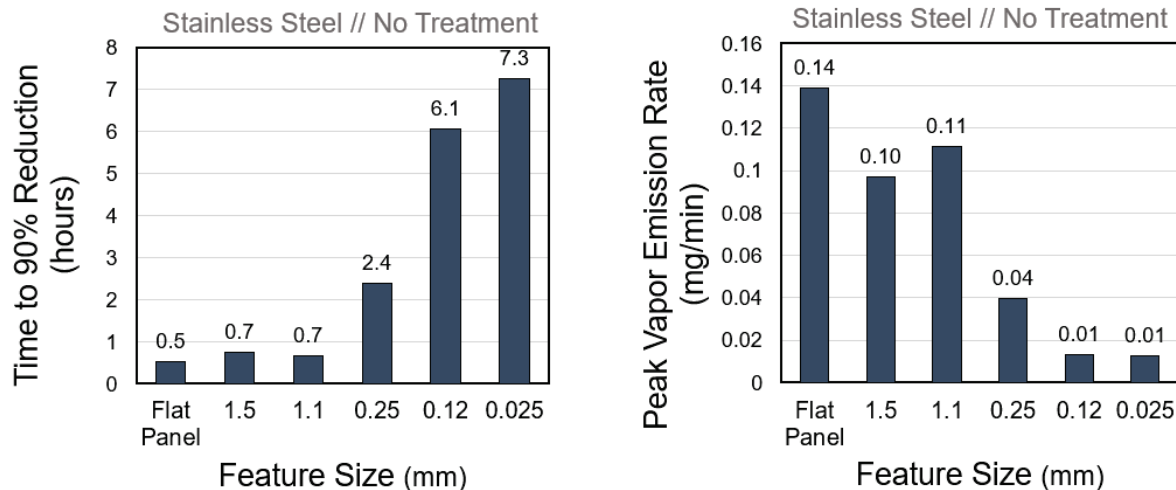
Figure 20. Vapor duration and peak emission rate for stainless steel capillaries.

For droplets placed on a PU-based coating, similar changes in emission rate were observed when contaminant was placed in a capillary feature. As shown in Figure 21, in all cases, vapor emission profiles of capillary entrained contaminants were different from profiles for flat panels. As feature size decreased, vapor duration increased. For the smallest feature size tested, 90% of the vapor was emitted after 90 min, which represents a 10-fold increase in emission duration as compared to a flat surface. Similar to the results for the stainless steel surface, the VEM for all features with the PU coating was 4.50 ± 0.13 mg. This indicates that all of the applied contaminant had eventually emitted as a vapor.
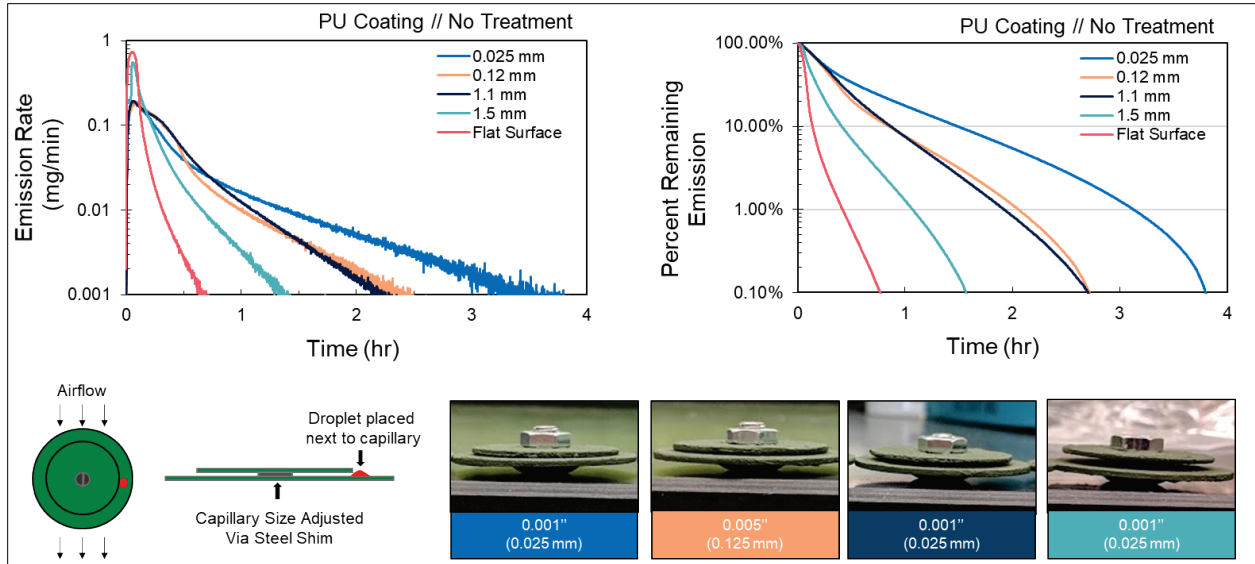
Figure 21. Influence of capillary feature size on vapor source terms for PU-based coating.

Although vapor duration increased as feature size decreased for both stainless steel and PU-coated surfaces, the relationship between vapor emission and capillary size was different across these materials. On the stainless steel features, entrainment influenced vapor emission only beyond a critical dimension. When features were larger than the critical dimension, the vapor emission rate closely matched the behavior of a flat panel. For PU-coated materials, the emission profile differed from that of a flat panel in every case, even for large capillaries, as shown in Figure 22.
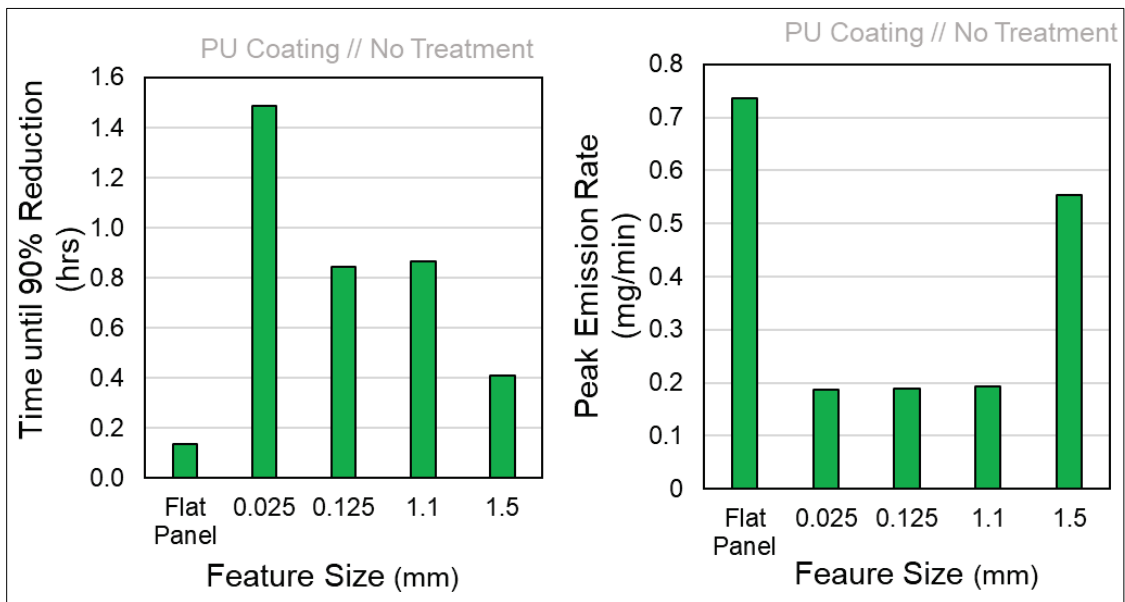
Figure 22. Vapor duration and peak emission rate for capillaries created from coated surfaces.

The difference in emission rate profiles may be attributed to liquid spreading behavior. Droplets largely remained sessile on stainless steel surfaces, whereas they readily spread on painted surfaces. Droplets on stainless steel exhibited little fluid transport if no capillary action occurred. Capillary action occurred if the feature size was smaller than the critical dimension and was the only contributor to liquid motion. However, on the PU-coated material, liquid spread across the surface throughout the duration of vapor emission. Liquid spreading provided the mechanism for liquid transfer both into and out of the complex feature. This led to a significant difference in vapor emission, as shown in Figure 23. The influence of liquid spreading on vapor emission is covered more extensively in Section 3.6.
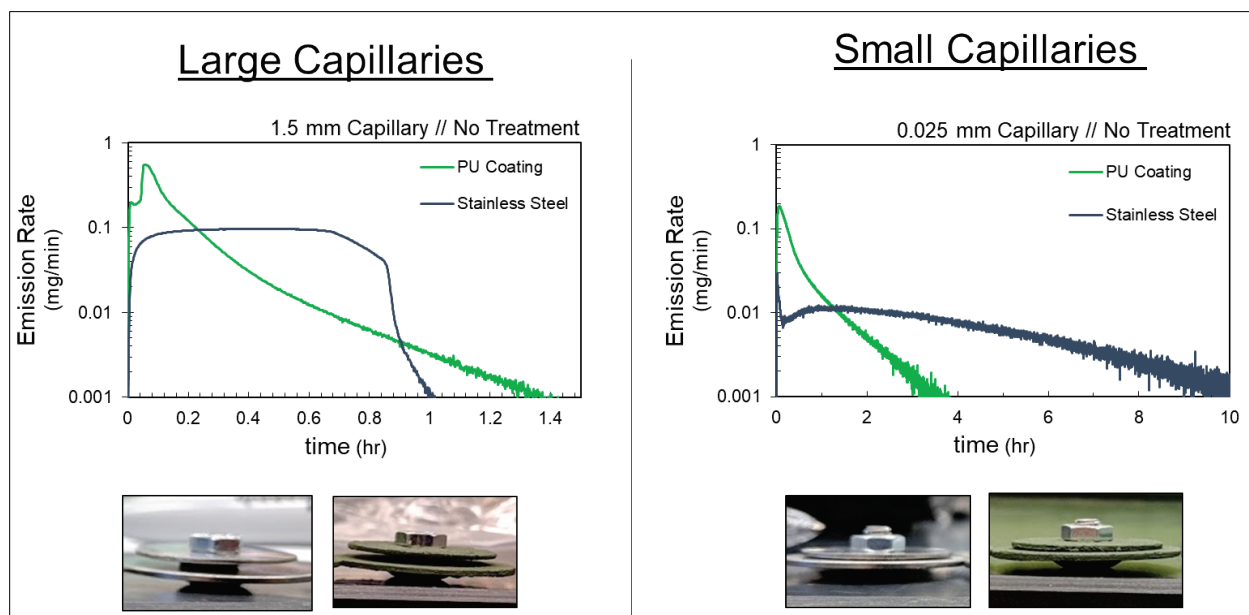
Figure 23. Comparison of vapor emission profiles on different materials for large (left) and small (right) capillaries. Note the significant difference in time to reach minimum emission rates between large and small capillaries.

3.5   Influence of Feature Geometry

The role of feature geometry was studied by investigating four types of laboratory-scale complex features: capillaries, recessions (i.e., holes), threads, and interfaces. Capillaries represent grooves or gaps in a material and were studied as described in Section 3.4. Recessions represent a hole or cavity, where trapped contaminant may be protected from airflow (wind). Threaded features represent a screw turned into a thread (i.e., nut or threaded standoff), where contaminant can spread through the threads and become entrained in the nut. Material interfaces are areas where two materials are directly adjacent to each other and thereby form a capillary. The geometries studied along with the critical dimension and dosing location for each feature are provided in Figure 24.
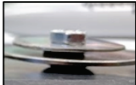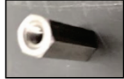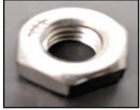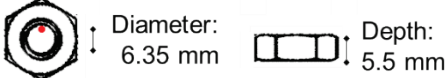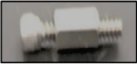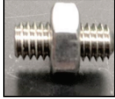
Figure 24. Critical dimensions for capillaries, recessions, and threads. Objects not drawn to scale.

Vapor emission rate was measured from contaminated features of each geometry. The results for stainless steel features are provided in Figure 25. For all cases, the VEM was 4.37 ± 0.19 mg, which indicates that the majority of all contaminant was emitted over the experiment duration. Contaminants placed at the interface of a thread and a bolt exhibited a two-regime behavior. For large threads (¼ in.–20 bolt in a nut), a large initial spike in vapor emission was observed as the contaminant spread throughout the thread and emitted rapidly. A second regime was observed following the initial spike that likely reflected the slower emission of contaminant entrained within the nut. A similar, more pronounced trend was seen with the smaller threaded feature (a no. 4 screw in a standoff). Contaminant in a shallow recession with a large-diameter opening had emission similar to that for a flat panel, whereas contaminant placed in a deep recession with a narrow opening exhibited a significantly modified vapor profile. It is important to note that the emission rate of a contaminant contained within a recession is controlled by different factors than are capillary entrained features. However, in general, each of the small features provided a significant extension in vapor duration, whereas larger features exhibited vapor durations that were similar to those of flat surfaces. The results suggest that the feature dimensions, rather than specific geometry, had an outsized impact on influencing entrainment and vapor source terms.
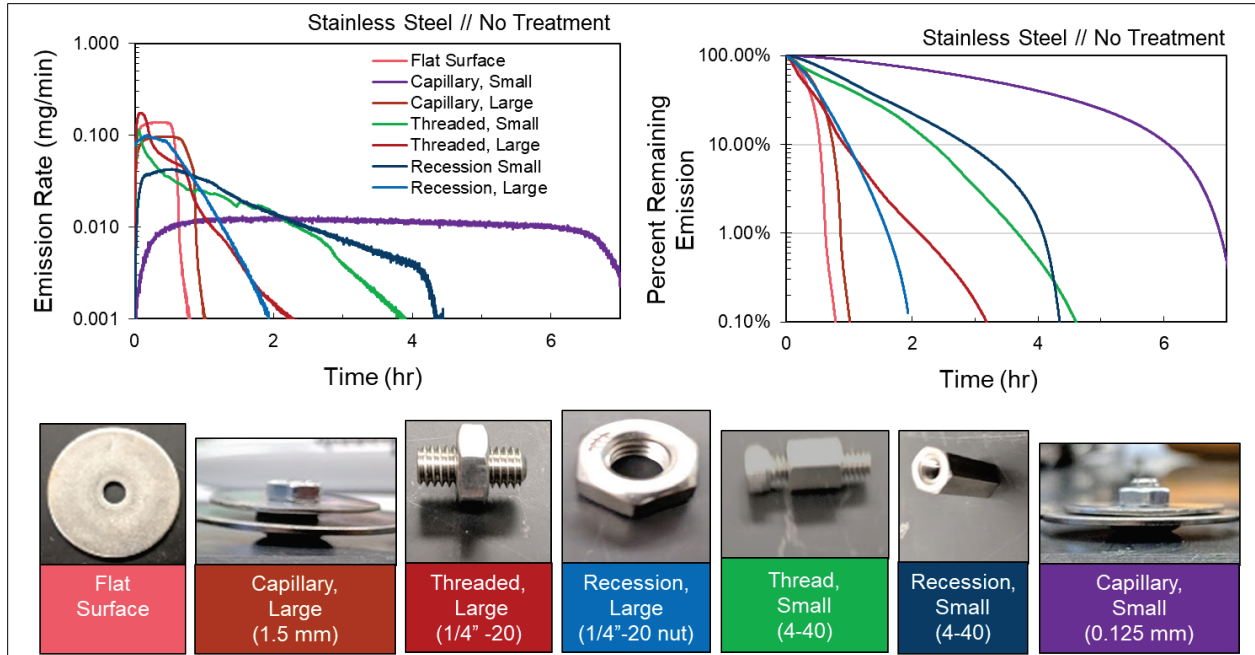
Figure 25. Vapor emission from stainless steel complex features in varying sizes and geometries.

A similar trend was observed for painted complex features. As shown in Figure 26, all contaminated complex features had extended vapor duration as compared with flat panels. For all cases, the VEM was 4.49 ± 0.10 mg, which indicates that the majority of all contaminant was emitted over the experiment duration. Vapor emission was generally more rapid on the coated materials than on the uncoated materials. This was likely due to the liquid spreading behavior increasing the exposed surface area for evaporation. Large features exhibited a small but measureable extension in vapor emission. Small features, particularly capillaries and recessed areas, seemed to have a large impact on the vapor source term.
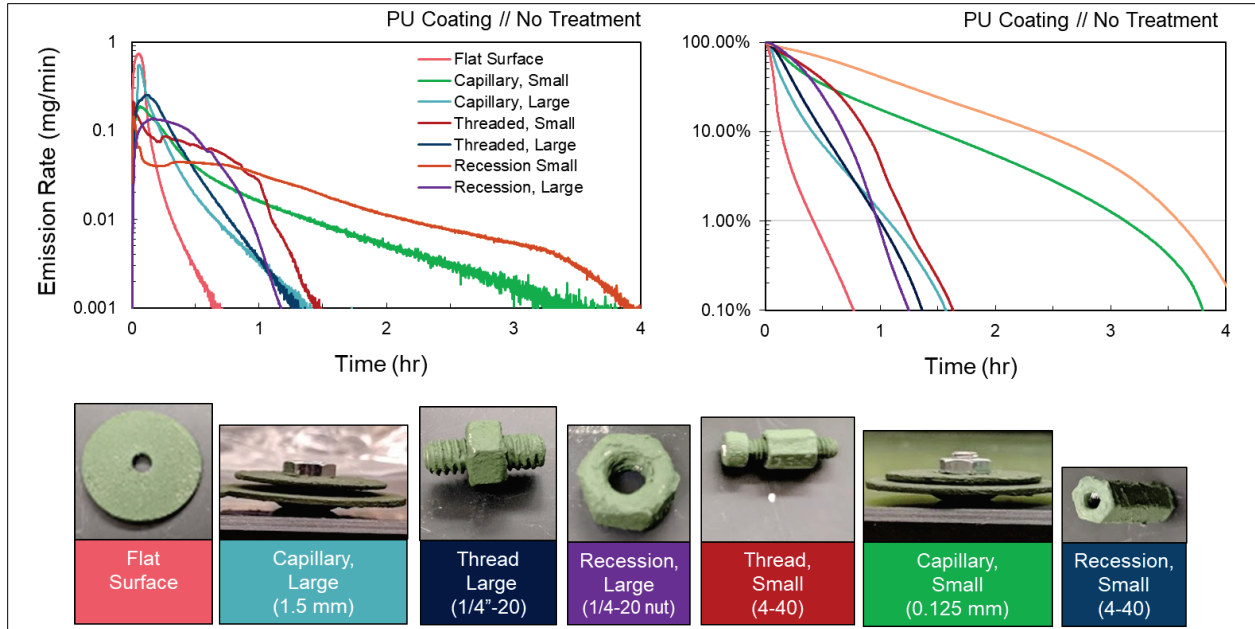
Figure 26. Vapor emission from coated complex features in varying sizes and geometries.

A comparison of the vapor duration for all measured geometries on both materials is provided in Figure 27. This analysis clearly shows that feature size has the largest impact on vapor emission. All of the small features exhibited significant extension in vapor duration, whereas the larger features had little to no influence on vapor duration. Geometry may play a secondary, minor role in dictating fluid movement before entrainment, but feature size largely controls the behavior once contaminant has been entrained. Studies were not performed with alternate dosing locations, but it is plausible that contaminants dosed at one end of a screw thread may travel down the thread and into the nut via capillary action. Thus, *geometry may influence how contaminant reaches an entrained area, and feature size influences how emission occurs once contaminant is entrained.*
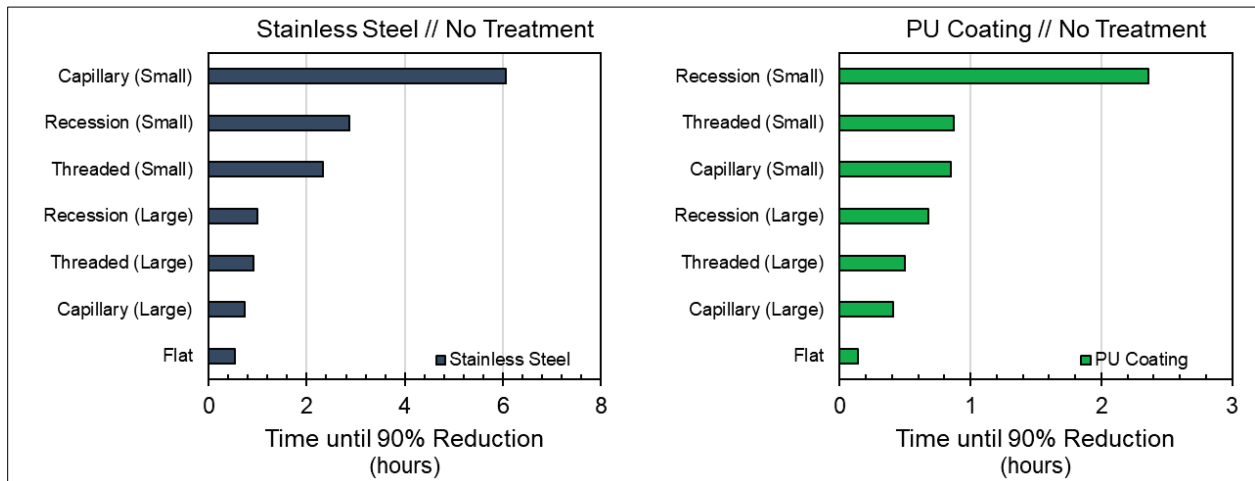
Figure 27. Comparison of vapor duration on untreated stainless steel (left) and coated materials (right).

Material interfaces were the fourth major category of complex features found on vehicles. This may include a capillary interface between a wetting surface and a non-wetting surface, such as a painted surface in close proximity to a bare metal surface. A brief investigation was performed to determine what controlled vapor emission at an interface between dissimilar materials. Washers made of two materials, stainless steel and a PU-based coating, were separated by a metal shim to create a 0.125 mm capillary. This represents an interface between a wetting surface (such as a paint coating) and a non-wetting surface (such as a bare metal) with either the wetting surface or the non-wetting surface on the bottom, where the droplet was deposited. The contaminant was dosed at the interface, and the vapor emission profile was measured using AP-MS. The results were compared to identical test conditions using stainless steel capillaries and PU-coated capillaries, as shown in Figure 28.
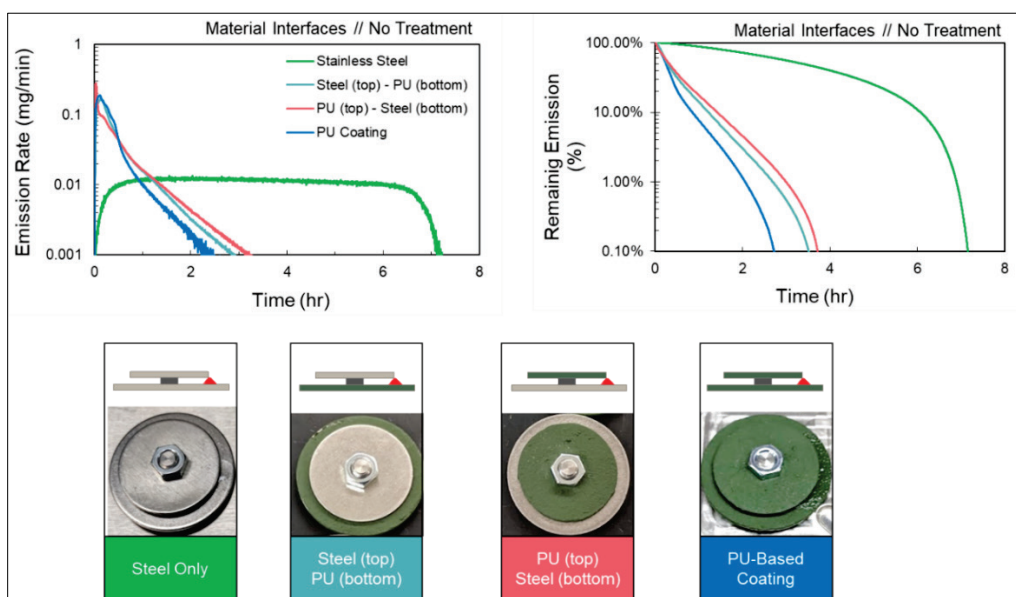
Figure 28. Influence of material interfaces on untreated vapor emission.

The results showed that vapor emission was dictated by the presence of a wetting material at the interface, regardless of orientation. The resulting vapor emission profile was quite similar to the vapor emission from a capillary created using the PU-based coating alone. This suggests that the wetting behavior dictated the fluid movement and thus, the vapor emission. The influence of multi-material interfaces was only tested using a small (0.125 mm) capillary; it may change with different capillary sizes, different droplet sizes, and absorption rates into materials.

3.6   Influence of Liquid Spreading

These results show clear differences in vapor emission across the two materials studied. The primary difference between these two materials is the wetting behavior of the contaminant. On the coated materials, liquids can readily spread across the surface after contamination. Wetting behavior can be attributed to surface morphology of the coating, wherein two-dimensional (2D) micron-scale capillaries can facilitate liquid spreading. The mechanism and supporting data are provided in Appendix A. In the case of stainless steel, the contaminant

droplet remains sessile, and no liquid spreading occurs on this visually smooth surface. The difference in entrainment and vapor emission between the materials is likely a result of the different liquid spreading behavior.

As shown in Figure 29, liquid spreading may influence the characteristics of how entrained agent is emitted as a vapor. For this discussion, capillary entrainment is focused on the large-scale feature being tested. In the case of steel, the emission rate is constant throughout most of the emission duration. This could be the result of the capillary interface limiting the surface area where liquid is evaporating. As surface area is a large driving force in emission rate, a constant surface area results in a constant emission rate. However, in the case of the PU coating, the emission peaked for a short time and decayed over the 600 min duration. In the first regime, bulk contaminant not contained within the large-scale feature spread and evaporated rapidly, which was similar to the vapor profile observed on a flat surface. Once the surface liquid had evaporated, the liquid entrained in the capillary slowly spread out of the feature. This led to the second regime of a slower vapor decay as the contaminant "drained" out of the texture in the surface of the capillary feature. These data may suggest that contaminant escapes entrainment on wetting materials but remains entrained on non-wetting features.
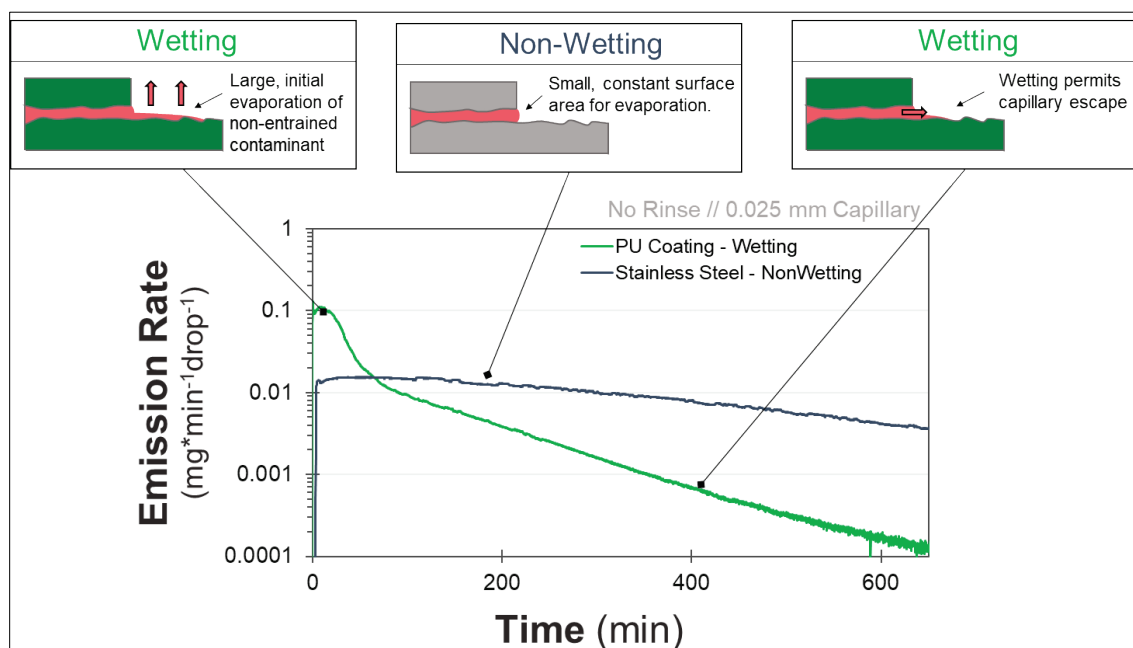
Figure 29. Comparison of vapor emission profiles for untreated 0.025 mm capillaries on wetting (PU coating) and non-wetting (stainless steel) surfaces.

This example shows that, on rough surfaces, liquid spreading provides a means for transport in and out of capillary features. This has competing impacts on vapor emission and entrainment. On one hand, contaminant that is entrained in a macroscopic capillary feature may gradually escape entrainment through liquid spreading. This accelerates vapor emission and presents a short-term hazard as compared to contaminant that does not readily spread. On the other hand, liquid spreading on wetting materials may also lead to capillary entrainment by

allowing liquid to travel across a flat surface to a complex feature. Thus liquid spreading both shortens the vapor hazard for contaminant entrained in a capillary but also increases the likelihood a droplet may interact with and become entrained in a capillary feature.

This work only included one material with wetting characteristics, and the material also presented significant surface roughness. On rough surfaces, capillary action drives the transport of contaminant into the macroscopic complex feature, and the spreading of the contaminant occurs through the microcapillaries in the texture or morphology of the surface. Capillary pressure increases as features become smaller; thus, capillary action through the smaller microcapillaries will be dominant. The higher capillary pressure may explain how entrained contaminant can spread out from a macroscopic complex feature through microcapillaries contained in the rough surface. However, liquid spreading on smooth materials occurs by a different mechanism and may not exhibit the same behavior observed for spreading on rough materials. Further study will be needed to understand the liquid transport that occurs when contaminant is entrained in a complex feature composed of a wetting, smooth surface.

4.   INFLUENCE OF COMPLEX FEATURES ON VAPOR EMISSION: WATER RINSE

4.1   Background and Approach

Contaminant entrained within a complex feature may provide a significant decontamination challenge. Section 3 described how contaminant was entrained in most of the feature sizes and geometries tested, which led to prolonged vapor emission. Some contaminant–material interactions, such as liquid spreading, can facilitate capillary entrainment and further compound the problem. Liquid decontaminants must either displace the contaminant from the capillary feature or solubilize the contaminant into a reactive solution to facilitate decontamination. Similar chemical–material interactions influence how the decontaminant can spread and displace entrained contaminants. Decontaminants effective at removing contamination from capillary features must be designed to access the same entrained areas as the contaminant. This requires tuning of decontaminant–material interactions, reactivity, and contaminant solubility.

A water-rinse process is used to demonstrate how capillary entrainment may affect post-treatment vapor emission. Water-rinse treatments are common in many decontamination procedures and are often the first step of hazard mitigation to perform physical removal of any adsorbed contaminant. Moreover, a water-rinse procedure in the laboratory mimics the spray application of many fielded water-based decontaminants such as Dahlgren Decon solution (First Line Technology; Chantilly, VA), Joint General Purpose Decontaminant, or bleach. The reactive components of these decontaminants are only effective if the decontamination solution can reach the contaminated area and solubilize the contaminant. Thus, the effectiveness of a rinse procedure is a reasonable predictor for how well a water-based decontaminant can access a contaminated surface.

To quantify this effect, the AP-MS methodology was used to measure the effectiveness of a rinse process at reducing the vapor emission rate for a contaminated complex feature. In this study, a complex feature was contaminated with 5 µL of 2,5-lutidine and rinsed

15 s after contamination (three 5 mL rinses). Contaminant dosing timing and procedures are provided in Section 4.2. This represents a "best case" decontamination scenario, where the contaminant can be removed before any significant absorption occurs for materials susceptible to chemical permeation. The rinsed feature was then placed in the vapor microchamber, and the emission was monitored using AP-MS.

In Figure 30, the vapor emission of the rinsed panel (red) is compared with vapor emission from the unrinsed panel (blue). The integrated area of this plot correlates with the total VEM, which is a measure of the total vapor emission. The higher the VEM, the larger the vapor hazard posed to unprotected personnel in a contaminated area. By comparing the VEM with and without the rinse procedure, the efficacy of the rinse process can be determined. In the example shown in Figure 30, the rinse procedure reduced the VEM from 5.0 to 0.08 mg, yielding an overall 22-fold reduction in total VEM. One method of measuring the efficacy is log reduction (LR), calculated as

$$LR = \log(VEM_{no\ rinse}) - \log(VEM_{rinse}) \tag{4}$$

This number represents the overall reduction in vapor emission due to the rinse process. This value can be presented on a log scale, with a 1 LR correlating to a 90% reduction in total vapor emission, and a 2 LR correlating with 99% reduction. The data generated using this method were analyzed based on the ability to reduce overall VEM. These results can be compared to vapor emission from a flat panel to determine the effect that the complex feature has on the rinse process. As with the previous study on weathering, a wetting (PU-based coating) and a non-wetting (stainless steel) material were studied.
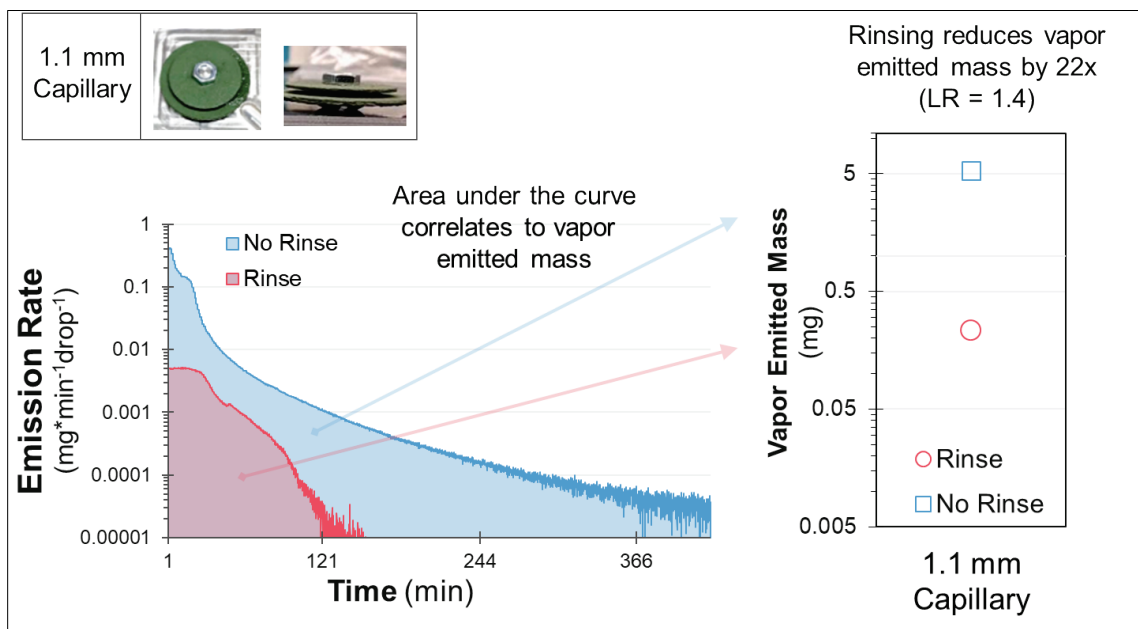
Figure 30. LR in VEM through a rinse process.

4.2   Post-Rinse Vapor Emission: Stainless Steel

Using stainless steel substrates as a non-wetting material for 2,5-lutidine, the influence of feature size on the efficacy of a rinse process was investigated. The vapor emission profiles of contaminant entrained in four different capillary feature sizes were measured. As shown in Figure 31, flat features exhibited no measurable vapor emission, as all of the contaminant was rinsed from the surface. However, for capillaries smaller than 0.010 in. (0.25 mm), significant vapor emission was observed after the rinse process. The feature size significantly impacted the duration of vapor emission after rinsing, and the smallest feature (0.025 mm) showed measurable vapor emission for longer than 500 min. It is worth noting that the dynamic range of emission rates spans 4 orders of magnitude. This creates experimental challenges for characterizing this large range while also providing a context for how these features can influence the evaluation of decontaminant performance on more realistic assets.
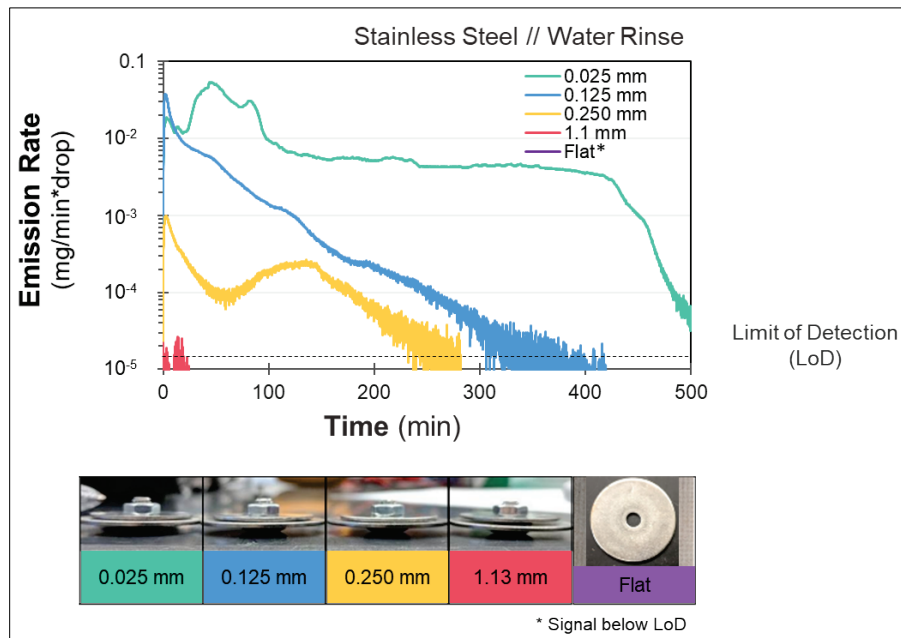
Figure 31. Influence of capillary size on post-rinse vapor emission from complex features.

The total VEM was calculated to determine the total amount of emission after the rinse procedure for the different capillary sizes. As shown in Figure 32, this value was compared to the VEM measured for the no-rinse condition. This figure shows that rinsing stainless steel was highly effective and reduced the vapor emission to below measureable levels. However, the effectiveness (LR) decreased with decreasing feature size, likely because the smaller features restrict the flow of the rinse treatment. For the smallest capillary feature (0.025 mm), rinsing was almost totally ineffective and led to only slight reductions in total vapor emission. *These data demonstrate that rinsing a flat stainless steel panel is a highly effective decontamination procedure, but decontaminating a small capillary feature composed of the same material is a significant challenge. Furthermore, assessing decontamination technology effectiveness using flat panels only may not fully describe the effectiveness of a given hazard mitigation approach on real-world assets.*
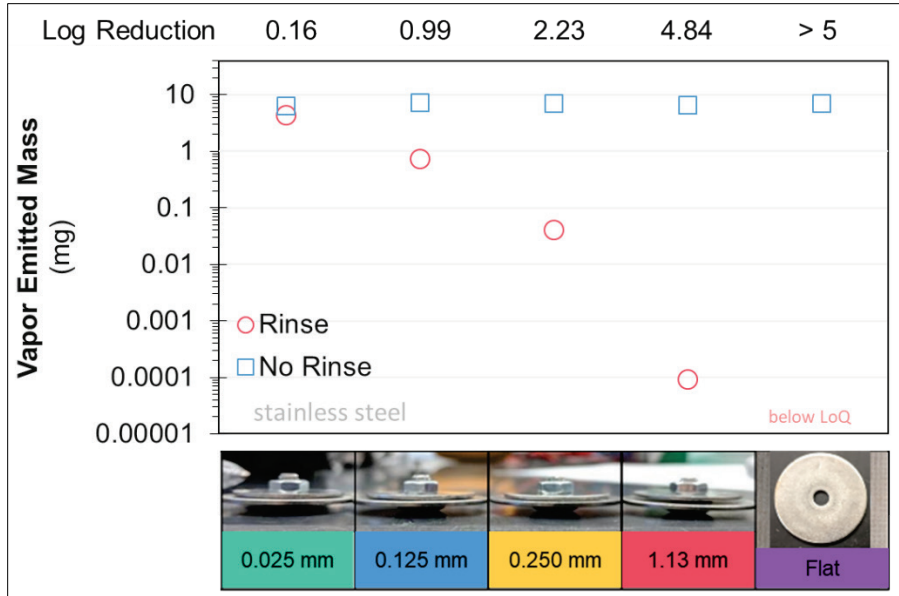
Figure 32. Influence of capillary size on post-rinse VEM for stainless steel complex features.

The influence of feature geometry on the efficacy of the rinse procedure was also measured. As shown in Figure 33, post-rinse vapor emission was significant for all geometries tested and was most pronounced in the small thread and recession. Even the large thread resisted decontamination by a rinse procedure.
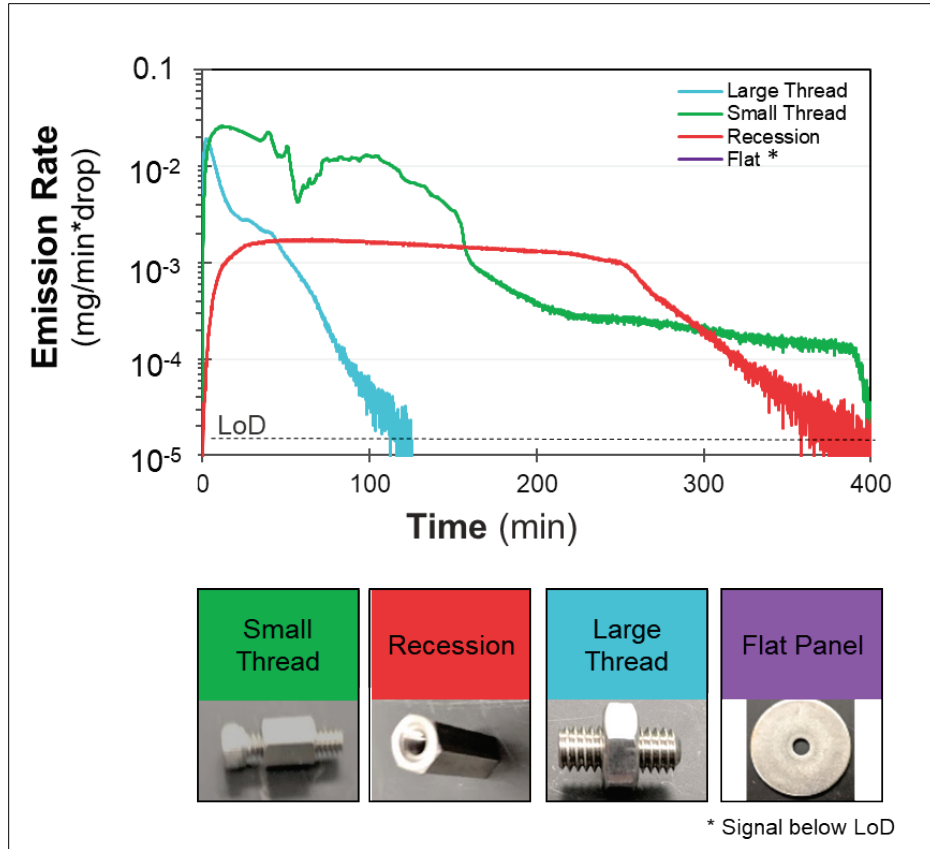
Figure 33. Influence of feature geometry on post-rinse vapor emission rate from stainless steel complex features.

As shown in Figure 34, after rinsing, a large amount of contaminant was emitted from entrainments and small recessions. Regardless of the feature geometry, decontamination of complex features is likely significantly more difficult than decontamination of a flat stainless steel surface. The strong correlation between capillary entrainment and feature size suggests that it is not the specific geometry, but rather the critical dimensions of the feature that most influence decontamination. Geometry may influence the likelihood of a feature becoming contaminated, but this has not been investigated experimentally. Geometries that contain a large surface area of capillary features are likely to be contaminated. For non-wetting materials, contamination must fall directly on or adjacent to a capillary feature to become entrained.
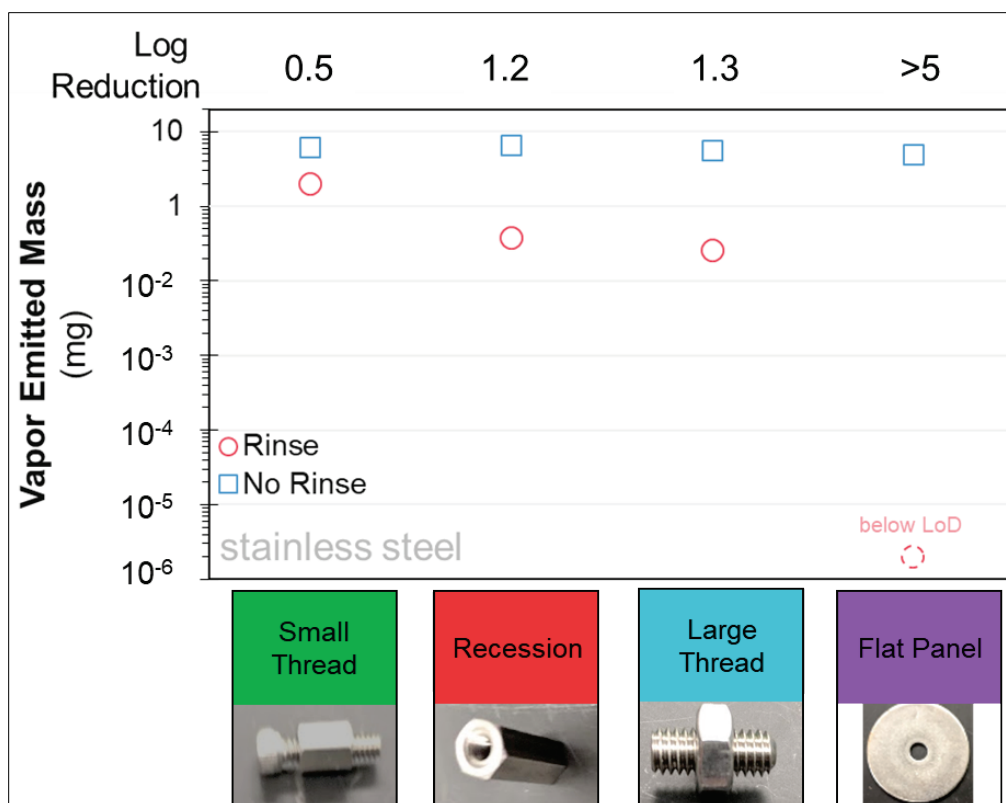
Figure 34. Influence of feature geometry on post-rinse VEM
for stainless steel complex features.

4.3   Post-Rinse Vapor Emission: PU-Based Coating

The influence of capillary size on the post-rinse vapor emission of 2,5-lutidine from a PU coating material was investigated. In contrast with stainless steel, contaminant surface wetting is significant with this material. Capillaries of varying sizes were contaminated with 2,5-lutidine and rinsed after 15 s. As shown in Figure 35, the vapor emission profiles varied greatly depending on the feature size. The emission rate from flat panels rapidly decreased upon measurement, which ceased after approximately 20 min. For the smallest capillary (0.025 mm), vapor emission steadily decayed over the course of 800 min (>13 h).
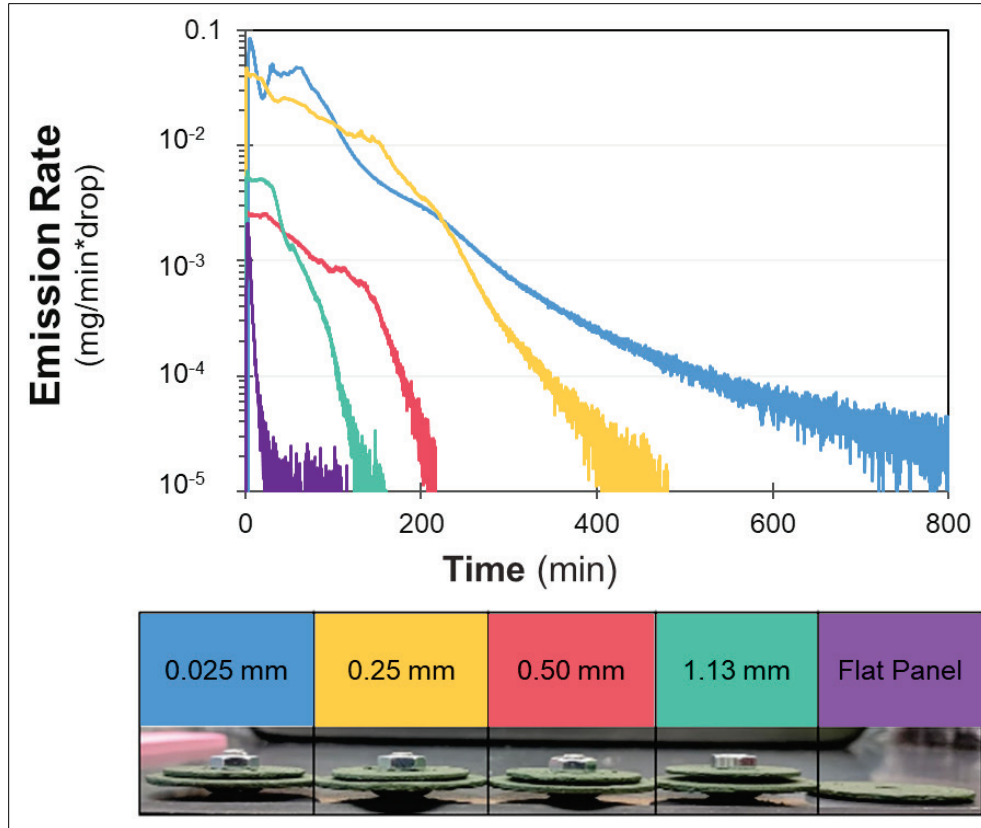
Figure 35. Influence of capillary feature size on vapor emission profile for PU-based coatings.

Comparing the total VEMs between the rinse and no-rinse conditions demonstrated that capillary features greatly hindered the ability to physically remove contamination. Only 0.007 mg of 2,5-lutidine was emitted after a rinse procedure for flat panels, which demonstrated that more than 99% of the vapor emission was mitigated. However, contaminant entrained within capillary features smaller than 0.25 mm was not influenced by the rinse procedure, and nearly all of the initial contaminant was released via vapor emission (Figure 36). This demonstrated that physical removal of contamination using a rinse procedure was significantly more difficult on complex features than on flat surfaces. *The ability to access or remove contaminant from a material is highly influenced by the contaminant distribution and whether it is entrained in a capillary, absorbed into the material, or residing on the material surface as a liquid.*
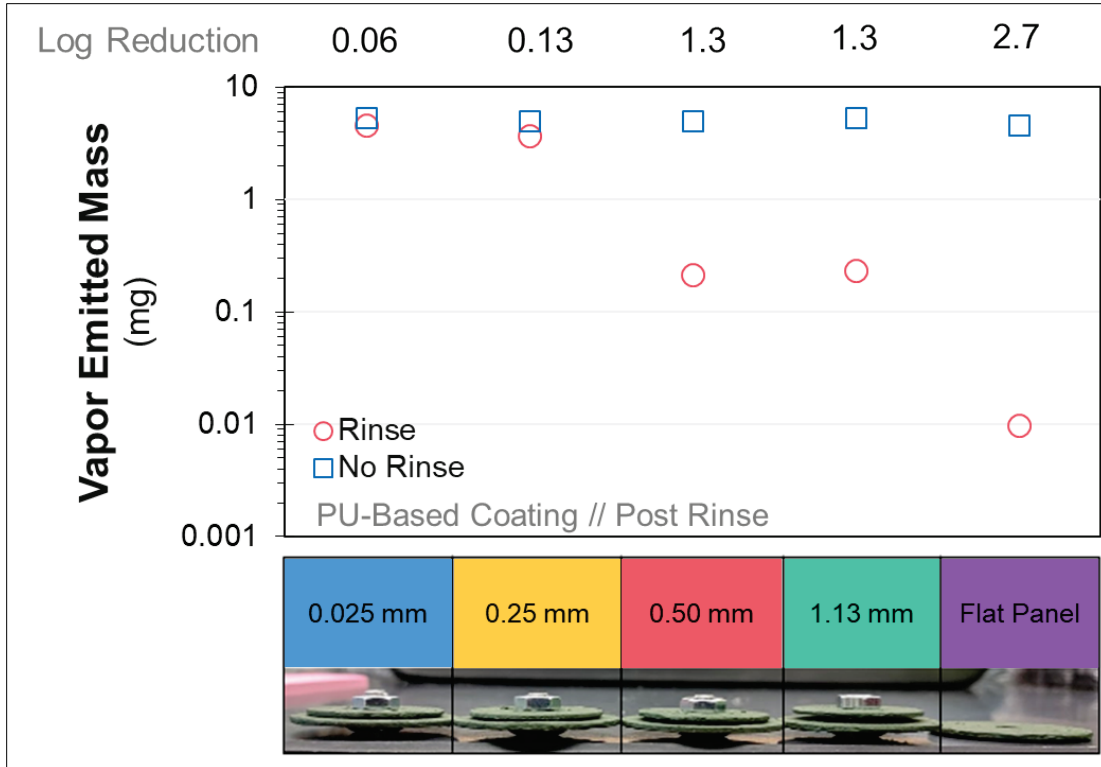
Figure 36. Influence of capillary size on post-rinse VEM of PU-based coatings.

Similarly, the post-rinse vapor emission was measured for a variety of different feature geometries that had been painted with a PU-based coating. As shown in Figure 37, contaminant contained in screw threads (small and large entrainments) exhibited an emission profile that was significantly more intense and longer than the profile seen for flat panels. Vapor emission from the small screw thread (entrainment) and the recession continued for 5–9 h after contamination, whereas vapor emission from flat panels decreased below detectable levels after only 1 h. As with the stainless steel features, capillary feature size (critical dimension) is the driving factor behind entrainment. Geometry may influence the likelihood that contamination reaches a capillary feature. However, on a wetting surface, a contaminant may traverse a surface to reach a capillary feature and allow for a contaminant deposited away from a capillary feature to still be entrained.
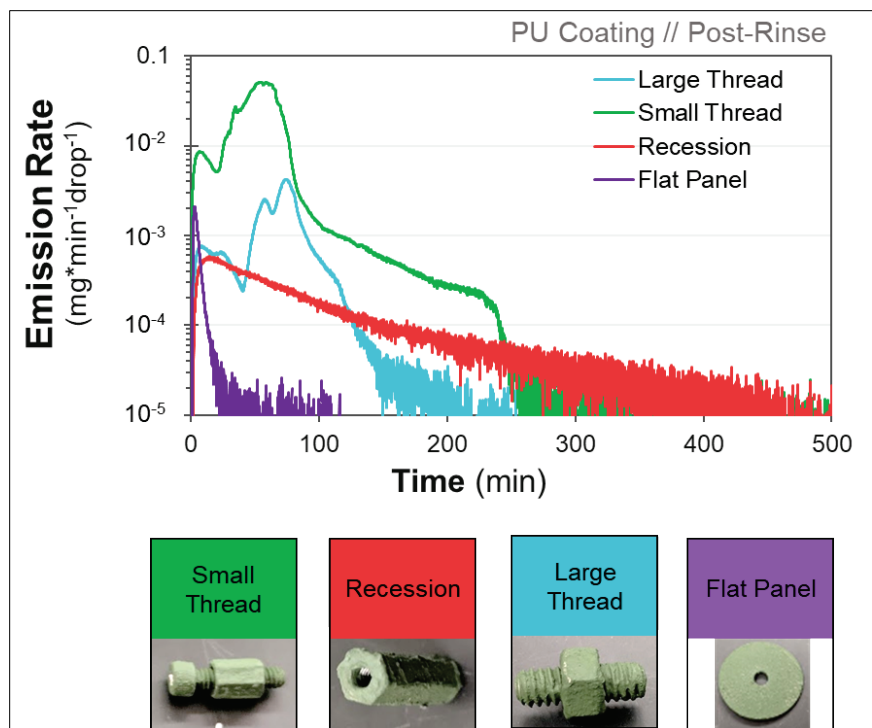
Figure 37. Influence of feature geometry on post-rinse vapor emission from PU-based coatings.

Analysis of the total VEM for a variety of feature geometries is described in Figure 38. This analysis shows that the small screw thread (entrainment) significantly resisted contaminant removal by rinsing. The large entrainment and recession also decreased the efficacy of the rinse process by nearly 10-fold. This shows that the rinse process was significantly more difficult for complex features, especially those containing capillaries smaller than 0.25 mm, regardless of their geometry. This translates to increased difficulty in decontaminating these assets with water-based liquid decontaminants.
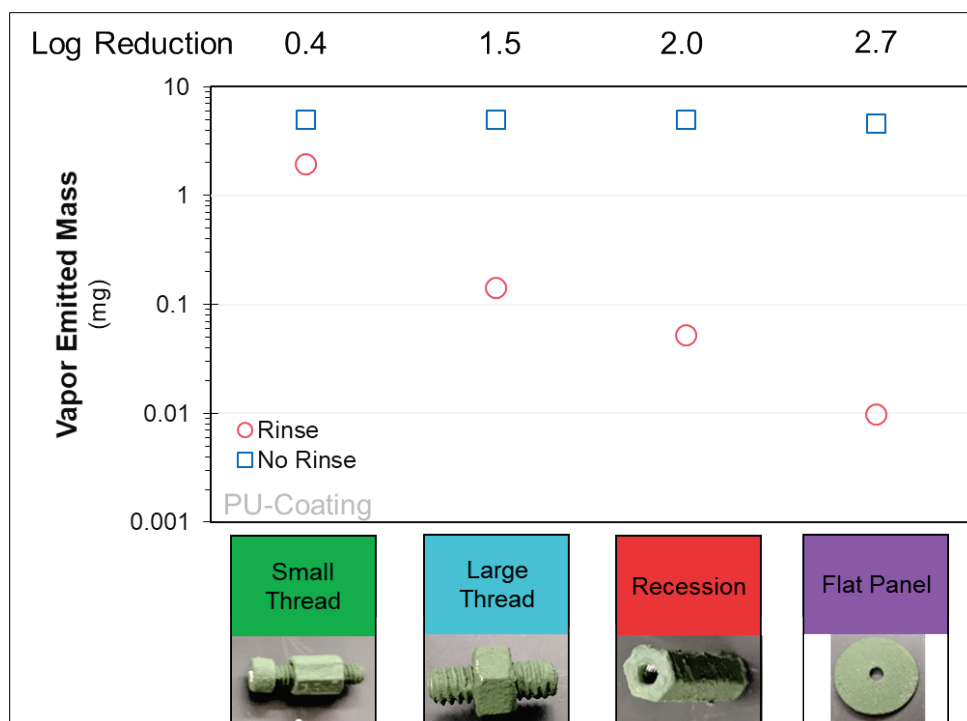
Figure 38. Influence of feature geometry on post-rinse VEM on PU-based coatings.

## 4.4	Data Analysis and Conclusions

In nearly all of the conditions tested, rinsing was less effective when the contaminant was placed on a complex feature. Contamination falling on flat panels of unpainted stainless steel was easily removed through rinsing and resulted in a very low post-rinse vapor emission. However, if the droplet becomes entrained in a capillary feature, the rinse procedure is significantly less effective. Up to 70% of the contamination may remain entrained in the feature, slowly emitting and presenting a significant vapor source. From a deposition of 4.6 mg of 2,5-lutidine, a total of 4.4 mg of contaminant was emitted from the rinsed smallest stainless steel capillary, as compared to 20 ng emitted from the rinsed flat panel (Figure 39). This represents over a 5 order of magnitude (100,000-fold) increase in vapor emission as compared to the flat panel condition. Flat stainless steel surfaces are generally considered to be a relatively simple material to decontaminate, but these results show complex steel surfaces can be a significant decontamination challenge.
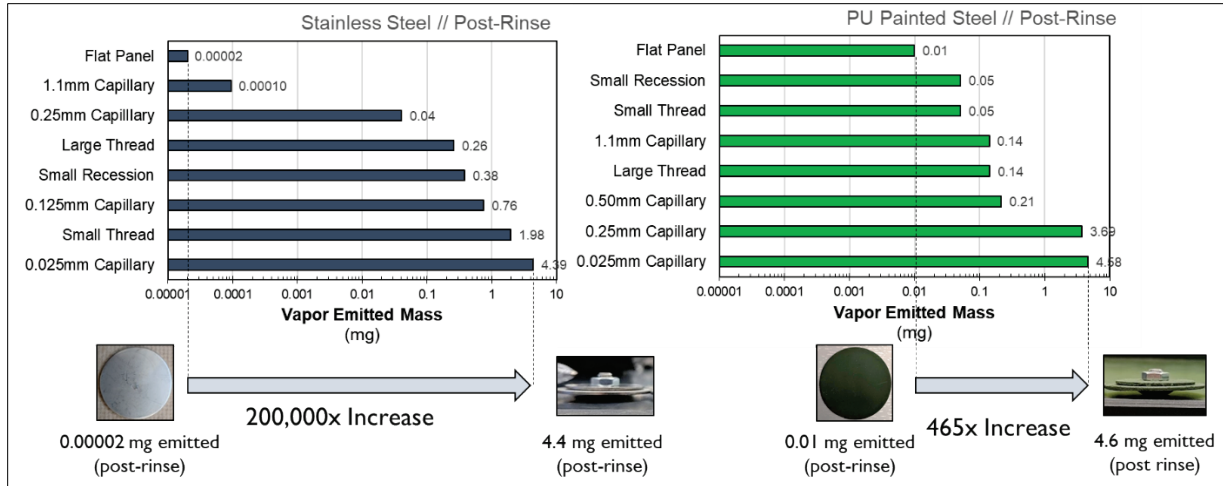
Figure 39. Rinse efficacy comparison between small capillaries and flat panels.

The surfaces painted with a PU-based coating presented a significant decontamination challenge. The rinsed flat panel gave off 1 µg of total VEM, which was nearly 200 times higher than the emission from flat stainless steel. This was likely due to some residual contaminant adhering to the surface during the rinsing procedure. Contaminant entrained within painted capillary features produced significant vapor emission that ranged from 10 µg to 4.6 mg. This shows that nearly all of the sizes and geometries tested resulted in at least a 5-fold increase in post-rinse vapor emission. Contaminant readily spread on the PU-based coating, making it possible for contaminant to migrate across a flat surface and become entrained in a capillary feature. This may provide an additional challenge not accounted for in the data. The overall efficacy of the rinse process can be evaluated with the LR calculation (eq 4). This number represents the overall reduction in VEM due to the rinse process (Figure 40). For example, rinsing a painted flat panel results in a 2.7 LR, or 99.8%, reduction in the overall vapor emission. However, the same procedure may only remove 14% of contaminant landing at a small capillary interface (0.06 LR). This analysis confirms that, in nearly every case, the painted material provided the most significant decontamination burden and a significantly smaller LR as compared to stainless steel.
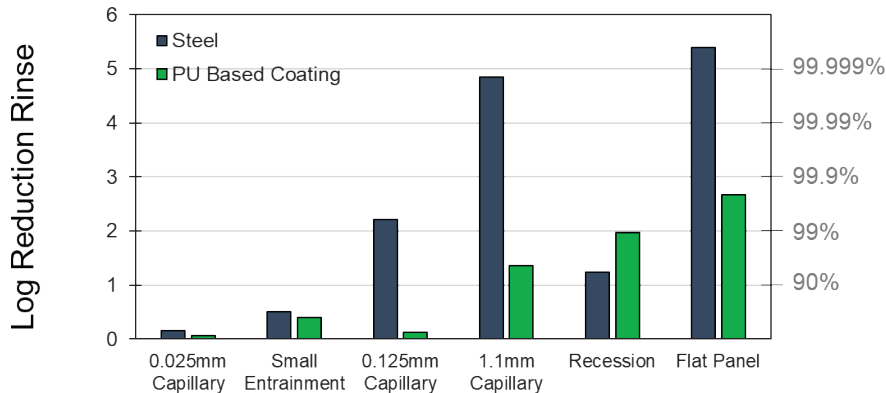
Figure 40. Efficacy of rinse procedure at removing contamination from various complex features using the LR of VEM for each condition.

44

In general, it appears that feature size has the largest impact on the ability to rinse contamination from a panel. For both materials, small threads and small capillaries resulted in little reduction in VEM. A comparison of post-rinse vapor emission versus feature size is shown in Figure 41, which clearly demonstrates that the efficacy of the rinse process decreased with decreasing capillary feature size. For any given feature, critical dimensions likely have a larger influence than geometry. Although the absolute dimensions will vary for different materials and contaminants, feature size clearly drives capillary entrainment. Recall that the capillary pressure that draws contaminant into the feature is a function of material surface energy and liquid surface tension (Section 1.2). This is likely coupled with fluid dynamic factors associated with the decontamination application process that would influence how the decontaminant could access contaminant in the capillary feature.
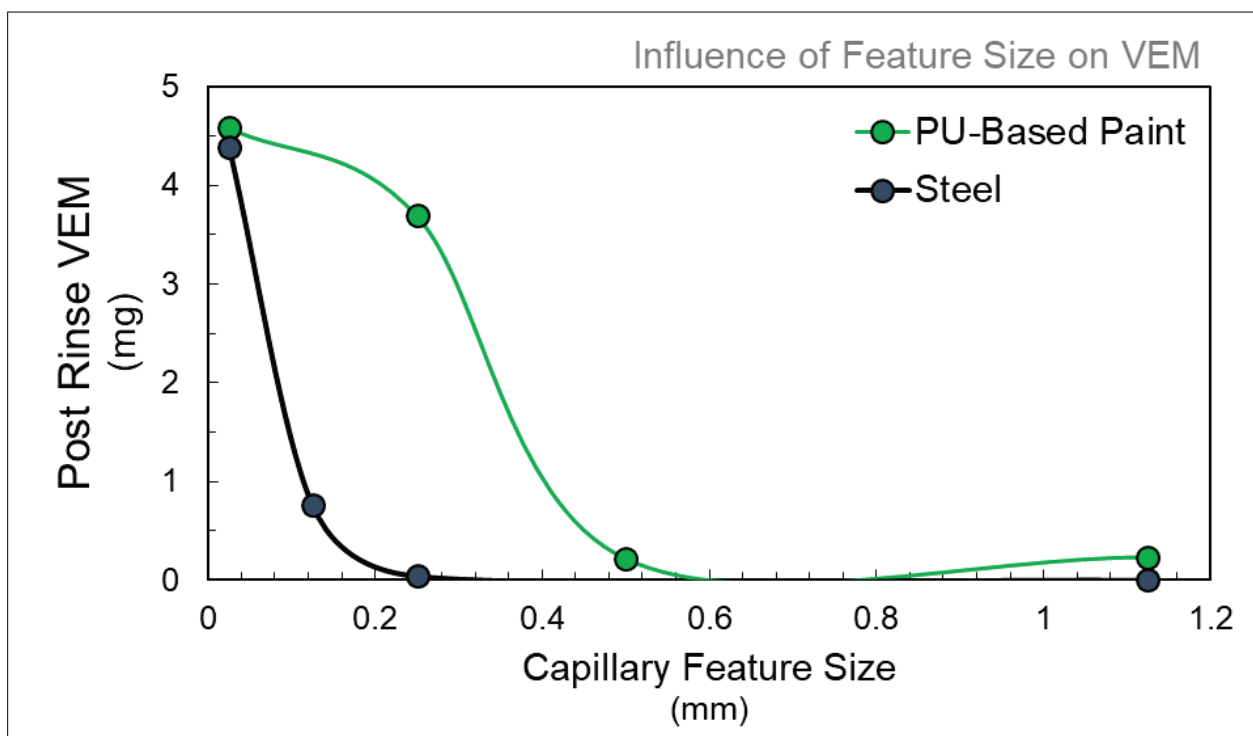
Figure 41. Influence of capillary feature size on VEM.

The post-rinse VEM describes the total hazard posed by a decontaminated asset, whereas vapor duration and peak emission describe the duration and magnitude of the associated vapor source terms. Peak emission rate represents the maximum value of the vapor source term, which is correlated with the maximum potential exposure risk. The peak emission rate for various geometries and feature sizes are provided in Figure 42. In general, most painted features had a higher vapor emission rate than their unpainted counterparts. This increased emission rate was likely due to liquid spreading. The scatterplot in Figure 42 shows that increased VEM typically correlated with a higher peak emission rate, which shows a link between the source term magnitude and the total vapor emission.
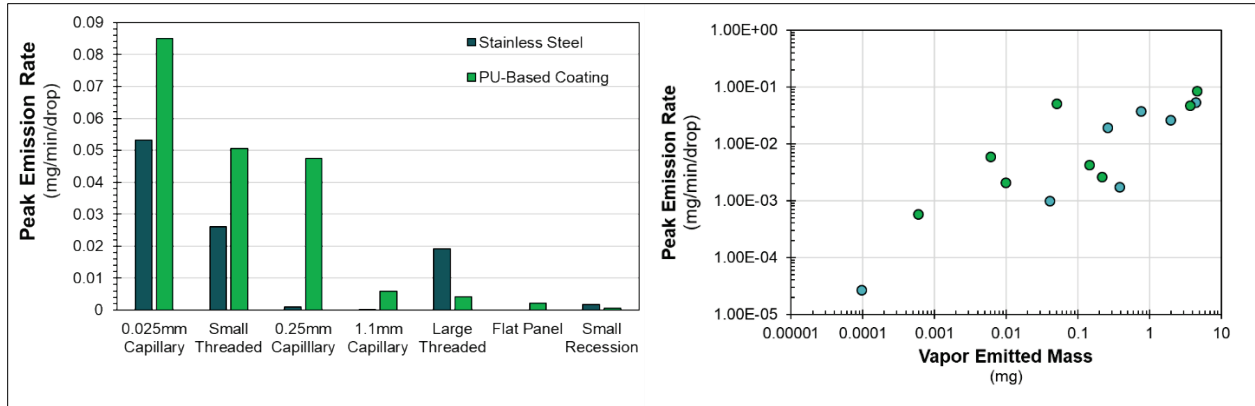
Figure 42. Peak emission rate for rinsed complex features (left) and
comparison of post-rinse VEM with post-rinse peak vapor emission rate (right).

The duration of the source term also played a key role in clarifying how exposure changed over time. One method of examining vapor duration is to look at how the remaining contaminant changes over time. As shown in Figure 43, an initial portion of the contaminant was removed via the rinse process, and the remaining contaminant decreased over time due to vapor emission. Vapor duration can be assessed by determining how long it took for the total contaminant to reduce by a certain factor. For this analysis, vapor duration was defined as the time to reach 99.9% removal of the contaminant (0.1% of the contaminant remaining).
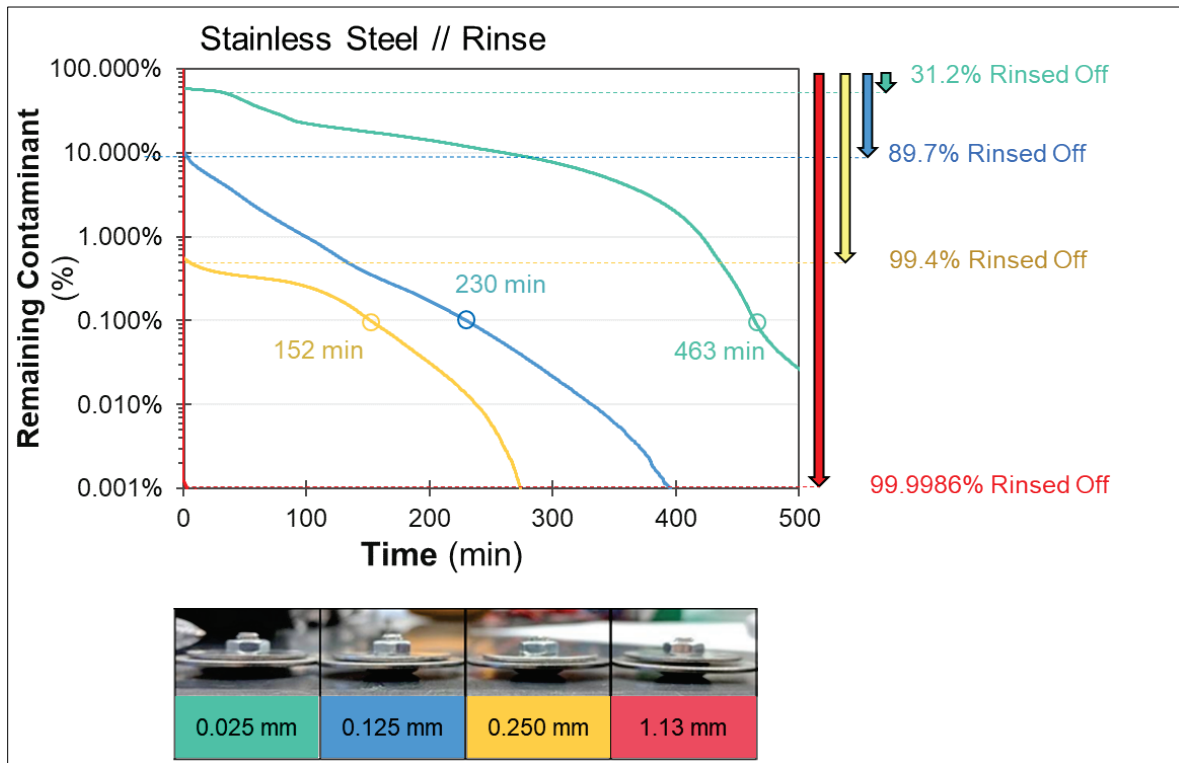
Figure 43. Remaining contaminant over time for rinsed stainless steel features.

A comparison of the vapor duration for a variety of complex features is given in Figure 44. These results show that most painted surfaces took longer to reach high levels of removal as compared with steel surfaces. This was likely due to the decreased effectiveness of the rinse process on the painted surfaces. Small capillaries, threads, and recessions were the longest-duration source terms. This analysis shows that the post-rinse source term duration was significantly increased by complex features.
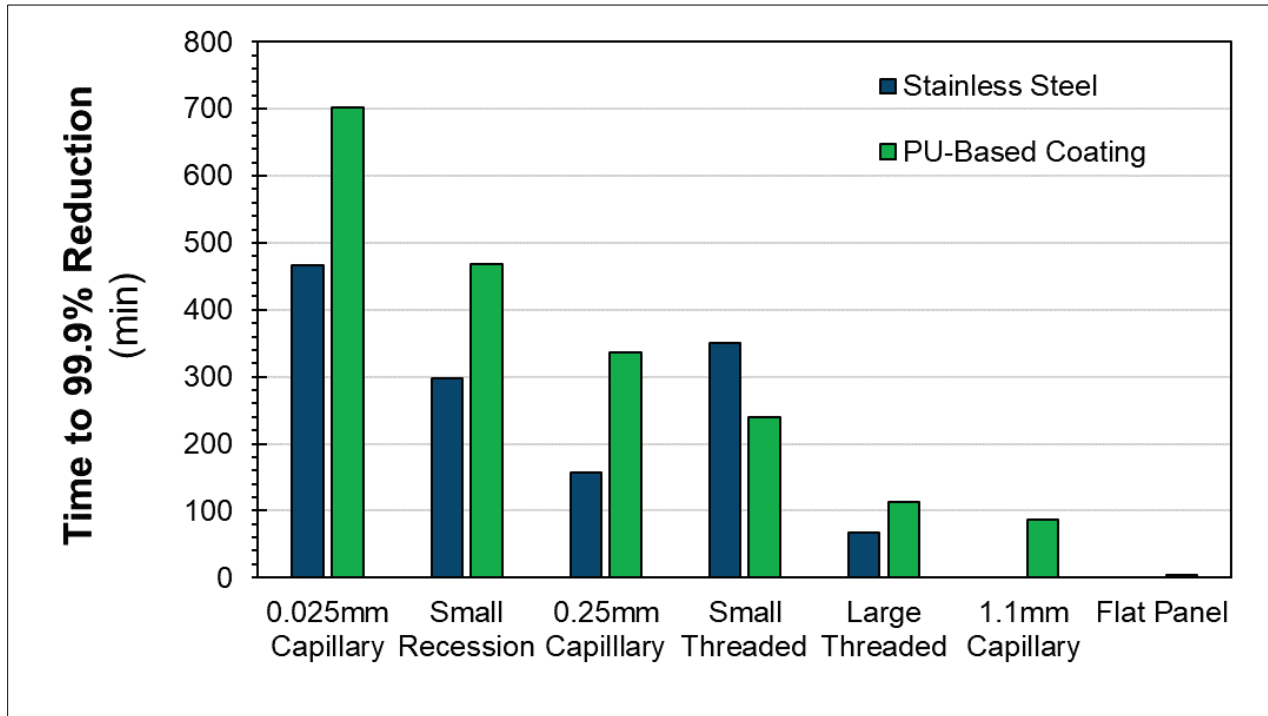
Figure 44. Vapor duration, measured as the time required for a 99.9% reduction in the starting contaminant.

Overall, these results show that the total amount of vapor emission after a rinse or liquid decontamination can be greatly increased when a droplet is entrained in a capillary feature. The inability of a rinse procedure to remove contamination from within capillary features is a result of restricted fluid flow to the contaminated area. This results in a larger amount of remaining contaminant and, therefore, an increase in the magnitude and duration of the vapor source terms. Thus, complex features may contribute significantly to the total source term of a decontaminated asset. If complex features are in fact a significant contributor to post-decontamination hazard, they must be incorporated in the process of decontaminant development and testing.

5.   VAPOR SCALE-UP CALCULATIONS

5.1   Vignette and Methodology

Translating laboratory-scale data to a real-world context requires appropriately summing or combining the individual vapor sources to represent the real-world asset. Specifically, the abundance of each material and presence of complex features are used to determine a composite asset emission rate. The composite source terms are used to approximate vapor exposure to personnel and can also be used to determine how each material contributes to the exposure. This work has shown that, regardless of material type, contaminated complex features create decontamination challenges and greater-magnitude and longer-duration vapor sources as compared to flat horizontal surfaces. This in turn suggests that vapor emission sources from liquids in capillaries may significantly contribute to the overall vapor source term for a contaminated asset. To test this hypothesis and determine whether these types of vapor emission sources need to be included or accounted for in research and development (R&D) or T&E procedures for technology development and evaluation, the contribution of contamination vapor emission from complex features relative to the vapor emission from all other types of features will be assessed on a full-scale asset.

A sensitivity analysis was performed to determine whether complex features significantly contribute to the overall vapor emission in a conceptual vignette (e.g., personnel standing near a vehicle after contamination and after decontamination). The analysis focused only on the total vapor source term of the asset; a full exposure assessment considering vapor dispersion into the environment and location of personnel was not conducted. The conditions of the vignette were as follows:

- The asset of interest was a vehicle with a total surface area of 50.5 m^2 (details are in Table 2).

- For the contamination event, the vehicle was contaminated with a GB simulant at a contamination density of 10 g/m^2. This was a total of 101,010 drops over a 50.5 m^2 surface. The behavior of the total number of droplets was treated as the behavior for the sum of non-interacting, single droplets.

- The vehicle consisted of both painted and non-painted materials.

- Vapor emission from painted materials was estimated using the data from the PU-based coating.

- Vapor emission from non-painted materials was estimated using the data from the stainless steel coating.

- In each case, vapor source terms were estimated with 0, 1, and 5% of the drops entrained in complex features and the remainder on flat horizontal materials.

- In the first case, vapor source terms were estimated as the vehicle weathered, (i.e., no treatment).

- In the second case, vapor source terms were estimated after the vehicle had undergone an immediate water-rinse procedure.

The data generated for complex features and flat panels (from previous sections of this report) were scaled up to determine the extent that complex features contributed to weathering (no liquid decontamination process) and post-rinse vapor source terms. The example vehicle was estimated to comprise mostly painted, wetting materials, as shown in Table 2. The number of drops to achieve the specified starting challenge on the material area was determined by

$$ n_{\text{drops}} = \frac{SC \; A_{\text{material}}}{\rho \; V_{\text{drop}}} \tag{5} $$

where

n_{drops} is the number of droplets on the material (drops),
SC is the starting challenge (g/m^2),
A_{material} is the material surface area (m^2),
ρ is the liquid density (g/mL), and
V_{drop} is the droplet volume (mL).

For this scaling, it was assumed that the droplet volume used in this calculation matches the droplet volume used in testing to acquire the vapor source terms.

Table 2. Materials Considered for Vehicle Decontamination

Category	Areas	Actual Material	Source Term Material	Contam. Area (m^2)	No. Drops (10 g/m^2)
Painted Materials (wetting)	Hood, Top, Sides, Mounts	Water Based Paint	PU-Based Coating	48.375	96,750
Non-Painted Materials (non-wetting)	Headlights, Viewports, Weather Stripping, Tow Hooks	Stainless Steel, Polycarbonate, EPDM	Stainless Steel	2.13	4,260

For any real-world asset, many materials may be present. However, it is not realistic to expect that all materials can be evaluated in laboratory testing. In some cases, it is expected that some asset materials will be approximated with different testing materials. This is shown in Table 2, where it is indicated that multiple "actual materials" were represented with a different source term material. All non-wetting materials, such as polycarbonate and tire rubber, were approximated using stainless steel source terms. Although all of these materials are similar with respect to liquid spreading, they may vary significantly in other properties, namely, absorption. The calculations in Section 5.2 provide a demonstration.

Although this vignette represents just one of many potential real-world scenarios, it provides a starting point for determining the importance of complex features in decontamination and weathering processes. The emission rate depends on the material, the contaminant, and the decontaminant, so conclusions here do not directly apply to all

decontamination contexts. The influence of these factors on the entrainment and emission from complex features is considered in the discussion.

Procedure 6 in the SD2ED includes the methodology for a vapor composite system calculation that scales individual panel vapor test data to represent an asset.[3] In this implementation of scale-up, the test material area was used as the vapor emission normalization metric, and vapor flux was reported in mass per unit of material area per unit time. The area-based approach is straightforward for mapping laboratory test panels to flat horizontal regions of an asset. However, scaling capillary features by material area will not capture how this particular vapor source may contribute to overall vapor emission. Typically, contaminant drop volumes are constant throughout a test or research program (e.g., the 5 µL droplets used here), and the same droplet volume is used for flat panel or the complex capillary panels considered in this report. Therefore, per-droplet normalization was used for all scale-up calculations. The laboratory droplet volume is assumed to be representative of the real-world contamination.

5.2   Influence of Complex Features on Vapor Emission from an Untreated Vehicle

As a baseline, the vapor emission from the vehicle was estimated when contamination to a level of 10 g/m^2 only fell on flat surfaces (0% interaction with complex features). Traditional laboratory testing has been limited to these flat surfaces. The vehicle emission rate was calculated as shown in Figure 45 using the estimates from Table 2, where most of the contamination was on painted surfaces (96,750 drops, 95.8%), and a small percentage was on unpainted stainless steel surfaces (4,260 drops, 4.2%); drop distribution was chosen semi-arbitrarily for demonstration purposes. The droplets falling on the PU-based coating dominated the overall vapor emission. The overall emission rate decreased by 99.9% over the course of 1 h and by 99.99% (4 LR) after 2 h.
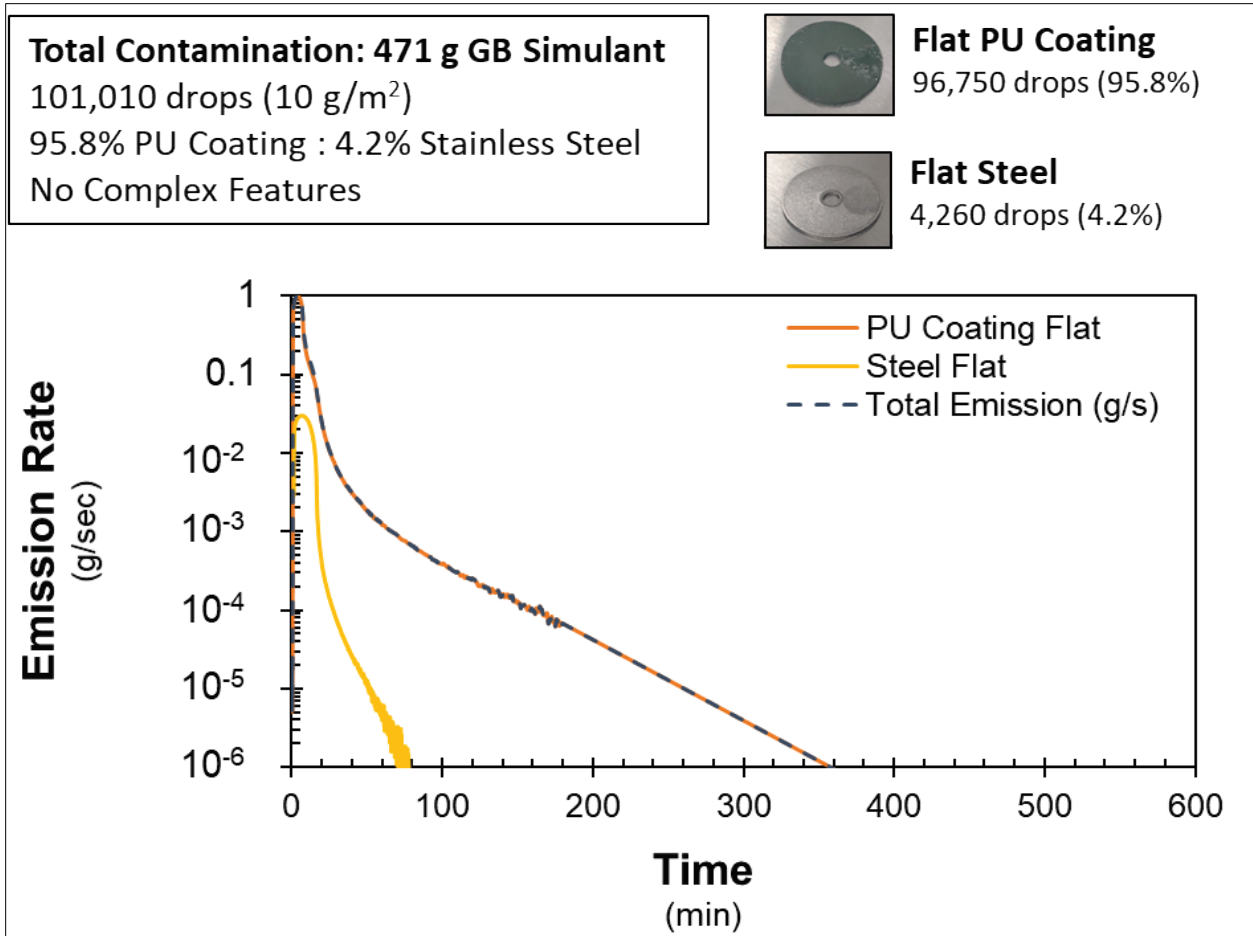
Figure 45. Predicted vehicle emission rate with no complex features present (no rinse).

A similar analysis was performed with 1% of the droplets becoming entrained in a complex feature (Figure 46). Entrainment was spread out across four feature types: a small capillary, a large capillary, an entrainment, and a recession. Recall that the presence of capillary entrainment tends to decrease the magnitude of the vapor source term and extend the duration. To characterize relative contributions from flat and complex features, the fraction emission is calculated as the ratio of total emission rate from each feature type to the total asset emission rate (upper right graph in Figure 46). During the initial hour of vapor emission, the source terms from the flat surfaces dominated the overall vapor emission. As the vapor emission progressed, the vapor emission from complex features became significant. After roughly 3 h, vapor emission was dominated by complex features. The inclusion of complex feature entrainment significantly extended the vapor source term.

Total Contamination: 471 g GB Simulant
101,010 drops (10 g/m^2)
95.8% PU-Coating : 4.2% Stainless Steel
99% Flat Features : 1% Complex Features

Flat PU Coating
95783 drops
94.83%

Flat Steel
4,217 drops
4.17%

Capillary (.025mm)
580 drops
0.57%

Capillary (0.25 mm)
25 drops
0.02%

Capillary (1.1mm)
195 drops
0.19%

Small Thread
10 drops
0.01%

Small Thread
192 drops
0.19%

Recession
8 drops
0.01%
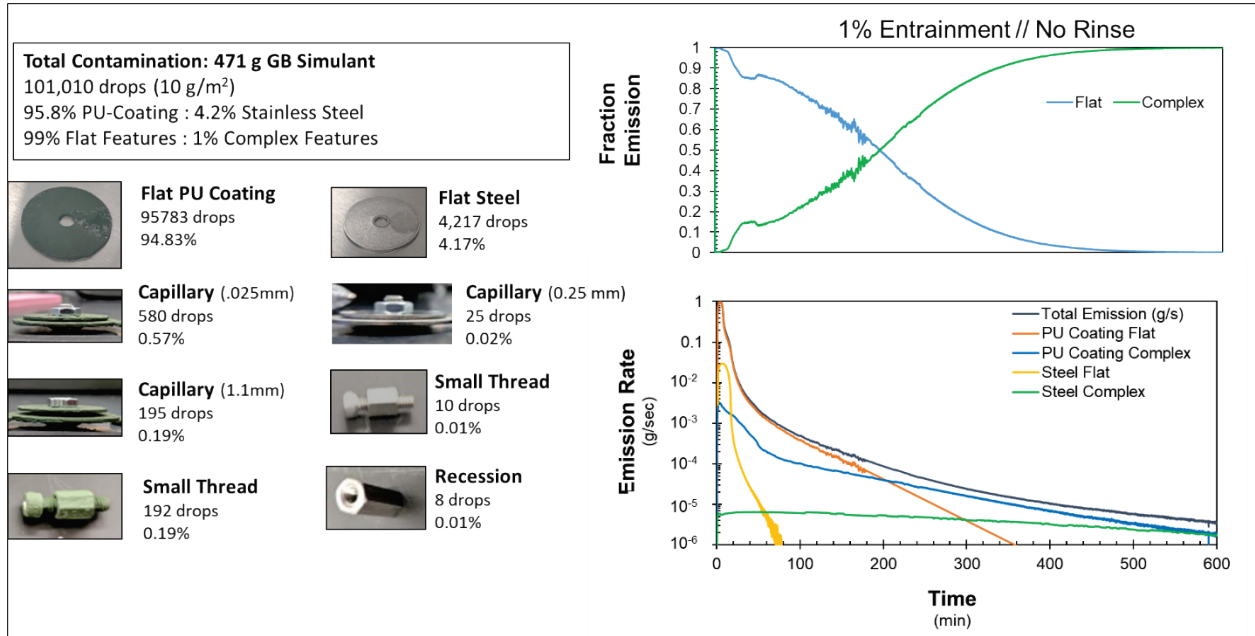
Figure 46. Predicted vehicle emission profile with 1% entrainment in capillary features (no rinse).

Analysis using 5% entrainment in capillary features gives a more pronounced impact (Figure 47). Complex features account for more than 40% of the emission just 40 min after contamination. A significant increase in vapor emission is observed after 3 h that corresponds to a nearly 10-fold increase in emission rate as compared to the flat panel. Inclusion of complex features in the analysis results in a significant increase in long-term, low-magnitude vapor emission. For the first 5 h, much of this can be attributed to the coated complex features; after that point, the steel complex features become significant vapor sources.
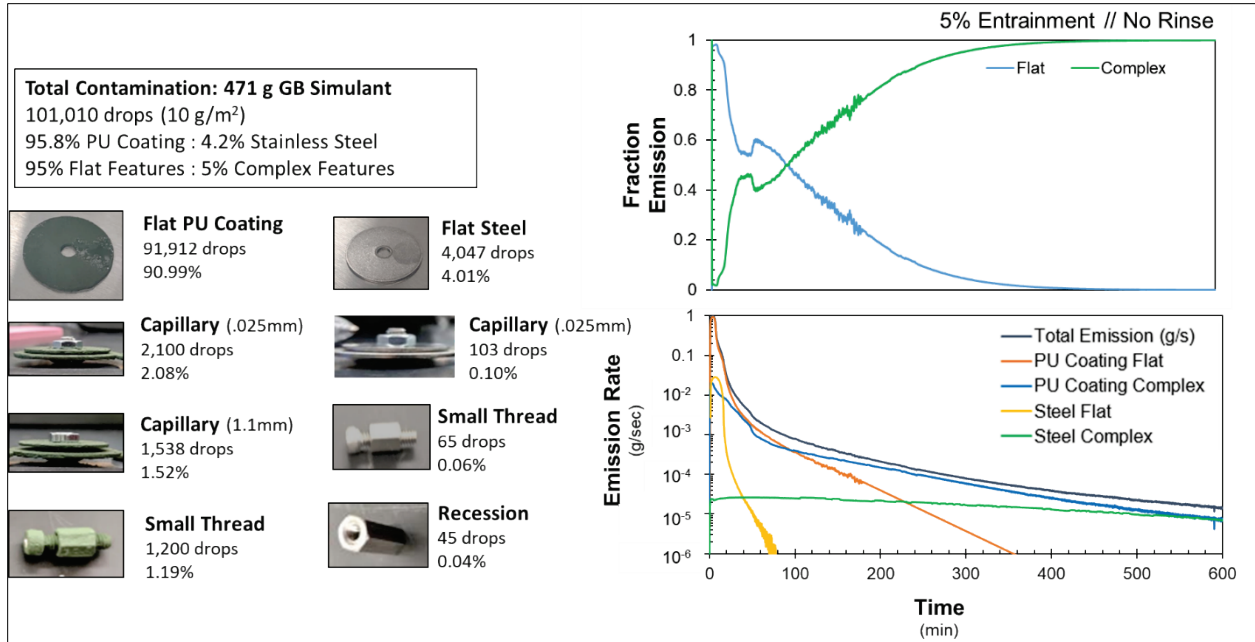
Figure 47. Predicted vehicle emission profile with 5% entrainment in capillary features (no rinse).

These results showed that complex features had a significant impact on vapor emission from a vehicle that had no decontamination treatment. The overall vapor emission rate for analysis cases of only flat surfaces, 1% entrainment in capillary features, and 5% entrainment in capillary features are shown in Figure 48. The initial 40 min of vapor emission area was dominated by the contribution from flat features; however, long-duration vapor emission was significantly higher when the analysis included complex features. After 5 h, vapor emission rates were 10–50 times higher when complex features were included, as compared to the case where only flat surfaces were assumed. This shows that contaminant trapped in complex features may lead to significantly longer-duration, lower-magnitude vapor emissions.
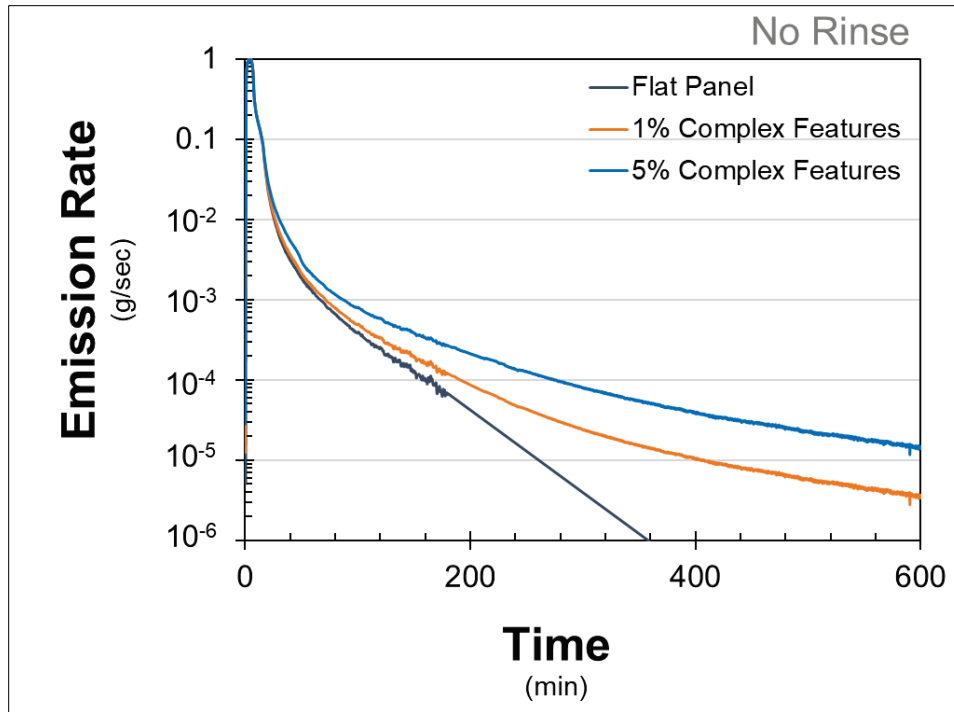
Figure 48. Comparison of vehicle emission profiles with varied entrainment in complex features (no rinse).

The vapor source term magnitude tends to be greatest at short time durations (i.e., shortly after decontamination treatment). However, in the operational context, it is unlikely that personnel would reduce personal protective posture until sometime later, when the asset could be monitored and reissued. Furthermore, it is the interactions of personnel with the assets for long time durations after protective posture is reduced that correspond to post-decontamination exposure. Therefore, the vapor magnitude at long time durations significantly influences potential personnel exposure and represents a critical factor to capture in experimental characterizations. Including the effects of complex panels on vapor source durations may be significant toward understanding and accurately characterizing hazard mitigation technologies.

This analysis suggests that contaminant entrained in complex features may lead to a lower-magnitude, longer-duration vapor emission. Whether this leads to a significant impact on the emission duration of an asset depends on the contaminant, the asset, and the environmental conditions. As shown in Table 3, the time it takes to reduce vapor source terms to low levels is increased when entrainment in complex features is considered. This impact can more than double the time it takes to reach low threshold levels. Although source terms play a role in exposure assessments, they cannot be directly used to calculate a vapor exposure. For some contaminants under certain environmental conditions, these low-level source terms may pose a significant exposure risk. However, the exposure risk may be negligible at these levels in other conditions. These data do not and cannot be used to make direct assessments on weathering. However, it does show that complex features may be a significant contributor and must be included when performing assessments on weathering of field assets.

Table 3. Time to Reach Emission Thresholds through Weathering (No Rinse)
for Varied Entrainment in Complex Features

Reduction in VEM (%)	Time to Reach Threshold (min)		
	Flat Panel	1% Entrainment	5% Entrainment
90	12	13	14
99	42	51	87
99.9	136	201	368
99.99	235	512	669

5.3　　　　**Influence of Complex Features on Vapor Emission after Rinse Treatment**

The post-rinse vapor emission rate was also considered. Data collected after an immediate water rinse was scaled up to estimate the emission rate of a vehicle, as described in Section 5.1. As with the non-treated case, 96% of the drops were assumed to land on painted (PU-based coating) surfaces, and approximately 4% of the droplets were assumed to fall on a stainless steel surface. As a baseline condition, the post-rinse vapor emission was estimated using only flat surfaces, as shown in Figure 49. As compared with the no-rinse condition, a significant portion of the contaminant was removed. No significant vapor emission was estimated from the flat stainless steel surface, as nearly all of the contaminant was rinsed from the surface. A small level of vapor emission was predicted from the flat painted surface. The magnitude of the emission after the rinse treatment was more than 100-fold smaller than it was under identical conditions for an untreated surface. An estimate that only considers flat panels suggests that a rinse procedure will greatly reduce both the magnitude and duration of vapor emission.
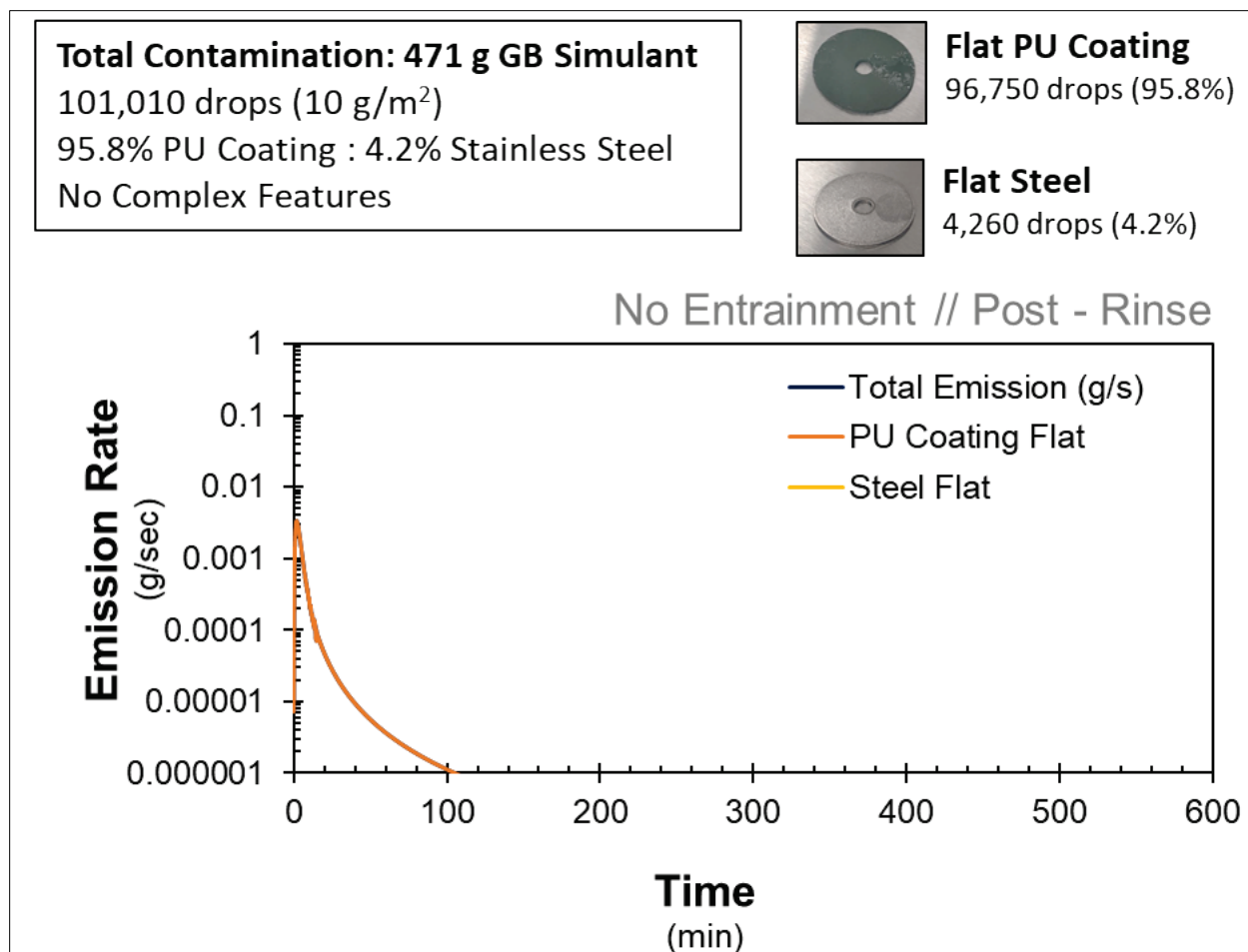
Figure 49. Prediction of vehicle vapor emission after a rinse procedure
where no complex features are present.

The overall vapor emission was then estimated with 1% of the droplets entrained in complex features, as shown in Figure 50. In this estimate, a significant portion of the vapor emission can be attributed directly to complex features. Inclusion of complex features in the estimate predicts a low-magnitude, long-duration tail to the vapor emission profile. This suggests that entrainment of a small percentage of droplets into complex features can significantly increase the vapor emission duration. In this case, the painted complex features were the most significant source of vapor emission and accounted for nearly 75% of the VEM. Droplets entrained in steel complex features only accounted for 43 of the 101,010 droplets (0.04%) but contributed to 3% of the overall vapor emission. On the other hand, *flat surfaces accounted for 99% of the droplet count, but contributed to only 23% of the overall vapor emission. This shows that a small minority of droplets entrained in complex features can contribute significantly to the overall vapor source terms*.
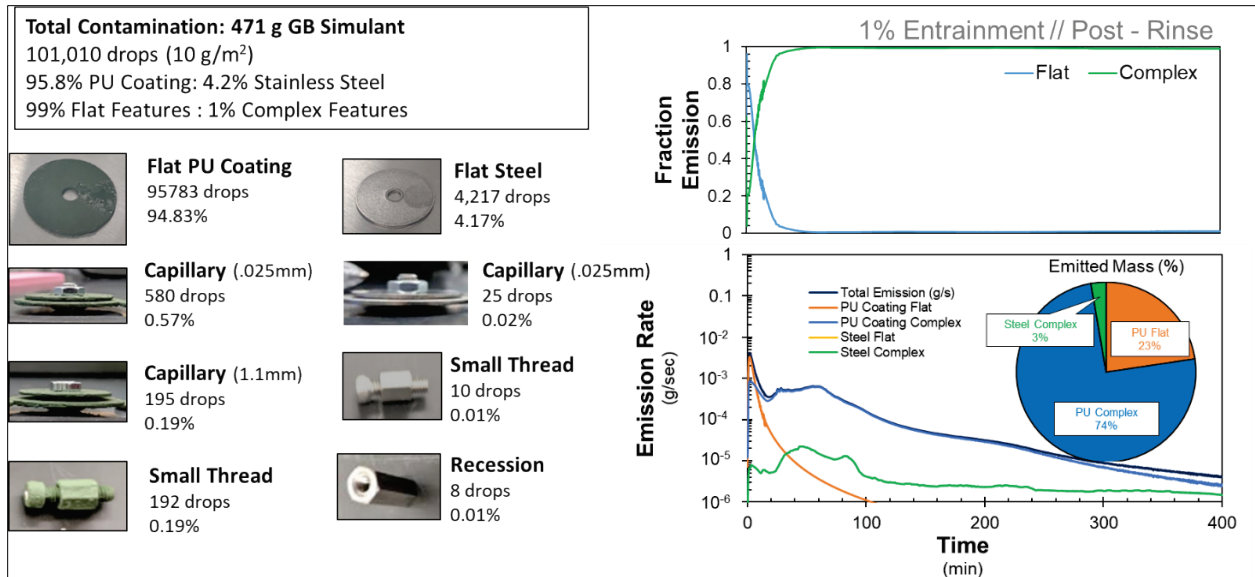
Figure 50. Predicted post-rinse vapor emission from a vehicle with 1% entrainment in capillary features.

The overall vapor emission was estimated with 5% entrainment of complex features, as shown in Figure 51. A similar low-magnitude, long-duration vapor emission was observed, and nearly all vapor sources arose from droplets contained within capillary features. In this case, nearly 95% of the overall vapor emission came from entrained droplets. Droplets entrained in painted surfaces accounted for 90% of the overall vapor emission, whereas those entrained in steel surfaces accounted for 4%. This further demonstrates that vapor source terms may be drastically underestimated if only data from flat horizontal surfaces are used.
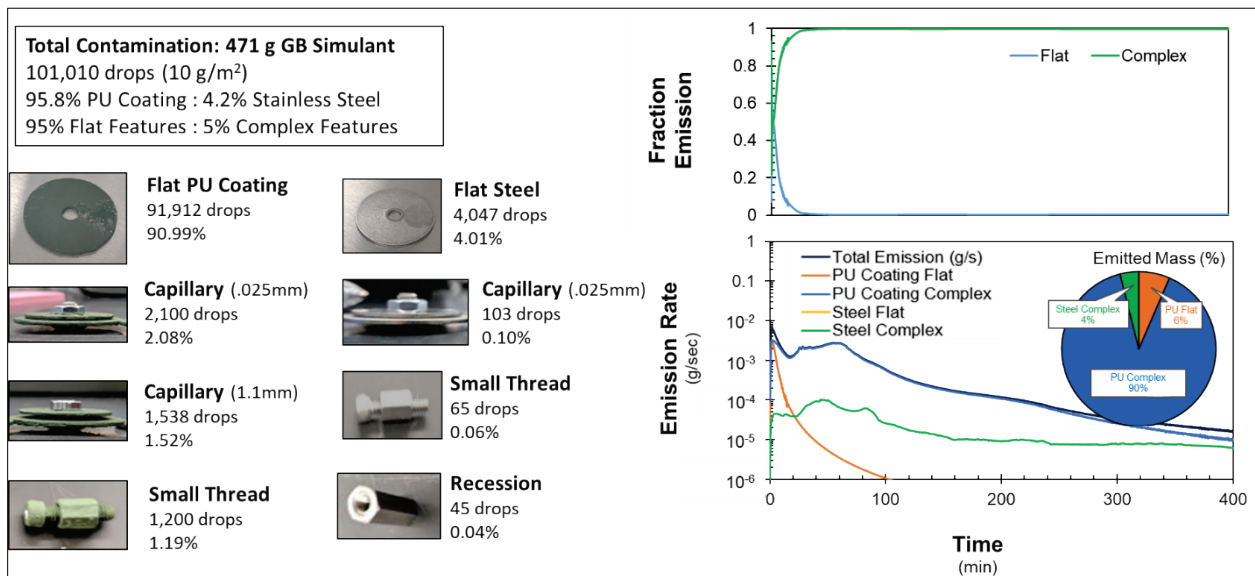
Figure 51. Predicted post-rinse vapor emission from a vehicle with 5% entrainment in capillary features.

The post-rinse vapor emission profiles are compared in Figure 52. The estimated vapor emission rate was significantly higher and it persisted for significantly longer when entrainment in capillary features was considered. The vapor emission rate declined to 0.00002 g/s (1.2 mg/min) after approximately 40 min when the analysis was performed using only flat surfaces. However, when entrainment in a capillary was accounted for, vapor emission stayed above that threshold for more than 4 h. The overall VEM was significantly higher for cases in which contaminant entrainment was considered because water rinses were shown to be less effective at removing contamination from complex features as compared with flat surfaces. Analysis with only flat panel surfaces predicted a total of 0.9 g of overall vapor emission. This can be compared with 4.1 and 13.9 g for analyses that included 1 and 5% entrainment, respectively. These results demonstrate that even a small percentage of droplets entrained in capillary features can significantly increase the duration and magnitude of vapor emission after a rinse procedure.
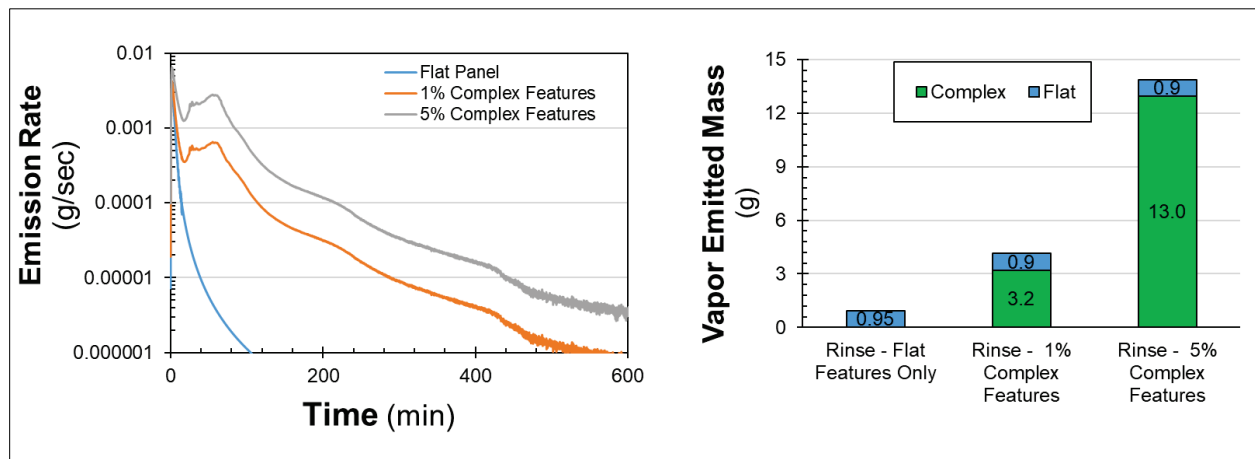
Figure 52. Comparison of predicted post-rinse vapor emission from a vehicle at varied levels of entrainment.

These results focused on a specific operational vignette wherein a vehicle is contaminated with a simulant and is immediately rinsed after contamination. As shown in Figure 53, a significant portion of the vapor emission can be attributed to the painted surfaces. These contributions are specific to this operational context and may change when different materials and contaminants are considered. Total asset source terms are used to assess potential post-decontamination hazards to personnel. These data illustrate that if only flat panel source terms are used, the resulting source term may significantly underestimate the actual asset emission rate. This example is not intended for the estimation of post-decontamination exposure hazards or for translation to different operational scenarios. Rather, this exercise is intended to demonstrate that even small levels of capillary entrainment may be lead to significantly higher vapor source terms. This demonstrates that hazard assessments and decontaminant development must consider entrainment in complex features as a potentially large contributor to the overall hazard posed by CWA contamination. Furthermore, the optimization of a decontaminant on flat panels alone may miss some of the considerations for improving performance on capillary features (which may be the most significant hazard sources).
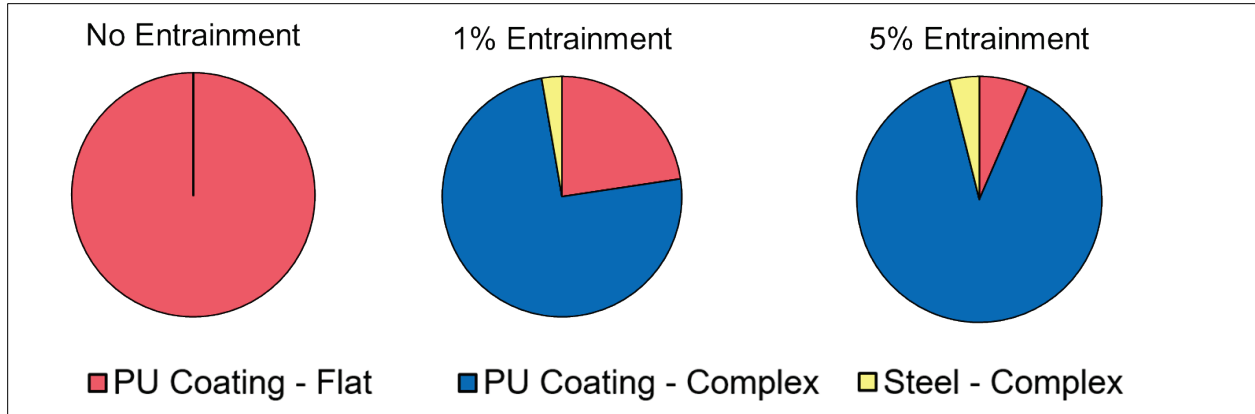
Figure 53. Comparison of total VEM after a rinse procedure with varied levels of entrainment. The contribution of a flat steel panel was negligible in all cases.

5.4   Conclusions

These data demonstrate that even small levels of entrainment may have significant consequences on vapor duration and magnitude for the simulated asset. In cases where the asset receives no treatment, entrainment in capillary features significantly influences vapor duration. If even 5% of droplets become entrained in a capillary feature, the vapor emission duration is significantly extended, as shown in Figure 54. Capillary entrainment has an even larger influence on the effectiveness of a rinse procedure. As the figure shows, entrained contaminant resists removal via rinse and results in a significantly higher post-rinse vapor emission hazard.
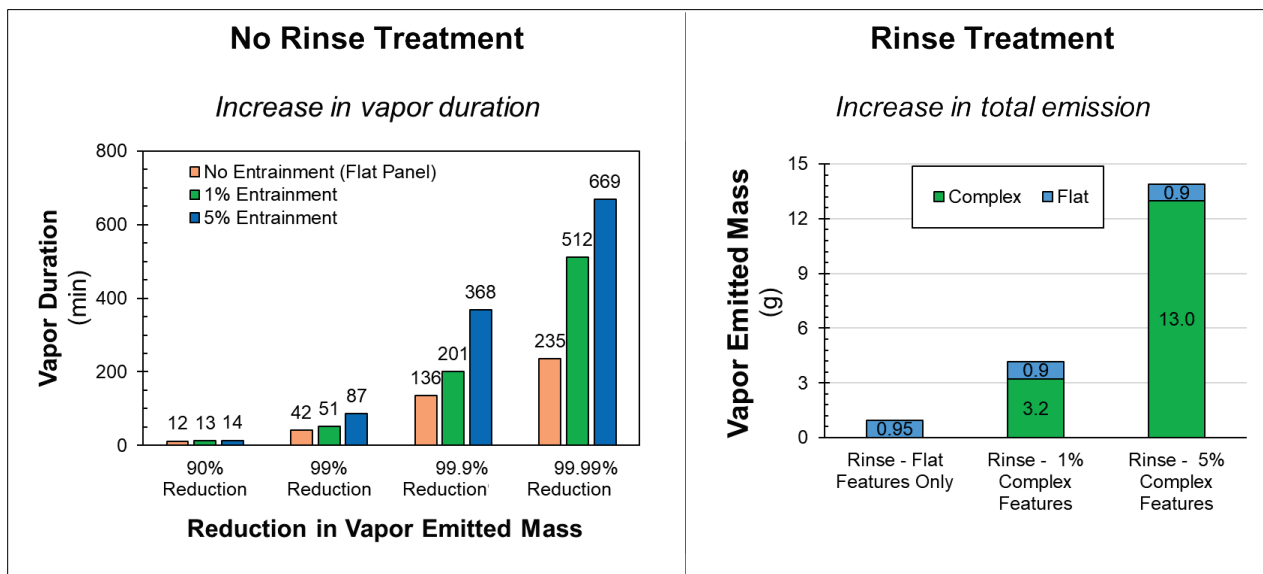
Figure 54. Influence of capillary entrainment on vapor emission duration, based on scale-up calculations.

59

5.5   Future Considerations Toward Complex Panel Test Methodologies: Simplified Testing

Previous data demonstrations illustrated how the inclusion of capillary features could influence the characterization of hazard mitigation technologies. However, there are many types of capillary features that could be considered, and the generation of a test matrix to test them all is unrealistic. The effects of capillary features were shown to be related to how agent is entrained within small gaps. Between the laboratory test panels and the real features found on assets, there can be significant variation in the volume of a feature that could entrain agent. It is not envisioned that a laboratory complex test panel will exactly replicate the features (e.g., depth, width, length, and internal volume) found on a real-world asset. Rather, it is assumed that the laboratory test panels *approximate the effects of capillary entrainment*. This approach is necessary to prevent the testing of every feature variation that may be present on an asset, which would result in unrealistic test loads.

The use of a composite system calculation enables the representation of vehicle vapor source terms with variable levels of resolution. For example, the vehicle could be represented using only flat horizontal panels for one material or for multiple materials (lower resolution). The composite calculation could include some features with the complex capillary source terms developed here (higher resolution). Including or excluding various types of source terms will influence the accuracy of the output calculation, as compared to the actual asset being represented, and will determine the amount of data required to conduct the analysis. Significantly contributing sources should be identified and prioritized for testing. In these demonstrations, only PU paint and steel materials were used. In future studies, the inclusion of more material source terms should be considered to ensure the asset is represented as accurately as needed.

As a brief example, in the following analysis, the composite emission rate that is obtained when all of the features are addressed (i.e., two flat surfaces and six different capillary features) is compared to that obtained when two flat surfaces and only one complex feature source term are used. The vapor source terms presented in Figure 35 or 37 share many similarities in magnitude and duration. Based on previous observations that feature size seemed more influential than feature geometry, the small capillary features were the most challenging to decontaminate and created the longest-duration vapor sources. It may provide acceptable accuracy to use the worst-case condition of a small capillary feature to represent all complex features on an asset. Alternately, this test condition could be the focus of efforts to improve decontaminant performance on complex features. To evaluate the accuracy of using one feature type and size on an asset-level evaluation, the condition of 1 and 5% contamination of complex features is repeated here, but the two flat panel source terms (for PU coating and steel), the 0.025 mm PU and steel features, and the corresponding flat panels are used here. These emission rate profiles were similar for each level of entrainment, regardless of whether a single material source term or multiple source terms were used (Figure 55).
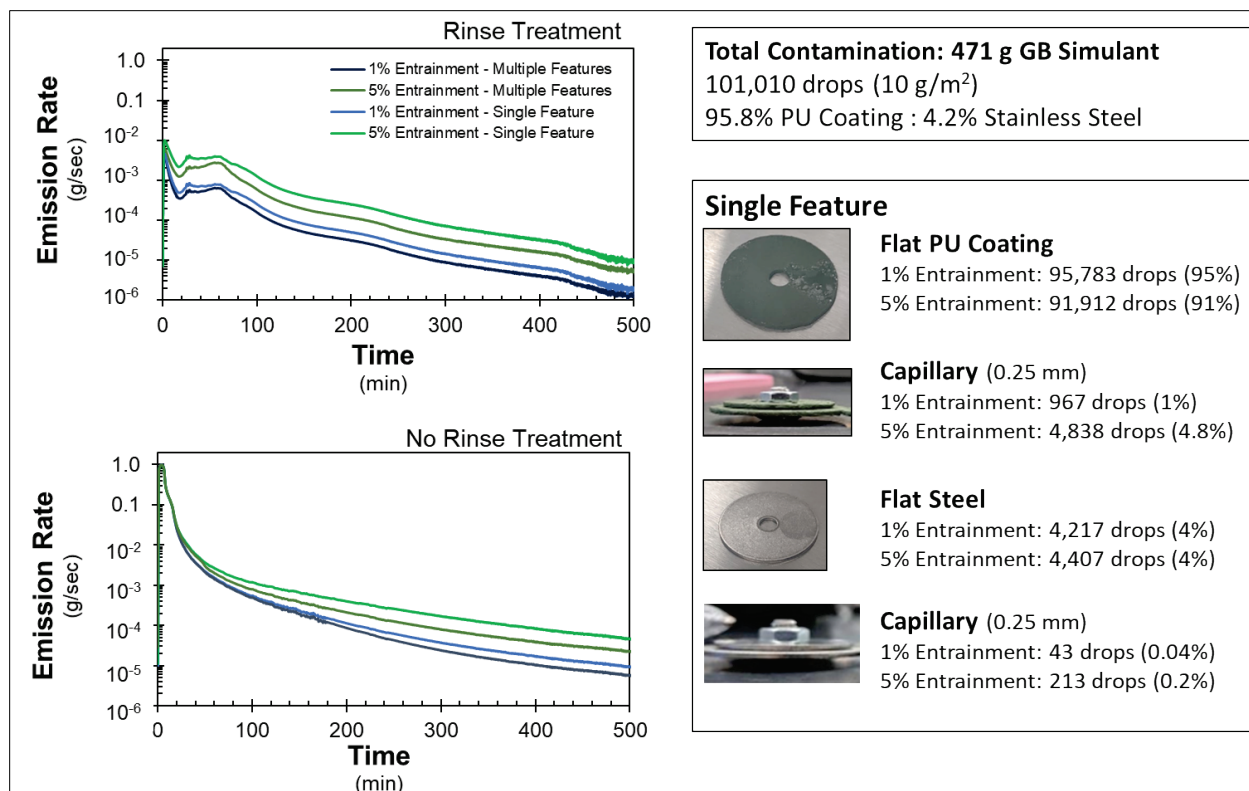
Figure 55. Emission rate of rinsed (top) and no-rinse (bottom) panels at various levels of entrainment, using a single or multi-material set.

As shown in Figure 56, the error expressed as the ratio of the source terms obtained using a single complex feature as compared with using multiple complex features shows that the use of five times more data of specific objects is within a factor of 1.5–2. The collection of multiple capillary features had a small impact on the overall asset source term as compared to that obtained using a single source term. As shown in Table 4, the VEM captures the difference of the total mass emitted, where the use of a single complex feature provided results that were within 1.3 to 1.7 times greater than estimates using multiple features. For features that did not receive a rinse, the VEM was the same, regardless of whether one source term or multiple source terms were used for the given material set. Therefore, depending on the needs of a test program, the effects of capillary features could be represented using the more-challenging-to-decontaminate features (like small capillary features), rather than attempting to test all possible variations of capillary features.

61
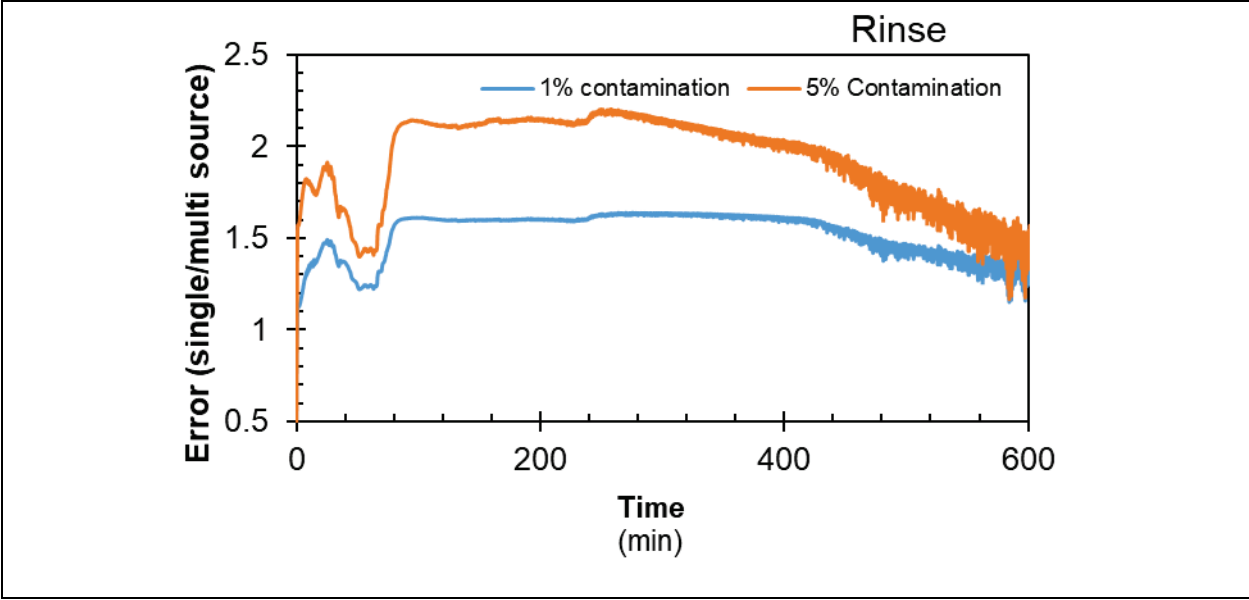
Figure 56. Ratio of emission rate calculated using one complex source term vs six complex source terms for the rinsed case; the use of a single complex feature tended to overestimate the use of six specific source terms by a factor of 1.5–2.

Table 4. Comparison of VEM Determined Using
a Single Source Term or Multiple Source Terms

| Condition | Droplets Entrained (%) | VEM (g) | | Ratio: Single/Multiple |
		Single Material	Multiple Materials	
Rinsed	1	5.578	4.151	1.34
	5	24.099	13.872	1.74
No rinse	1	0.988	0.989	1.00
	5	0.943	0.944	1.00

6.   DISCUSSION OF RESULTS

6.1   Data Summary and Overview

This study investigated how complex features influence vapor emission from contaminated materials. The roles of feature geometry, size, material type, and rinse treatment were explored. This work resulted in several key findings:

- Complex features tend to increase the vapor emission duration and decrease the magnitude of vapor emission for untreated surfaces.

- Complex features decrease the efficacy of a rinse procedure and lead to greater VEM per droplet of contaminant as compared with flat horizontal panels.

- Decreased emission rate magnitude can be attributed to a smaller exposed surface area for contaminants entrained in a complex feature through capillary action.

- Feature size has significant influence on vapor emission duration and magnitude.

- Feature size has significant influence on rinse efficacy, which is attributed to its limited access (e.g., flow restriction) to the contaminant due to the capillary feature.

- The smaller the feature size, the more significant the influence on vapor source emission duration, magnitude, and treatment efficacy.

- There seems to be a critical feature size range, on the order of 0.5 mm, where larger features behave similarly to flat panels and smaller features exhibit significant entrainment effects.

- Feature geometry has limited influence on vapor duration, magnitude, and rinse efficacy.

- Liquid spreading can have a significant impact on vapor emission and capillary entrainment.

- Scale-up of source terms to the asset level can be performed using a per-contaminant-droplet normalization, rather than the per-material-area approach previously used.

- Vapor scale-up calculations demonstrate that even small levels of capillary entrainment can significantly contribute to the overall vapor source term for an asset.

This study demonstrated that complex features likely have a significant impact on vapor emission and decontaminant performance. These conclusions were supported by a series of laboratory studies and scale-up calculations. This section explores the caveats, implications, and impact of this study and proposes future directions for further study. Section 6.2 focuses on

understanding how results from this study can be translated to other contaminants and materials. Section 6.3 aims to discuss how the findings of this study can inform development of decontaminants to better address the issue of complex features. The final section explores future directions of this work that can be done to further our understanding of decontaminant development.

6.2   **Translation of Results to Different Contaminant–Material Combinations**

Although the scope of this work was limited to two materials and one contaminant, some observed trends may be broadly applied to other materials and contaminants. Capillary entrainment in complex features is fundamentally governed by physical properties of the contaminant, the feature, and the material. The ability to translate the results of this study to a broader set of chemicals, materials, and features depends on how much each of these properties influences capillary retention. The influence of many of these factors is currently unknown, but reasonable hypotheses can be formed based on this limited data set. Further study is needed to determine which physical properties have the most significant influence on capillary retention and decontamination. Some general trends are likely to be observed across varying contaminant–material combinations:

- Capillary entrainment leads to increased emission duration and decreased decontaminant access.

- Capillary entrainment increases as feature size decreases.

- Liquid spreading on rough surfaces provides a means for liquid to enter or exit a complex feature.

These general trends likely hold true across different contaminants and materials, but the magnitude of the impact may vary. Entrainment leads to decreased surface area, slowing evaporation, and limiting decontaminant access, regardless of the contaminant. However, the capillary size that leads to entrainment may vary based on the material and the contaminant. As factors such as interfacial tension and contact angle change the capillary pressure, the size regime necessary for entrainment may shift. For 5 µL droplets of 2,5-lutidine on the materials studied, entrainment was significant for features 0.5 mm and smaller. However, this critical size may change for other materials and contaminants.

It was observed that liquid spreading had a significant influence on both entrainment and vapor emission. Liquid spreading on rough surfaces provided a means for transport out of a macroscopic capillary feature, which led to decreased vapor emission duration. The impact of wetting on entrainment will vary, based on how quickly the contaminant wets the surface. Highly wetting contaminant–material combinations may easily "drain" from a complex feature, whereas slower wetting combinations may remain entrained. The wettability of a contaminant on a rough surface depends on several factors, including the size of the material microcapillaries (correlated with surface roughness), contaminant viscosity, interfacial tension, liquid–material adhesion, and contact angle. These factors play a significant role in defining the liquid transport of the contaminant into and out of the complex feature.

Although some trends may be relevant across most contaminant–material combinations, other key factors may significantly change results for different contaminants, materials, and conditions. Some factors that were not extensively investigated in this study include the following:

- impact of contaminant absorption into materials;

- impact of varied surface wetting on rough versus smooth surfaces;

- effects of contaminant droplet size on critical dimensions for entrainment;

- influence of water solubility of a decontaminant on the efficacy of the rinse process;

- decontamination of complex features using solvent-based, viscous, or vaporous decontaminants with significantly varied rheology; and

- influence of decontaminant application pressure, angle, and flow rate on efficacy of decontamination of entrained contaminants.

The role of absorption was not investigated in this study. The simulant used (2,5-luditide) had a high vapor pressure and evaporated rapidly. In this case, the timescale of evaporation was significantly shorter than the timescale for absorption in material. Thus, studies using this simulant may not account for the influence of contaminant absorption. Absorbed chemicals are more difficult to access with a liquid decontaminant and may emit more slowly than a bulk liquid on a surface. The use of lower vapor pressure simulants will not only result in a longer vapor emission; more contribution from absorption of the contaminant into the material may also occur. Traditional CWAs and simulants such as HD, VX, GD, and methyl salicylate (an HD simulant) have lower vapor pressures than 2,5-lutidine. Based on this, it can be hypothesized that these compounds will emit over a longer duration and may potentially exhibit more absorption.

Liquid spreading on a smooth surface occurs by a different mechanism than liquid spreading on a rough surface. Namely, surface tension and the surface energy of the material dictate the wetting behavior on smooth materials. This varies from the rough-coated surfaces used in this study, wherein wetting was driven by capillary action through microchannels on the surface. The results from this study can only be used to infer dynamics on rough surfaces, and further study will be required to better understand how complex features interact with smooth, non-wetting surfaces.

Direct conclusions about feature size cannot be taken without considering the influence of droplet size. Large 5 µL droplets used in this study do not reflect the smaller droplet distributions anticipated in a contamination scenario. For capillary entrainment to occur, the deposited liquid layer thickness or droplet radius needs to be comparable to the size of the capillary gap. Thus, the ranges of capillary sizes that lead to entrainment may depend on deposition and droplet sizes. Although this study demonstrated that capillary size is a significant driver in contaminant entrainment, the specific feature sizes highlighted should only serve as estimates, not absolutes. Further study is required to understand how droplet size and deposition influence capillary entrainment.

Another factor that may influence the decontamination process is the solubility of the contaminant in the decontamination solution. For decontamination with an aqueous liquid, contaminant can be physically removed (via action of a sprayer) and dissolved. The ability to dissolve the contaminant, in this case into water, influences the efficacy of a reactive decontaminant. Poor mass transport (e.g., dissolution) into the decontaminant solution can decrease the ability of the decontaminant to reduce the contaminant concentration and lead to poor efficacy. 2,5-Lutidine has a higher aqueous solubility than HD, VX, GD, or methyl salicylate (Figure 12). This is one of many factors that may influence the ability to remove contaminant entrained in a surface. The influence of the solubility may be insignificant to other parameters such as application pressure, spray direction, decontaminant viscosity, and contaminant adsorption to the surface. This makes it difficult to predict how the rinse procedure used in this study will translate to other contaminants, materials, and treatment procedures with different technologies.

In summary, translating the findings from this study to other contaminants and materials requires an understanding of how physical properties influence capillary entrainment. Some factors, such as capillary feature size, are agnostic to the material being studied and the contaminant being used. Other factors, such as surface wetting, vary with contaminant and material. Although this study was limited in scope, the work described here shows that complex features can be significant vapor sources. Effective decontaminant development and hazard assessment must account for the influence of complex features to ensure that decontaminants vetted in the laboratory are also effective in the field.

6.3   Implications for Decontamination Development

Traditional decontaminant development has focused first on stirred reactor studies to measure liquid-phase homogenous reaction rates. However, this methodology ignores key decontaminant attributes necessary for effective decontamination. As shown in Figure 57, a decontaminant must be capable of accomplishing three key functions to facilitate effective decontamination:

- **Access:** A decontaminant must access contaminant that may reside as a liquid on a surface, be entrained in features, or be sorbed in materials.

- **Interact:** A decontaminant must interact with the contaminant, typically via dissolution of the contaminant into the decontaminant or the decontaminant into the contaminant.

- **Detoxify:** A decontaminant must detoxify contaminants through reaction or encapsulation.

Liquid-phase reactor studies only measure the ability of a decontaminant to react with and detoxify contaminant that has been dissolved in a decontaminant solution. A decontaminant must be able to accomplish all three functions to effectively decontaminate the materials of an asset. A decontaminant solution that is reactive, but cannot access the contaminant, will not be effective. Each essential decontaminant function is correlated with specific decontaminant attributes that can be measured using specific tests and optimized using laboratory studies. Decontaminant development that only focuses on liquid-phase reactivity risks late-stage problems because key decontaminant attributes were ignored during development.

66
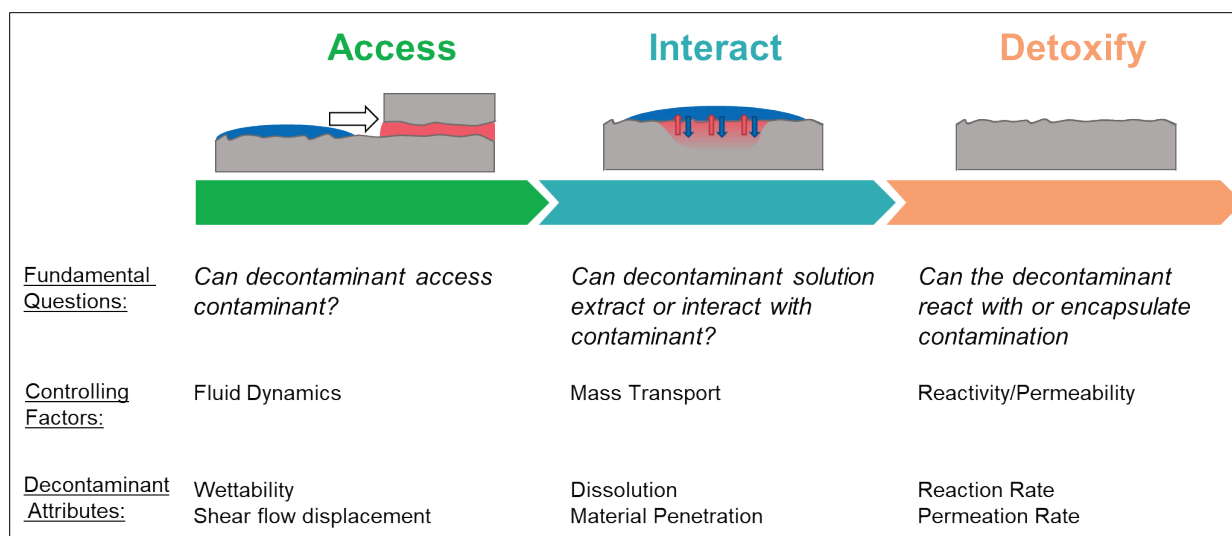
Figure 57. Essential functions for decontamination with associated decontaminant attributes.

This work highlights the importance of decontaminant access to entrained contamination. Entrained contaminant can be a significant vapor source and is more difficult to remove using water-based rinse procedures. Removal of contaminant from capillary features relies on fluid flow across the surface. Entrained contaminant may be removed through displacement, wherein a directed flow is applied to overcome the capillary forces retaining the contaminant. This depends on the application pressure and direction as well as the decontaminant wettability and viscosity. Another means of removal is through dissolution, which requires a decontaminant to extract the contaminant at the exposed interface. The solubility of the contaminant in the decontaminant can be optimized by addition of co-solvents.

The ability to optimize decontaminant access requires a testing methodology in the laboratory. Using shimmed-washer capillaries, the ability to remove entrained contaminant can be examined in the laboratory. Due to the outsized influence of capillary size on contaminant retention, it is suggested that 0.5 mm capillaries be used to study the case of moderate entrainment and 0.025 mm capillaries be used to study extreme entrainment. Although this study used AP-MS to measure VEM, residual contaminant measurements may involve a simpler method of analyzing the influence of capillary entrainment on decontaminant efficacy. However, additional studies are needed to develop reproducible methods of applying both the contaminant and the decontaminant to capillary features.

It is clear that simple reactivity studies alone are insufficient for development of an effective, field-ready technology for material decontamination. The ability of a decontaminant to access entrained contaminant, remain in place during decontamination, and extract bulk and absorbed contamination are essential. These processes are governed by different physical processes that must be considered and examined experimentally during decontaminant development. This allows for an early understanding of decontamination processes and limitations during R&D and avoids late-stage failures during product development.

6.4   Future Directions

Expand the study to different contaminants and materials. As discussed in Section 6.2, the influence of capillary entrainment on decontamination may vary based on the contaminant, material, and decontaminant used. Although some factors, such as capillary size, are largely agnostic to changes in material and contaminant, wetting behavior and absorption rates depend greatly on the physical and chemical properties of the contaminants and materials involved. Moreover, the short contaminant age time used in this study minimized the influence of contaminant absorption. Contaminant absorbed within a capillary feature may be a significant decontamination challenge and should be investigated. Additional studies correlating these results with agent (rather than simulant) data may provide a stronger case for the need to consider capillary entrainment during decontaminant development.

Determine the levels of entrainment occurring for fielded assets, and refine scale-up methods. This study demonstrated that even 1% entrainment in capillary features can significantly influence vapor source terms. However, no data exist for how much contaminant becomes entrained during a CWA attack. This data set would allow for more reliable hazard assessments and more accurate predictions of health effects. This type of information depends on the vignette, and capillary retention may vary greatly for different assets. However, several small-scale pilot studies on select high-value assets may help provide more reasonable estimates of capillary entrainment. These could be performed using CWA simulants loaded with a dye or tracer compound.

Determine influence of decontaminant rheology and application on removal of entrained contaminant. This study used a rinse-only decontamination procedure with three 5 mL aliquots of water delivered from a pipette. Commercial and fielded decontaminant sprayers will be applied at different flow rates, temperatures, and pressures, and these factors likely play a significant role in decontamination. The fluid flow of the decontaminant is also highly important, and the addition of rheology modifiers may help the decontaminant displace entrained contaminant. A small pilot study on the influence of decontaminant application methodologies and decontaminant rheology may help guide more informed decontaminant development in the future.

Development of a robust testing methodology for estimating decontaminant performance on complex features. This study highlighted that capillary entrained contaminant can pose a significant decontamination challenge. To effectively evaluate the ability of decontaminants to address this problem, robust methodologies must be developed. This will be important in both R&D and T&E phases for existing and upcoming decontaminant formulations. This requires outlined how-to procedures for applying contaminant and decontaminant to complex features, extracting contaminant, and analyzing results. Moreover, these methods can provide recommendations for creating reliable capillary features for laboratory-scale studies, including which feature sizes are most important.

Determination of the influence of droplet size and deposition methods on capillary entrainment. This study demonstrated that feature size is a large driver of contaminant entrainment in capillary features. However, the size regimes that lead to entrainment may depend heavily on the droplet size and how far it was deposited from the capillary feature. Further

studies should be performed to elucidate how capillary entrainment changes with droplet size and deposition method. These studies can provide a clearer operational picture of which features are most likely to entrain chemical agent and how to better design T&E procedures to determine decontaminant performance on complex features.

Blank

LITERATURE CITED

1. Kim, K.; Tsay, O.G.; Atwood, D.A.; Churchill, D.G. Destruction and Detection of Chemical Warfare Agents. *Chem. Rev.* **2011,** *111* (9), 5345–5403. https://doi.org/10.1021/cr100193y.

2. Jang, Y.J.; Kim, K.; Tsay, O.G.; Atwood, D.A.; Churchill, D.G. Update 1 of: Destruction and Detection of Chemical Warfare Agents. *Chem. Rev.* **2015,** *115* (24), PR1–PR76. https://doi.org/10.1021/acs.chemrev.5b00402.

3. Lalain, T.; Mantooth, B.; Shue, M.; Pusey, S.; Wylie, D. *Chemical Contaminant and Decontaminant Test Methodology Source Document*; ECBC-TR-980; U.S. Army Edgewood Chemical Biological Center: Aberdeen Proving Ground, MD, 2012; p 262.

4. Willis, M.P.; Mantooth, B.A.; Lalain, T.A. Novel Methodology for the Estimation of Chemical Warfare Agent Mass Transport Dynamics, Part I: Evaporation. *J. Phys. Chem. C* **2012,** *116* (1), 538–545. https://doi.org/10.1021/jp2087835.

5. Willis, M.P.; Mantooth, B.A.; Lalain, T.A. Novel Methodology for the Estimation of Chemical Warfare Agent Mass Transport Dynamics. Part II: Absorption. *J. Phys. Chem. C* **2012,** *116* (1), 546–554. https://doi.org/10.1021/jp2087847.

6. Boyne, D.A.; Varady, M.J.; Lambeth, R.H.; Eikenberg, J.H.; Bringuier, S.A.; Pearl, T.P.; Mantooth, B.A. Solvent-Assisted Desorption of 2,5-Lutidine from Polyurethane Films. *J. Phys. Chem. B* **2018,** *122* (7), 2155–2164. https://doi.org/10.1021/acs.jpcb.7b10656.

7. Varady, M.J.; Pearl, T.P.; Stevenson, S.M.; Mantooth, B.A. Decontamination of VX from Silicone: Characterization of Multicomponent Diffusion Effects. *Ind. Eng. Chem. Res.* **2016,** *55* (11), 3139–3149. https://pubs.acs.org/doi/10.1021/acs.iecr.5b04826.

8. Ismail, A.E.; Grest, G.S.; Heine, D.R.; Stevens, M.J.; Tsige, M. Interfacial Structure and Dynamics of Siloxane Systems: PDMS−Vapor and PDMS−Water. *Macromolecules* **2009,** *42* (8), 3186–3194. https://doi.org/10.1021/ma802805y.

9. Fox, H.; Taylor, P.; Zisman, W. Polyorganosiloxanes…Surface Active Properties. *Ind. Eng. Chem.* **1947,** *39* (11), 1401–1409. https://doi.org/10.1021/ie50455a607.

10. Xiao, Y.; Yang, F.; Pitchumani, R. A Generalized Analysis of Capillary Flows in Channels. *J. Colloid Interface Sci.* **2006,** *298* (2), 880–888. https://doi.org/10.1016/j.jcis.2006.01.005.

11. Gorzkowska-Sobas, A.A. *Chemical Warfare Agents and Their Interactions with Solid Surfaces*; FFI-rapport 2013/00574; Norwegian Defence Research Establishment: Kjeller, Norway, 2013.

12. Varady, M.J.; Pearl, T.P.; Bringuier, S.A.; Myers, J.P.; Mantooth, B.A. Agent-to-Simulant Relationships for Vapor Emission from Absorbing Materials. *Ind. Eng. Chem. Res.* **2017,** *56* (38), 10911–10919. https://doi.org/10.1021/acs.iecr.7b02323.

13. *Standard Guide for Small-Scale Environmental Chamber Determinations of Organic Emissions from Indoor Materials/Products*; ASTM D5116-17; ASTM International: West Conshohocken, PA, 2017.

14. Jolley, D.; Hanning-Lee, M.; Mamo, T.; Giessing, M.L. *TECMIPT Test Operations Procedures (TTOP) 8-2-196, Simulant Selection for Laboratory, Chamber and Field Testing*; West Desert Test Center: Dugway Proving Ground, UT, 2011.

Blank

ACRONYMS AND ABBREVIATIONS

2D	two dimensional
3D	three dimensional
AP-MS	atmospheric pressure mass spectrometry
CFD	computational fluid dynamics
CWA	chemical warfare agent
DEVCOM CBC	U.S. Army Combat Capabilities Development Command Chemical Biological Center
GB	sarin, (*RS*)-propan-2-yl methylphosphonofluoridate (nerve agent)
GD	pinacolyl methylphosphonofluoridate
GPL	general population limit
HD	sulfur mustard, bis(chloroethyl)sulfide (blister agent)
LR	log reduction
m/z	mass-to-charge ratio
PU	polyurethane
R&D	research and development
SD2ED	Source Document, Second Edition
SST	solid sorbent tube
T&E	test and evaluation
VEM	vapor emitted mass
VX	[2-(diisopropylamino)ethyl]-*O*-ethyl methylphosphonothioate (nerve agent)
WPL	worker population limit

(U) Blank

APPENDIX A:
LIQUID SPREADING

Droplets may be generically described as wetting or non-wetting. Often droplets are described as *sessile*, meaning immobile on the surface of a material or *not spreading over time*. Although a droplet may remain sessile on the surface, if the contact angle (θ) is <90°, then the presence of a capillary gap can still generate a positive capillary pressure that can result in capillary flow and produce entrained liquids. The more wetting the contaminant–material pair, the more significant the capillary pressure and resulting effects.

Most discussions of wetting consider nominally smooth surfaces. The presence of surface roughness can influence wetting characteristics. To some extent, surface roughness can present a two-dimensional (2D) capillary along the material surface. If a smooth surface is slightly wetting (θ < 90°), the rough surface will tend to result in more wetting (spreading) of the droplet than will the smooth surface. For the polyurethane (PU) coating investigated in this report, the material exhibits significant surface roughness and wetting of the liquids into the surface roughness. Discussions regarding capillary pressure or capillary flow for this material will be in reference to the feature created for testing rather than any capillary effects associated with the material roughness.

The rough surface of the coating can form 2D micron-scale capillaries that provide channels for liquid movement (i.e., spreading) across the surface, as seen in Figure A-1. Even if the material is only slightly wetting, the small 2D feature sizes associated with surface roughness can create significant capillary pressure (see Figure 8 within this report) that result in spreading across the material surface. Note that other smooth materials, not tested here, can exhibit spreading, such as the spreading on glass shown in Figure 6 within this report.
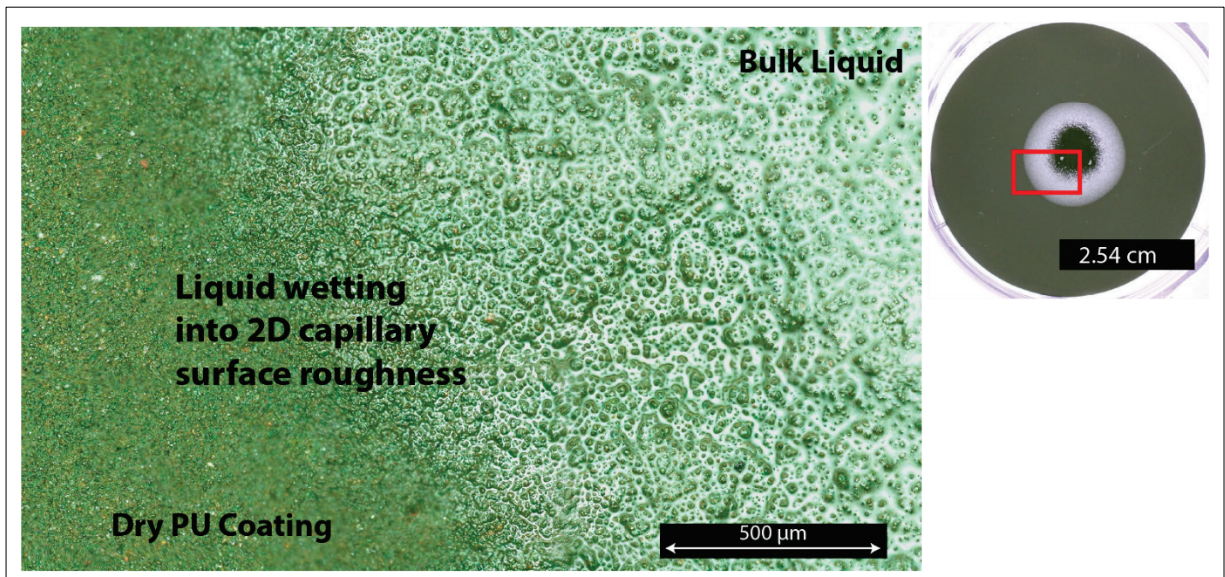

Figure A-1. (Left) Optical microscopy image of water (bright white regions) wetting into the surface roughness of a PU coating. (Right) Photograph of liquid spreading on a PU coating.

Blank

APPENDIX B:
SIMPLIFIED EMISSION RATE CALCULATION

B.1   Mass Balance Construct for Vapor Test Chambers

Traditional vapor test chambers use the mass balance equation to describe the relationship between the vapor source and the chamber concentration accounting for mass accumulation in the chamber volume.[B-1] A mass balance construct implies that mass introduced into the system must either leave or accumulate in the system. In the context of vapor testing, mass is introduced into the system by the object that is emitting agent vapors; in other words, by the vapor source. The accumulation of agent mass in the chamber generates a vapor concentration. The agent mass leaves the system due to air flowing into and out of the system (i.e., exhaust). Defining the mass balance system enables the derivation of a mass balance equation that relates the observed vapor concentration to the vapor source.

Within a closed system, mass must be conserved. An illustration of a generic dynamic vapor chamber with a contaminated item is shown in Figure B-1. For this type of system, the general mass balance equation can be expressed as

$$\text{Accumulation} = \text{In} - \text{Out} + \text{Generated} - \text{Consumed} \qquad \text{(B-1)}$$

Accumulation characterizes the quantity of mass within the chamber over time. *In* characterizes the mass of contaminant entering the chamber. Typically, the vapor entering the emission chamber does not contain contaminant vapor, so In is set to zero. *Out* characterizes the mass of contaminant exiting the chamber. *Generated* is the mass generated within the chamber by the vapor-emitting item. *Consumed* is a reduction of mass within the chamber, typically associated with a chemical reaction or a mass sink within the system (e.g., absorbent). The chamber walls can act as a sink and influence the results.[B-2] For the present system, Consumed is set to zero (i.e., it is assumed there are no sinks in the system). These definitions are used to derive an equation that describes the time evolution of the system.
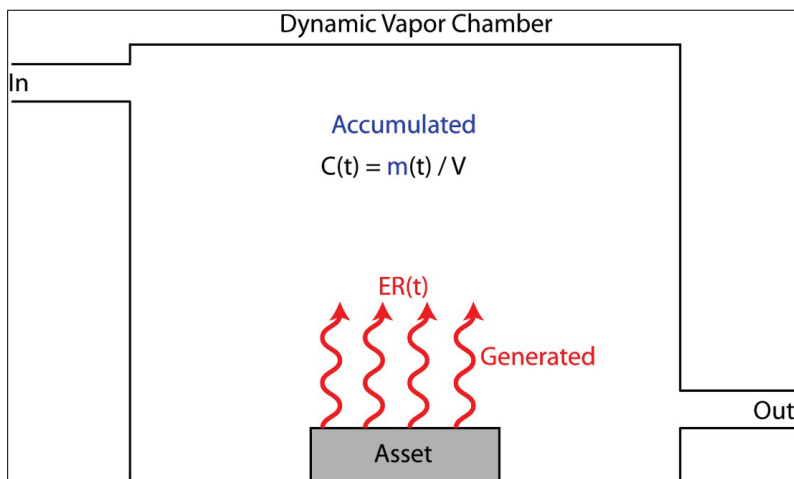

Figure B-1. Illustration of a dynamic vapor chamber.

A dynamic vapor chamber has a known chamber volume (V). The chamber is constructed such that the airflow in (Q) equals the airflow out of the exhaust. In a well-mixed environment, the vapor concentration in the chamber is uniform throughout the chamber, and the vapor concentration in the exhaust is the same as within the chamber. The chamber vapor concentration is determined by the mass of agent vapor in the chamber, divided by the chamber volume, expressed as

$$C(t) = \frac{m(t)}{V} \qquad (B\text{-}2)$$

where

   t is time (s),
   $C(t)$ is the chamber concentration as a function of time (mg/m^3),
   $m(t)$ is the mass of agent vapor in the chamber as a function of time (mg), and
   V is the chamber free air volume (m^3).

The agent vapor mass in the chamber (i.e., *accumulated*) changes as a function of time because of agent vapor mass introduced by vapor emission (i.e., *generated*) and agent vapor mass removed (i.e., Out) by air flowing out of the exhaust stream. Derivation of the mass balance equation considers a small time interval (Δt). The vapor source emits agent mass at a rate expressed as an emission rate [$E(t)$] that varies with time. During the small time interval, the emission source adds agent vapor mass to the chamber, which is determined by the product of the emission rate and the small time interval [$E(t)\Delta t$]. Simultaneously, agent leaves the chamber through the exhaust stream. Because the chamber is assumed to be well mixed, the mass of agent removed by exhaust (i.e., Out) is determined by the product of the agent vapor concentration, the chamber airflow rate, and the time interval [$C(t)Q\Delta t$]. Using the mass balance approach in eq B-1, the change in the total agent vapor mass in the chamber (Δm) is a function of the mass introduced by the emission source and the mass removed by the exhaust stream, expressed as

$$\Delta m = \text{Generated} - \text{Out}$$
$$\Delta m = E(t)\Delta t - C(t)Q\Delta t \qquad (B\text{-}3)$$

where

   Δm is the change in agent vapor mass in the chamber for a small time interval (mg);
   $E(t)$ is the emission rate (mg s^{-1});
   Δt is the small time interval (s); and
   Q is the chamber airflow rate (m^3 s^{-1}).

This equation is divided by Δt to produce

$$\frac{\Delta m}{\Delta t} = E(t) - C(t)Q \qquad (B\text{-}4)$$

The change in mass term (Δm) is converted to the change in vapor concentration (ΔC), by dividing by the chamber free air volume (V) to produce

$$\frac{\Delta C}{\Delta t} = \frac{E(t)}{V} - C(t)\frac{Q}{V} \qquad (B\text{-}5)$$

In the limit, as the small time step goes to zero ($\lim \Delta t \rightarrow 0$), the equation can be expressed as a linear first-order differential equation, referred to as the mass balance equation:

$$\frac{\mathrm{d}C}{\mathrm{d}t} = \frac{E(t)}{V} - C(t)\frac{Q}{V} \qquad \text{(B-6)}$$

For a given system, the ratio of Q/V is a fixed constant that represents the airflow rate per unit volume. This ratio is often referred to as the air change rate [n (s^{-1})], which represents the period for one chamber (or environmental) volume of air to flow into the system.

B.2   Flow in the Microchamber

Computational fluid dynamics (CFD) was used to calculate the airflow characteristics in the vapor microchamber at the U.S. Army Combat Capabilities Development Command Chemical Biological Center (DEVCOM CBC; Aberdeen Proving Ground, MD) (Figure B-2). Simulations were conducted using Autodesk CFD software (Autodesk, Inc.; San Rafael, CA). The chamber airflow rate for these simulations was 500 mL/min (8.3×10^{-6} m^3/s), using the chamber designs illustrated in Figure 9 within this report. A key design element of this vapor microchamber was the diffusion trough that disperses the airflow across the test panel. The particle trace plot (Figure B-2, part C) for this chamber design shows that the air at the inlet (bottom left) is dispersed by the diffuser trough and flows across the panel surface before being focused into the microchamber exhaust line (upper right). The straight-line path illustrates that minimal mixing occurs in this chamber; a laminar flow is maintained that collects vapor emission from the sample and transports it directly to the chamber exhaust. In this case, the mass balance equation used to describe a test chamber with a defined volume that is assumed to be well mixed can be simplified to a flow-through system (Figure B-3).
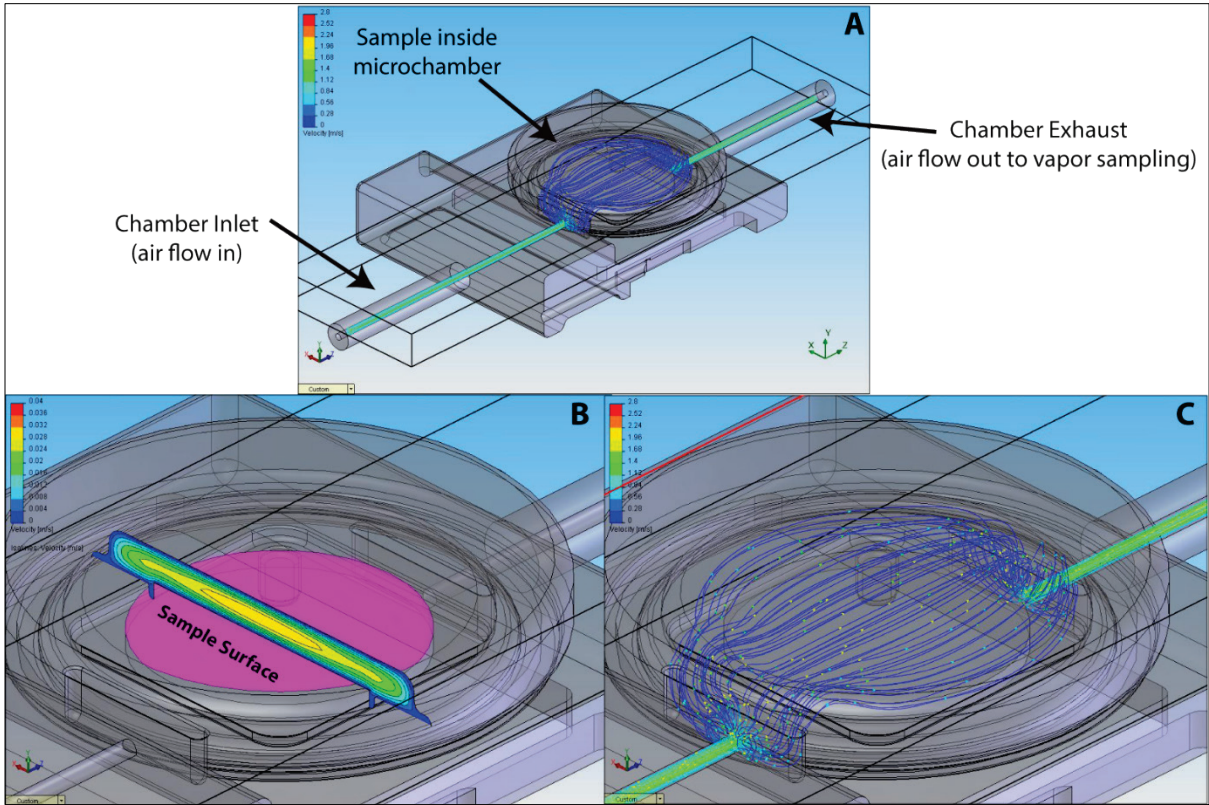
Figure B-2. (A) CFD air velocity calculations for the DEVCOM CBC vapor microchamber. (B) A contour cross section of the air velocity over the panel surface. (C) A particle trace, illustrating the trajectory of the airflow from inlet to exhaust.
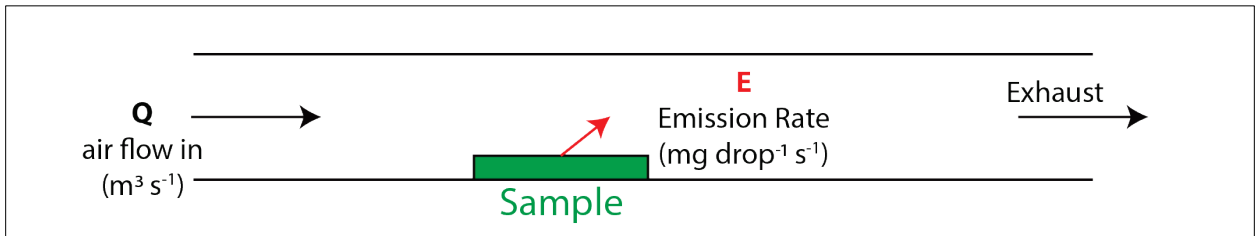
Figure B-3. Simplified flow geometry for the DEVCOM CBC vapor microchamber.

Using the simplified flow geometry (Figure B-3), the vapor concentration at the exhaust can be calculated as the mass emitted per unit time divided by the chamber flow rate:

$$C(t) = \frac{E(t)N}{Q} \tag{B-7}$$

where
$E(t)$ is the emission rate (mg drop^{-1} s^{-1});
N is the number of contaminant droplets applied to the test material (drops);
$C(t)$ is the vapor concentration (mg/m^3); and
Q is the airflow rate through the chamber (m^3 s^{-1}).

Solving for *E(t)*, the item emission rate can be determined from the experimentally measured exhaust concentration as

$$E(t) = \frac{C(t)Q}{N} \tag{B-8}$$

B.3   Approximation to the Mass Balance Equation for Microchambers

       The simplified flow geometry presented in eq B-8 assumes that mass accumulation within the chamber volume can be ignored. The CFD airflow analysis would tend to support this assumption; however, not all vapor microchambers present a similar flow-through pattern. For example, previous test chambers have used a simple cylinder geometry with inlet and exhaust flows at the top of the cylinder (Figure B-4). This creates a mixing volume: agent vapor could accumulate, and the flow could deviate from the simplified calculation in eq B-8, where this accumulation is ignored. The following analysis considers how the chamber volume and chamber flow rate for a well-mixed chamber may deviate from the assumptions used in eq B-7. The flow characteristics of the DEVCOM CBC chamber do not exhibit mixing; thus, the following calculation is thought to be a worst-case error to use with eq B-8 to estimate emission rates.

       To evaluate the accuracy of eq B-8, an ideal emission rate of

$$E_{\text{actual}}(t) = 1 \times 10^{-5}\exp(-t \times 0.005) \tag{B-9}$$

was input to the mass balance equation (eq B-6) using the DEVCOM CBC microchamber volume ($V = 3.2 \times 10^{-5}$ m^3) and flow rate ($Q = 150$ mL/min $= 2.5 \times 10^{-6}$ m^3/s), and an initial condition of $C(t = 0) = 0$ mg/m^3, to produce a simulated vapor concentration (Figure B-5, part A). This approach assumes the microchamber is well mixed (i.e., the vapor concentration is uniformly distributed within the chamber volume), which maximizes the accumulated mass that is ignored by eq B-8. The resulting estimated emission rate ($E_{\text{est}}(t)$), calculated by eq B-8, is shown in Figure B-5, part B. The accuracy of the estimated to the actual emission rate is compared as the ratio of $E_{\text{est}}(t)/E_{\text{actual}}(t)$ in Figure B-5, part C. It is observed that the error ratio stabilized around 1.07 after 6.9 air changes (6.9 × Q/V), which was the time for 99% of the air in the chamber to be flushed.[B-1] The results indicate that for the specified test conditions, eq B-8 may overestimate the emission rate by a factor of 1.07 if the chamber is well mixed. From this, it is expected that the actual deviation is less than this ratio because the CFD analysis shows the chamber is more of a direct flow-through chamber. As a last analysis, the vapor-emitted masses (VEMs) for the actual and estimated emission rates were compared, which produced a ratio of 0.997. This indicates that even when the well-mixed assumption is applied, the VEM of E_{est} is within 0.3% of the VEM for E_{actual}. The 0.3% missing emitted mass was likely due to error occurring during the first few seconds of the simulation, when the chamber concentration was increasing from the initial condition. Based on these results, eq B-8 was found to acceptably represent the item emission rate for the DEVCOM CBC microchambers and the test conditions used in this report.
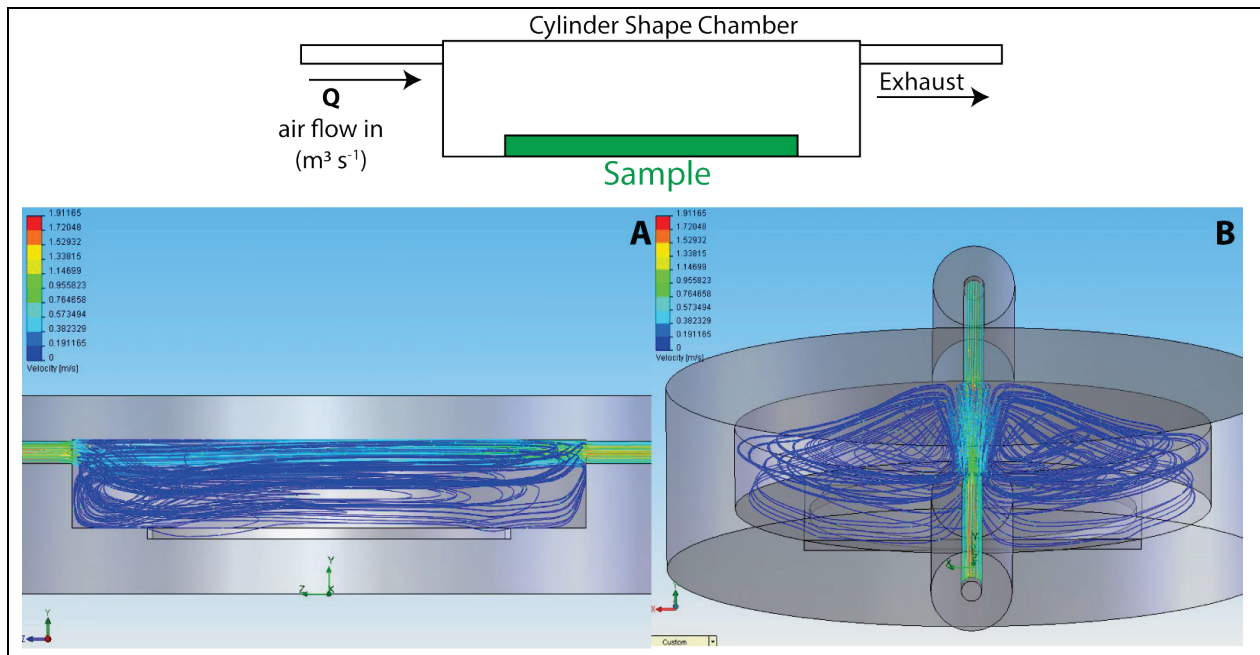
Figure B-4. Particle trace plots for a cylinder vapor chamber with a flow geometry that creates a mixing volume. (A) Side perspective of the particle flow trajectories shows circulating patterns. (B) A perspective view along the inlet flow path shows circulating flow in the chamber volume.
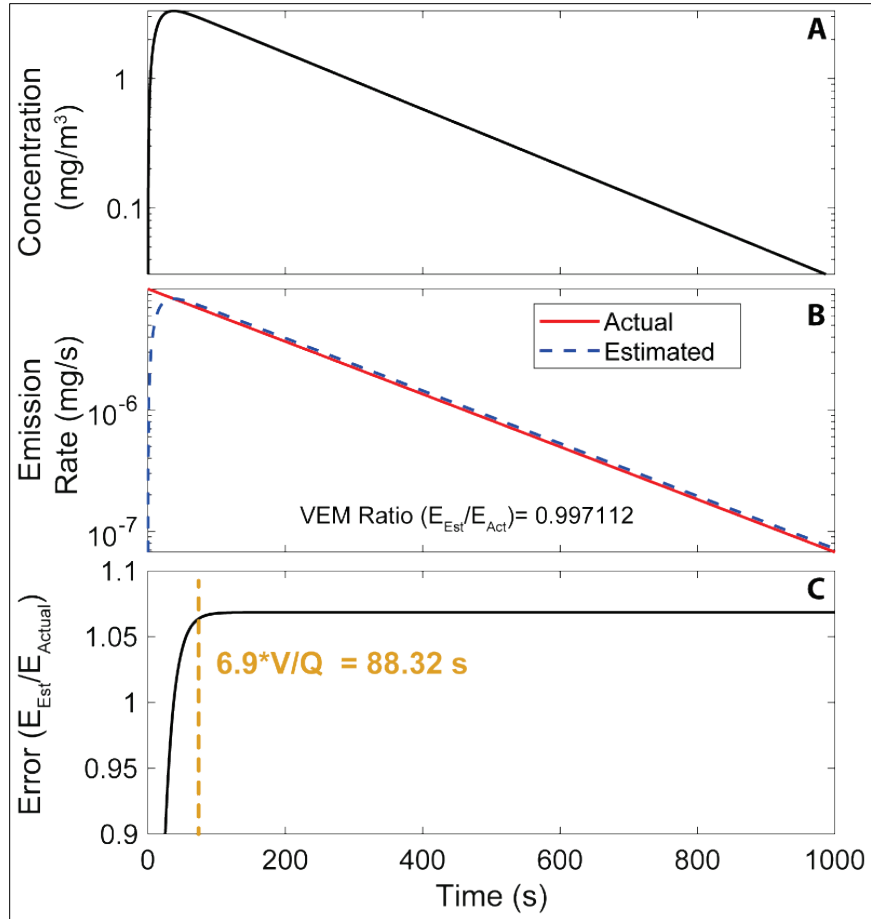
Figure B-5. (A) Microchamber-predicted concentration using the mass balance equation. (B) Actual and estimated emission rates. (C) Difference in the estimated and actual emission rates shown as the ratio between the rates.

APPENDIX B: LITERATURE CITED

B-1.   *Standard Guide for Small-Scale Environmental Chamber Determinations of Organic Emissions from Indoor Materials/Products*; ASTM D5116-17; ASTM International: West Conshohocken, PA, 2017.

B-2.   Tichenor, B.A. *Characterizing Sources of Indoor Air Pollution and Related Sink Effects*; STP1287; ASTM International: West Conshohocken, PA, 1996.

APPENDIX C:
ANALYTICAL METHOD AND DATA ANALYSIS

C.1   Mass Spectrometer Conditions

Atmospheric pressure mass spectrometry (AP-MS) was used to quantify the emission rate from complex features. The Cirrus 3-XD system (MKS Instruments; Andover, MA) a high-sensitivity instrument that includes capillary pressure reduction and mass spectrometry, was used for these studies. When sampling, a 150 mL/min nitrogen vapor stream was passed over a contaminated item that had been placed in the vapor microchamber. This flow rate was controlled using a mass flow controller. The chamber outlet was directed toward a sampling junction, where 20 mL/min of the flow was directed to the capillary inlet of the mass spectrometer. The remaining 130 mL/min was directed toward the exhaust. The capillary inlet flow into the spectrometer was fixed by the instrument configuration. The chamber flow rate was selected to give sufficient air exchanges in the microchamber. The sampled vapor stream was reduced from ambient pressure using a pressure-reduction capillary, a 2 m long fused silica tube with a 0.010 in. inner diameter. The capillary was wrapped in a heating jacket, and temperature was maintained at 150 °C to prevent gas condensation on the inner wall of the capillary tube. Figure C-1 shows the vapor sampling system.
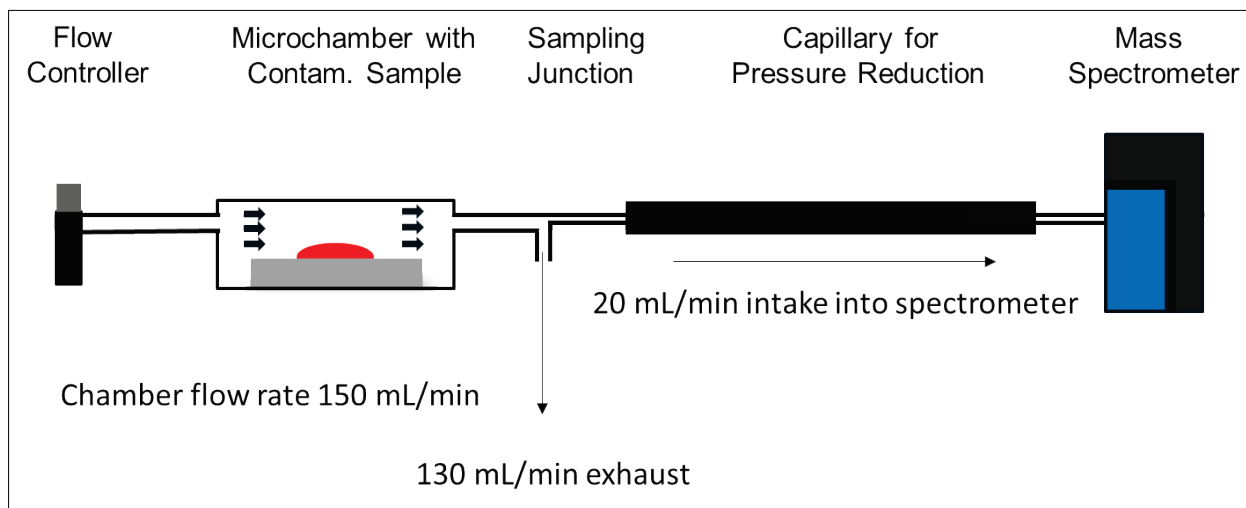

Figure C-1. Vapor emission sampling apparatus.

Upon exiting the capillary, the analyte was ionized using electron impact in a closed ion source. Electrons were generated using a tungsten filament. Ionization conditions are provided in Table C-1.

Table C-1. Electron Impact Ionization Conditions

Electron energy	70 eV
Ion energy	4.4 eV
Emission current	1.0 mA
Extractor potential	−16.1 V
Pole bias	0.3 V

As shown in Figure C-2, the analyte ion was generated using the ion source, and ions were mass filtered using the quadrupole. For 2,5-lutidine, the primary M^+ ion is generated at a mass-to-charge ratio (m/z) of 107. The quadrupole scanned the mass range from m/z 105 to m/z 108 at a peak resolution of 16 measurements per mass, for a total of 64 measurements. One scan was performed every 2.8 s (a dwell time of 0.7 s per m/z). Following mass selection at the quadrupole, analyte ions were amplified at two electron multiplier settings, high and low, for increased dynamic range. Ion detection could also be measured using a Faraday cup.
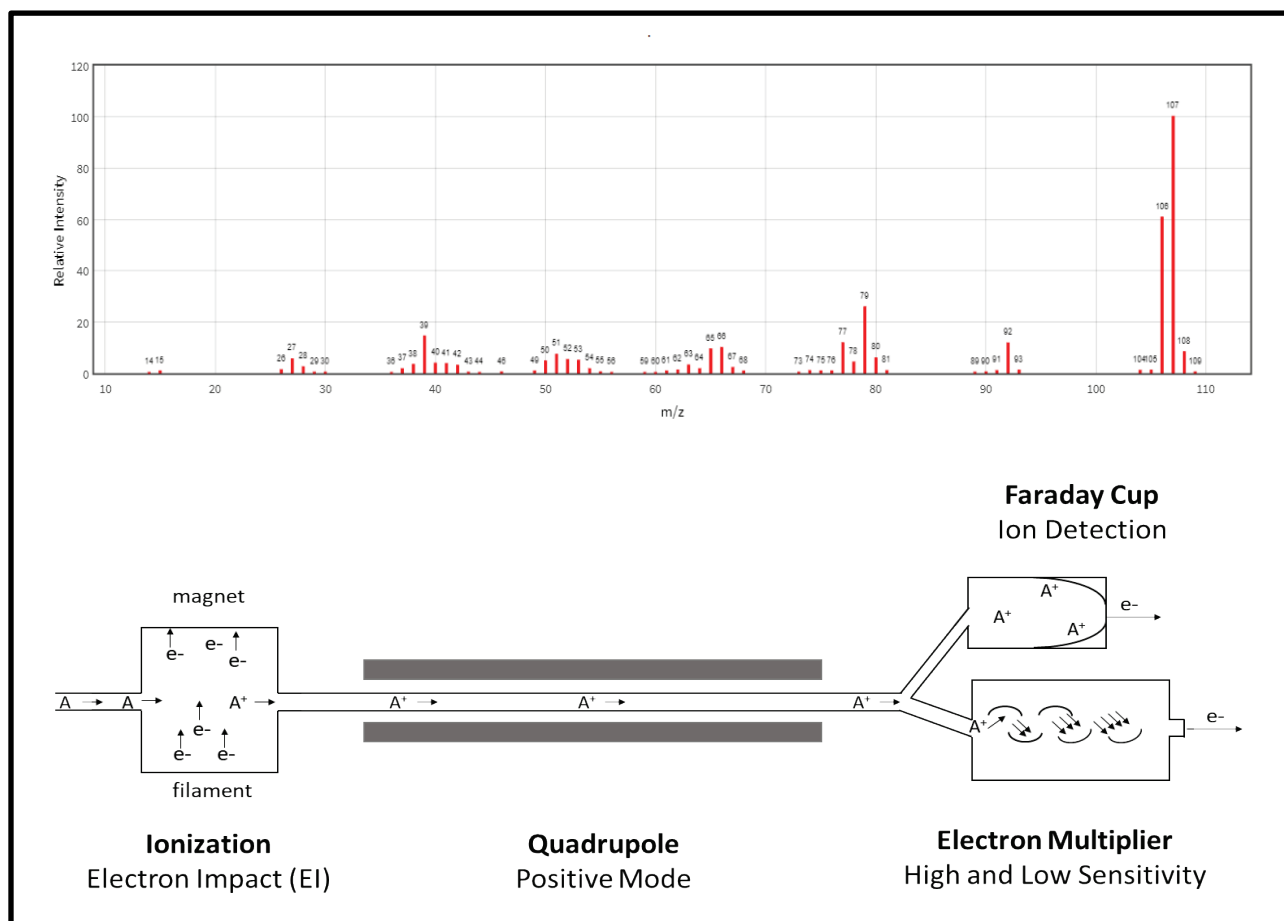
Figure C-2. (Top) Mass spectrum of 2,5-lutidine. (Bottom) Mass spectrometer ion path.

C.2   Calibration of Mass Spectrometer

The raw output of the mass spectrometer (from the electron multiplier) is in volts. The detector requires calibration to convert the raw detector output into analyte concentration. To do this, a saturated stream of 2,5-lutidine vapor was diluted to create known concentrations of 2,5-lutidine vapor. A saturator cell (Figure C-3) created a saturated vapor stream at 24,159 mg/m^3, which was further diluted by an additional nitrogen diluent line. The vapor concentration of the saturated stream was verified using gravimetric measurements to determine the mass loss in the saturator cell during calibration. During calibration, vapor flow rate was maintained at 150 mL/min total, and ionization conditions were identical to those used in the sampling procedure.
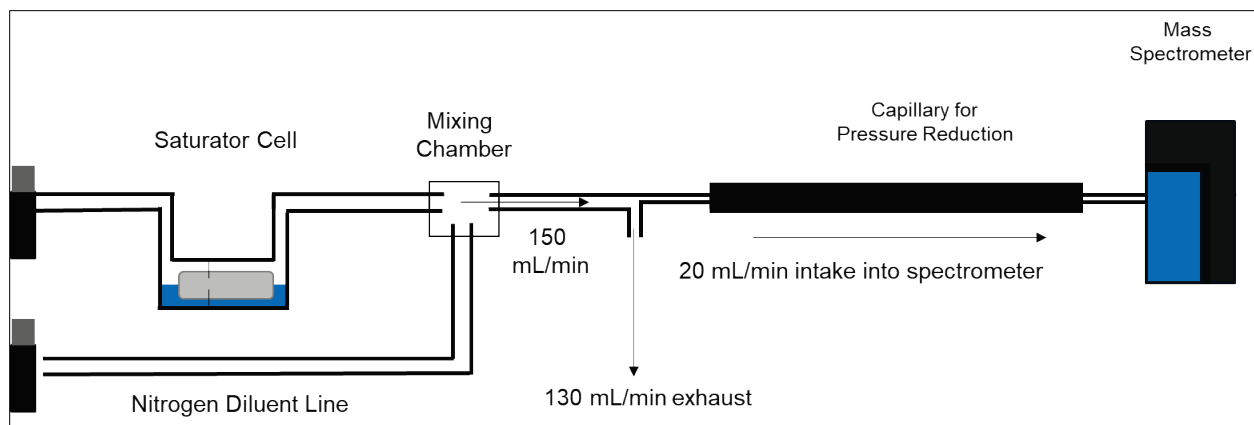
Figure C-3. Mass spectrometer calibration setup.

A calibration of the vapor stream was performed by serial dilution of the saturated 2,5-lutidine vapor stream at 30-, 15-, 10-, 7.5-, and 6-fold for a total of six calibration points and a blank. The calibration data exhibited a linear response up to approximately 2000 mg/m^3 before showing signs of saturation. A nonlinear (quadratic) calibration was used to calibrate beyond the linear range. Full calibrations for two electron multiplier settings are given in Figure C-4. The high and low settings on the electron multiplier correspond with two different gain settings on the instrument.

	Detector Response		
Dilution Factor	Vapor Concentration (mg/mL)	Multiplier = High (V)	Multiplier = Low (V)
Blank	0	0.0	0.0
30	805	3.6	7.8
15	1611	7.8	16.2
10	2416	14.2	30.1
7.5	3221	20.2	43.3
6	4026	27.3	59.8

$$y = -2.3304x^2 + 209.48x$$
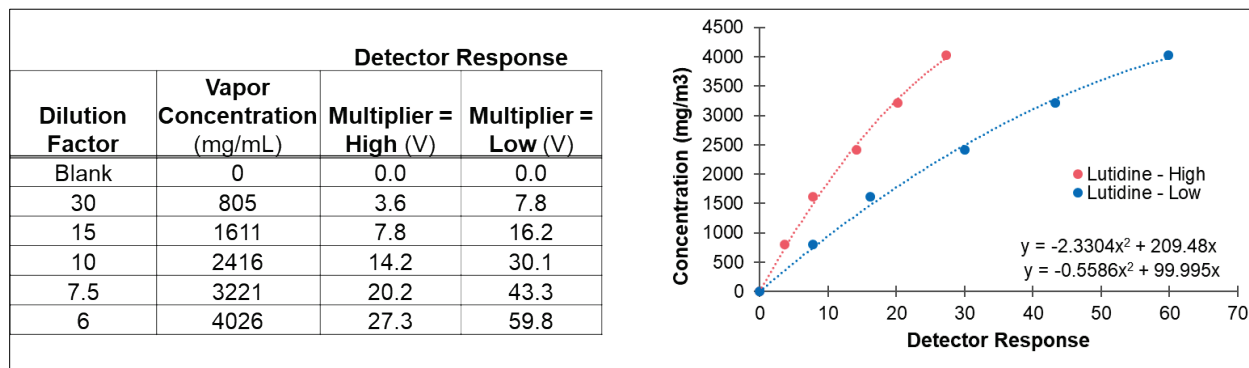$$y = -0.5586x^2 + 99.995x$$

Figure C-4. Calibration data for 2,5-lutidine.

Verification of the calibration was performed by introducing a known volume of 2,5-lutidine into the vapor microchamber and integrating the emission rate over time. As described in Section C-3, the vapor concentration and volumetric flow can be used to calculate the total vapor emitted mass (VEM). A 2 µL drop of 2,5-lutidine was added to a stainless steel panel, the mass of the contaminated panel was determined gravimetrically, and then the panel was placed in the vapor microchamber. The concentration of the effluent stream during emission was determined using AP-MS, and the total VEM was determined through integration of the data (see Section C-3). After vapor emission ceased, the panel mass was measured, and the difference between the pre- and post-emission panel was used to determine the gravimetric VEM. Valuation of the calibration was performed by comparing the VEM determined gravimetrically to the value

calculated from integration of the mass spectrometry data. As shown in Figure C-5, the calculated VEM largely fell within the range of the gravimetric measurements.
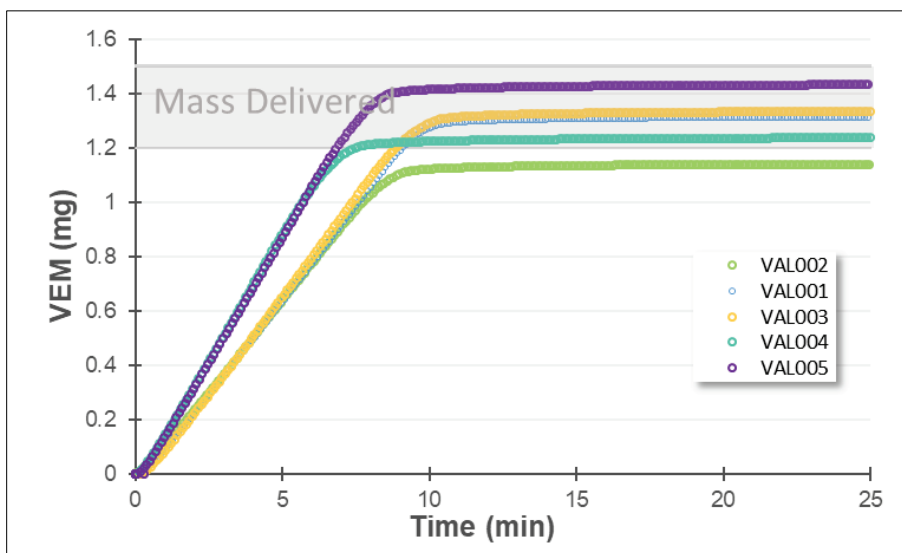

Figure C-5. Gravimetric validation of detector calibration. Grayed-out region corresponds to mass of 2 µL droplets of 2,5-lutidine delivered, determined gravimetrically.

C.3   Data Analysis Calculations

Vapor concentration was determined from the raw mass spectrometry, the quadratic calibration equation (eq C-1), and the calibration coefficients listed in Figure C-4. Typically, the low electron multiplier setting was used for data analysis.

$$C(t) = aR(t)^2 + bR(t) \qquad\qquad \text{(C-1)}$$

where

    $C(t)$ is the vapor concentration (mg/m^3);
    $R(t)$ is the detector response from mass spectrometer;
    a is the first calibration coefficient; and
    b is the second calibration coefficient.

The per-droplet emission rate from the object can be correlated to the vapor concentration $C(t)$ using the volumetric flow rate, Q. All measurements were performed using a single droplet, so $N = 1$ for all measurements through this study. Similarly, all studies were performed with $Q = 150$ mL/min (1.5×10^{-4} m^3/min).

$$E(t) = \frac{C(t)Q}{N} \qquad\qquad (C\text{-}2)$$

where
        $E(t)$ is the emission rate (mg/min) per N droplets;
        N is the number of contaminant droplets applied to the test material;
        $C(t)$ is the vapor concentration (mg/m^3); and
        Q is the airflow rate through the chamber (m^3/min).

Integration of the emission rate over time provides the cumulative VEM, as given in eq C-3. Integration over the course of the vapor emission provides the total VEM.

$$M_{VE}(t) = \int_0^t E(t)\,\mathrm{d}t \qquad\qquad (C\text{-}3)$$

where
        $M_{VE}(t)$ is the cumulative VEM per N droplets (mg); and
        $E(t)$ is the emission rate (mg/min) per N droplets.

DISTRIBUTION LIST

The following individuals and organizations were provided with one electronic version of this report:

U.S. Combat Capabilities Development
Command Chemical Biological Center
(DEVCOM CBC)
FCDD-CBR-PD
ATTN: Hawbaker, N.
Mantooth, B.
Morrissey, K.
Pearl, T.

Defense Threat Reduction Agency
DTRA-RD-IAR
ATTN: Lawson, G.
Bass, C.

DEVCOM CBC Technical Library
FCDD-CBR-L
ATTN: Foppiano, S.
Stein, J.

Defense Technical Information Center
ATTN: DTIC OA